

**SYNTHESIS AND MESOMORPHIC PROPERTIES OF  
SCHIFF BASE ESTERS WITH DIFFERENT  
TERMINAL SUBSTITUENTS**

**CHONG YEE TING**

**FACULTY OF SCIENCE  
UNIVERSITY OF MALAYA  
KUALA LUMPUR**

**2018**

**SYNTHESIS AND MESOMORPHIC PROPERTIES OF  
SCHIFF BASE ESTERS WITH DIFFERENT  
TERMINAL SUBSTITUENTS**

**CHONG YEE TING**

**DISSERTATION SUBMITTED IN FULFILMENT OF  
THE REQUIREMENTS FOR THE DEGREE OF  
MASTER OF SCIENCE**

**DEPARTMENT OF CHEMISTRY  
FACULTY OF SCIENCE  
UNIVERSITY OF MALAYA  
KUALA LUMPUR**

**2018**

**UNIVERSITY OF MALAYA**  
**ORIGINAL LITERARY WORK DECLARATION**

Name of Candidate: **CHONG YEE TING**

Matric No: **SGR120038**

Name of Degree: **MASTER OF SCIENCE**

Title of Project Paper/Research Report/Dissertation/Thesis ("this Work"):

**SYNTHESIS AND MESOMORPHIC PROPERTIES OF SCHIFF BASE  
ESTERS WITH DIFFERENT TERMINAL SUBSTITUENTS**

Field of Study: **MATERIAL SCIENCE**

I do solemnly and sincerely declare that:

- (1) I am the sole author/writer of this Work;
- (2) This Work is original;
- (3) Any use of any work in which copyright exists was done by way of fair dealing and for permitted purposes and any excerpt or extract from, or reference to or reproduction of any copyright work has been disclosed expressly and sufficiently and the title of the Work and its authorship have been acknowledged in this Work;
- (4) I do not have any actual knowledge nor do I ought reasonably to know that the making of this work constitutes an infringement of any copyright work;
- (5) I hereby assign all and every rights in the copyright to this Work to the University of Malaya ("UM"), who henceforth shall be owner of the copyright in this Work and that any reproduction or use in any form or by any means whatsoever is prohibited without the written consent of UM having been first had and obtained;
- (6) I am fully aware that if in the course of making this Work I have infringed any copyright whether intentionally or otherwise, I may be subject to legal action or any other action as may be determined by UM.

Candidate's Signature

Date:

Subscribed and solemnly declared before,

Witness's Signature

Date:

Name:

Designation:

# SYNTHESIS AND MESOMORPHIC PROPERTIES OF SCHIFF BASE ESTERS WITH DIFFERENT TERMINAL SUBSTITUENTS

## ABSTRACT

Liquid crystal is a class of fascinating material showed unique properties such as thermochromism and photochromism which allowed applications in display devices, anisotropic networks, photoconductors and semiconductor materials. The study in liquid crystal science led to development of understanding the mesomorphic properties with small changes in terminal groups, carbon chains and incorporated heteroatom into mesogenic units. Four series of Schiff base esters comprising either thiophene or aromatic rings were successfully prepared via imination, and Steglich esterification which was widely reported. The chemical structure of the esters was confirmed by Fourier-transform infrared spectroscopy (**FTIR**), proton and carbon nuclear magnetic resonance ( $^1\text{H}$  and  $^{13}\text{C}$  **NMR**) together with CHN elemental analysis. The mesomorphic properties were determined using differential scanning calorimetry (**DSC**) and polarized optical microscopy (**POM**). DSC results revealed that most of the prepared esters exhibited multi-transition either in heating or cooling process or both. This had evidenced by the presence of several phase transition peaks between crystals and isotropic liquid. The liquid crystal textures were later confirmed with the POM analysis by comparing with the reported literature. First series (**nSB-R**) comprising different terminal groups (**R** =  $\text{CH}_3$ ,  $\text{OCH}_3$  and  $\text{N}(\text{C}_2\text{H}_5)_2$ ). Methoxy group series showed nematogenic properties whereas methyl group series displayed both nematic and smectic A or B phases for its compound, **14SB-CH<sub>3</sub>**. However, diethylamino group series showed direct isotropization behavior. The results suggested that a bulky substituent may disrupt the mesogen arrangement that enable liquid crystal mesophase. A small non-polar group such as methyl group was minimized the steric hindrance

between the molecules and allowed them to be orientated and interacted closer. Second series (**nSHB-OCH<sub>3</sub>**) comprising the additional lateral hydroxy group of previous series. The DSC and POM results revealed that additional hydroxy group increased liquid crystal phase stability and enhanced lateral interaction. Although methoxy group reported as one of the terminal groups which favors in nematic phase, but the impact of lateral hydroxy group was significant and allow the lamellar packing smectic A phase. In third series, only **OBSB-Cl** and **OBSB-OCH<sub>3</sub>** showed the liquid crystal properties while the rest are non-mesogenic. The results displayed that a bulky substituent at the terminal flexible chain will increase the steric hindrance effect between the molecules and diminished the mesomorphic properties. The present of heteroatom in fourth series (**nAFTP**) impacted on its anisotropy and enhanced the phase stability. The heteroatom such as S, O and N significantly impart lateral and/or longitudinal dipoles as it was more polarizable than carbon. Thiophene group reduced the linearity of the molecules and this had enhanced the molecule to tilt with an angle and led to favor in Smectic C phase. The liquid crystal properties are greatly influenced by the small changes in the molecular architecture and this will lead to existence of different mesophase and phase stability.

**Keywords:** liquid crystal; smectic A; smectic C; nematic; benzylideneaniline

# SINTESIS DAN SIFAT-SIFAT CECAIR HABLUR BAGI SEBATIAN ALKALI SCHIFF ESTER DENGAN PENUKAR GANTI YANG BERLAINAN

## ABSTRAK

Hablur cecair adalah kelas bahan yang menarik dengan menunjukkan sifat-sifat unik seperti termachromisme dan fotochromisme yang membolehkan aplikasi dalam paparan peranti, rangkaian tak isotropi, bahan-bahan fotokondutor dan semikondutor. Kajian sains dalam hablur cecair membawa kepada pembangunan dan pemahaman sifat-sifat mesomorf dengan penukaran dalam kumpulan terminal, rangkaian karbon dan heteroatom ke dalam struktur teras. Empat siri alkali Schiff ester yang terdiri daripada thiofene atau aromatik telah berjaya disediakan melalui proses iminasi dan pengesteran Steglich yang dilaporkan secara meluas. Struktur kimia ester tersebut telah disahkan melalui kaedah spektroskopi terbitan inframerah Fourier (FTIR), proton dan karbon resonans magnet nukleus (NMR  $^1\text{H}$  dan  $^{13}\text{C}$ ) bersamaan dengan analisis unsur CHN. Sifat-sifat mesomorf telah ditentukan menggunakan kaedah kalorimetri pengimbasan pembezaan (DSC) dan mikroskopi optik terkutub (POM). Keputusan DSC mendedahkan bahawa kebanyakan ester mempamerkan pelbagai suhu peralihan. Ini telah dibuktikan dengan kewujudan beberapa fasa peralihan antara kristal dan cecair isotropi. Tekstur hablur cecair telah disahkan kemudian dengan bantuan analisis POM dan membandingkan dengan struktur yang dilaporkan. Siri pertama (**nSB-R**) terdiri daripada kumpulan terminal yang berlainan (**R = CH<sub>3</sub>, OCH<sub>3</sub> dan N(C<sub>2</sub>H<sub>5</sub>)<sub>2</sub>**). Siri kumpulan metoksi menunjukkan sifat-sifat nematogenik manakala siri kumpulan metil telah memaparkan fasa-fasa nematik dan smektik A atau B bagi kompaun, **14SB-CH<sub>3</sub>**. Tetapi, siri kumpulan dietilamino menunjukkan isotropi secara langsung dari fasa kristal. Keputusan mencadangkan bahawa kemungkinan kumpulan yang besar telah mengganggu mesogen daripada susunan fasa-fasa hablur cecair. Kumpulan kecil tidak

berkutub seperti metil telah mengurangkan halangan sterik antara molekul dan membenarkan orientasi dan interaksi yang lebih dekat. Siri kedua (**nSHB-OCH<sub>3</sub>**) terdiri daripada tambahan kumpulan hidroksi di sisi struktur. Keputusan DSC dan POM mendedahkan kumpulan hidroksi tambahan tersebut meningkat kestabilan fasa hablur cecair dan interaksi. Walaupun kumpulan metoksi yang dilaporkan sebagai salah satu daripada terminal yang dalam mempamerkan fasa nematik, tetapi kesan daripada kumpulan hidroksi telah membenarkan susunan lamela bagi fasa smektik. Dalam siri ketiga, hanya **OBSB-Cl** dan **OBSB-OCH<sub>3</sub>** menunjukkan sifat-sifat hablur cecair manakala selebihnya tidak menunjuk sifat hablur cecair. Keputusan telah menunjukkan bahawa kumpulan yang sangat besar di terminal akan meningkat kesan halangan sterik antara molekul dan sifat hablur cecair akan berkurangan. Kehadiran heteroatom dalam siri keempat (**nA<sub>2</sub>TP**) meningkatkan sifat tak isotropi dan kestabilan fasa mesomorf. Heteroatom seperti S, O dan N memberikan kesan berkutub sama ada di sisian dan/atau membujur kerana ia adalah lebih berkutub daripada karbon. Kumpulan tiofena menyebabkan struktur yang kurang linear dan ini telah meningkatkan kecondongan sudut molekul dan condong ke arah fasa Smektik C. Sifat-sifat hablur cecair amat dipengaruhi oleh perubahan kecil dalam struktur molekul dan membawa kepada kewujudan pelbagai mesofasa dan kestabilan fasa.

**Kata kunci:** hablur cecair; smektik A; smektik C; nematik; benzilidenaanilina

## ACKNOWLEDGEMENTS

I would like to express my great appreciation and gratitude to my supervisors, Dr. Norazilawati binti Muhamad Sarih (University of Malaya), Dr. Ha Sie Tiong (Universiti Tunku Abdul Rahman) and Prof. Dr. Md. Rezaul Karim Sheikh (Rajshahi University, Bangladesh) for their guidance, advice and encouragement along my study. I want to thank my laboratory mates, Dr. Siti Nor Atika Baharin, Dr. Syed Shahabuddin and Ms. Fatem Hamime Ismail for all their helps, supports, discussions and valuable suggestions through the entire period in our laboratory. I would also like to convey my appreciation to the technical staff from Department of Chemistry for the continuous helps either directly or indirectly involved in my research work. Many thanks also to University of Malaya for the research facilities and financial support through Postgraduate Research Fund with the vote PG013-2013A and Fundamental Research Grant Scheme (FRGS) with the vote FP031-2014B. Finally, I owe my special gratitude to my parents that giving me a lot of support and patient during the project in running. Without their support, I think I might not be able to complete my dissertation as well.



## TABLE OF CONTENTS

Abstract .....	iii
Abstrak .....	v
Acknowledgements.....	vii
Table of Contents.....	viii
List of Figures.....	xii
List of Tables.....	xvi
List of Symbols and Abbreviations .....	xix
List of Appendices.....	xxi
<b>CHAPTER 1: INTRODUCTION .....</b>	<b>1</b>
1.1 General Aspect of Liquid Crystals .....	1
1.2 Structure of Calamitic Liquid Crystals.....	5
1.2.1 Terminal Substituents (R and R') .....	5
1.2.1.1 Polar Groups .....	6
1.2.1.2 Straight Alkyl/ Alkoxy Chains.....	9
1.2.2 Linking Groups.....	10
1.2.3 Lateral Substituent .....	13
1.2.4 Center Core.....	14
1.3 Research Objective .....	17
1.4 Scope of Study.....	17
1.5 Significance of Study.....	18
1.6 Thesis Outline.....	18

<b>CHAPTER 2: LITERATURE REVIEW.....</b>	<b>19</b>
2.1 Rod-like Liquid Crystals.....	19
2.1.1 Schiff Base Liquid Crystals.....	20
2.1.2 Terminal Substituted Flexible Alkyl Chain Liquid Crystals.....	29
2.2 Heterocyclic Liquid Crystals.....	33
2.2.1 Thiophene-based Liquid Crystals .....	34
 <b>CHAPTER 3: MATERIALS AND METHODS.....</b>	 <b>36</b>
3.1 Chemicals.....	36
3.2 Synthesis .....	36
3.2.1 Synthesis of Series 1 .....	36
3.2.1.1 Synthesis of 4-hydroxybenzylidene-4'-methyl, 4'-methoxy, 4'-(N,N-diethyl-amino)aniline .....	37
3.2.1.2 Synthesis of Series 1A (nSB-CH <sub>3</sub> ).....	38
3.2.1.3 Synthesis of Series 1B (nSB-OCH <sub>3</sub> ) .....	39
3.2.1.4 Synthesis of Series 1C (nSB-NDEA).....	40
3.2.2 Synthesis of Series 2 .....	41
3.2.2.1 Synthesis of 2,4-dihydroxybenzylidene-4'-methoxyaniline....	41
3.2.2.2 Synthesis of Series 2 (nSHB-OCH <sub>3</sub> ) .....	42
3.2.3 Synthesis of Series 3 .....	43
3.2.3.1 Synthesis of 4-hydroxybenzylidene-4'-substituted aniline.....	43
3.2.3.2 Synthesis of Series 3 (OBSB-R) .....	44
3.2.4 Synthesis of Series 4 .....	45
3.2.4.1 Synthesis of intermediate 1 for series 4.....	46
3.2.4.2 Synthesis of intermediate 2 for series 4.....	47
3.2.4.3 Synthesis of Series 4 with different alkyl chain (nAFTP).....	47

3.3	Characterization Method.....	48
3.3.1	Fourier Transform Infrared (FTIR).....	48
3.3.2	Nuclear Magnetic Resonance (NMR).....	49
3.3.3	Differential Scanning Calorimetry (DSC).....	49
3.3.4	Polarized Optical Microscope (POM).....	50
3.3.5	Elemental CHN Analysis. ....	50
3.3.6	Thin Layer Chromatography. ....	50
<b>CHAPTER 4: RESULTS AND DISCUSSION.....</b>		<b>51</b>
4.1	Series 1.....	51
4.1.1	Structural Elucidation.....	52
4.1.2	Thermal Behavior and Mesomorphic Properties.....	75
4.1.2.1	Series 1A.....	75
4.1.2.2	Series 1B.....	81
4.1.2.3	Series 1C.....	86
4.1.3	Chemical Structure-Liquid Crystal Property Relationship .....	88
4.2	Series 2.....	90
4.2.1	Structural Elucidation.....	90
4.2.2	Thermal Behavior and Mesomorphic Properties.....	100
4.3	Series 3.....	107
4.3.1	Structural Elucidation.....	107
4.3.2	Thermal Behavior and Mesomorphic Properties.....	116
4.4	Series 4.....	121
4.4.1	Structural Elucidation.....	121
4.4.2	Thermal Behavior and Mesomorphic Properties.....	130

<b>CHAPTER 5: CONCLUSION &amp; FUTURE WORK.....</b>	<b>136</b>
5.1 Series 1.....	136
5.2 Series 2.....	137
5.3 Series 3.....	137
5.4 Series 4.....	138
5.5 Recommendations for Future Work .....	138
References .....	139
List of Publications and Papers Presented .....	146
Appendices .....	148

## LIST OF FIGURES

Figure 1.1:	Molecular structure of cholesteryl benzoate.....	1
Figure 1.2:	Molecular structure of 4-cyano-4'-pentylbiphenyl.....	2
Figure 1.3:	General classification of liquid crystals .....	3
Figure 1.4:	Structure of thermotropic liquid crystal .....	3
Figure 1.5:	Molecular structure and mesophase of liquid crystal (Kato <i>et al.</i> , 2007) .	4
Figure 1.6:	General structural templates for calamitic mesogens .....	5
Figure 1.7:	Structure of <i>p</i> -phenylenedi- <i>p</i> -aminobenzoate .....	7
Figure 1.8:	Illustration of the terminal and lateral attraction between molecules .....	9
Figure 1.9:	Structure of 2-(4'- <i>n</i> -alkoxyphenylazo)-6-methoxybenzothiazoles.....	10
Figure 2.1:	Structures of Schiff Base Liquid Crystals (Shanker & Pisipati, 2011)...	20
Figure 2.2:	Schiff base liquid crystal with different polar substituent.....	24
Figure 2.3:	Molecular structure and their phase transition temperature of 1O.5, 1O.O5 and 1O.OOC5 (Taylor & Francis, 1984) .....	25
Figure 2.4:	Molecular structure of Schiff base esters by Yeap and co-worker .....	28
Figure 2.5:	Structure of nCB .....	28
Figure 2.6:	Molecular structure of $\omega$ -substituted alkoxycyanobiphenyls.....	29
Figure 2.7:	Molecular structure of $\omega$ -substituted 2-alkoxy-5-phenylpyrimidines ....	30
Figure 2.8:	Molecular structure of bromoalkyloxy chain derivatives and their related compounds.....	31
Figure 2.9:	Structural formula of thiophene.....	33
Figure 2.10:	Molecular structure of 2-[4-(4'- <i>n</i> -alkoxybenzoyloxy) benzylidene-amino]-3-cyano thiophene.....	34
Figure 3.1:	Synthetic route towards the formation of the intermediate and the compounds named as nSB-CH <sub>3</sub> , nSB-OCH <sub>3</sub> and nSB-NDEA.....	37

Figure 3.2:	Synthetic route towards the formation of the intermediate and the compound named as nSHB-OCH <sub>3</sub> .....	41
Figure 3.3:	Synthetic route towards the formation of OBSB-H, OBSB-CH <sub>3</sub> , OBSB-OCH <sub>3</sub> , OBSB-Cl, OBSB-Br and OBSB-NDEA.....	43
Figure 3.4:	Synthetic route towards the formation of the intermediate and the compound named as nAFTP.....	46
Figure 4.1:	Structural formula of nSB-CH <sub>3</sub> , nSB-OCH <sub>3</sub> and nSB-NDEA .....	51
Figure 4.2:	FTIR spectrum of 10SB-CH <sub>3</sub> .....	56
Figure 4.3:	FTIR spectrum of 12SB-OCH <sub>3</sub> .....	57
Figure 4.4:	FTIR spectrum of 16SB-NDEA .....	58
Figure 4.5:	Atomic numbering scheme for 12SB-CH <sub>3</sub> , 10SB-OCH <sub>3</sub> and 14SB-NDEA .....	59
Figure 4.6:	<sup>1</sup> H NMR spectrum of 12SB-CH <sub>3</sub> .....	61
Figure 4.7:	<sup>13</sup> C NMR spectrum of 12SB-CH <sub>3</sub> .....	63
Figure 4.8:	<sup>1</sup> H NMR spectrum of 10SB-OCH <sub>3</sub> .....	66
Figure 4.9:	<sup>13</sup> C NMR spectrum of 10SB-OCH <sub>3</sub> .....	68
Figure 4.10:	<sup>1</sup> H NMR spectrum of 14SB-NDEA .....	71
Figure 4.11:	<sup>13</sup> C NMR spectrum of 14SB-NDEA .....	73
Figure 4.12:	DSC thermogram of 10SB-CH <sub>3</sub> .....	76
Figure 4.13:	DSC thermogram of 14SB-CH <sub>3</sub> .....	77
Figure 4.14:	DSC thermogram of 18SB-CH <sub>3</sub> .....	77
Figure 4.15:	Optical photomicrographs of compound 12SB-CH <sub>3</sub> exhibiting nematic phase during cooling cycle .....	78
Figure 4.16:	Optical photomicrographs of compound 14SB-CH <sub>3</sub> exhibiting nematic phase during cooling cycle .....	79
Figure 4.17:	Plot of transition temperatures of nSB-CH <sub>3</sub> during cooling cycle as a function of the number of carbon atoms .....	80
Figure 4.18:	DSC thermogram of 12SB-OCH <sub>3</sub> .....	82

Figure 4.19:	DSC thermogram of 16SB-OCH <sub>3</sub> .....	82
Figure 4.20:	Optical photomicrographs of compounds nSB-OCH <sub>3</sub> exhibiting nematic phase during cooling cycle .....	84
Figure 4.21:	Plot of transition temperatures of nSB-OCH <sub>3</sub> during cooling cycle as a function of the number of carbon atoms .....	85
Figure 4.22:	DSC thermogram of 12SB-NDEA.....	86
Figure 4.23:	DSC thermogram of 14SB-NDEA.....	87
Figure 4.24:	Structural formula of nSHB-OCH <sub>3</sub> .....	90
Figure 4.25:	FTIR spectrum of 12SHB-OCH <sub>3</sub> .....	93
Figure 4.26:	Molecular structure with atomic numbering scheme for 10SHB-OCH <sub>3</sub> .....	94
Figure 4.27:	<sup>1</sup> H NMR spectrum of 10SHB-OCH <sub>3</sub> .....	96
Figure 4.28:	<sup>13</sup> C NMR spectrum of 10SHB-OCH <sub>3</sub> .....	98
Figure 4.29:	DSC thermogram of 14SHB-OCH <sub>3</sub> .....	101
Figure 4.30:	DSC thermogram of 16SHB-OCH <sub>3</sub> .....	101
Figure 4.31:	Optical photomicrographs of compound 12SHB-OCH <sub>3</sub> exhibiting nematic phase only during cooling cycle .....	103
Figure 4.32:	Optical photomicrographs of compound 16SHB-OCH <sub>3</sub> exhibiting nematic phase and smectic A phase during cooling cycle .....	104
Figure 4.33:	Optical photomicrographs of compound 18SHB-OCH <sub>3</sub> exhibiting smectic A phase only during cooling cycle.....	105
Figure 4.34:	Plot of transition temperatures of nSHB-OCH <sub>3</sub> during heating cycle as a function of the number of carbon atoms .....	106
Figure 4.35:	Plot of transition temperatures of nSHB-OCH <sub>3</sub> during cooling cycle as a function of the number of carbon atoms .....	106
Figure 4.36:	Structural formula of OBSB-R .....	107
Figure 4.37:	Infrared spectrum of OBSB-Br.....	109
Figure 4.38:	Molecular structure with atomic numbering scheme for OBSB-OCH <sub>3</sub> .....	110
Figure 4.39:	<sup>1</sup> H NMR spectrum of OBSB-OCH <sub>3</sub> .....	112

Figure 4.40:	$^{13}\text{C}$ NMR spectrum of OBSB-OCH <sub>3</sub> .....	114
Figure 4.41:	DSC thermogram of OBSB-OCH <sub>3</sub> .....	117
Figure 4.42:	DSC thermogram of OBSB-CH <sub>3</sub> .....	117
Figure 4.43:	DSC thermogram of OBSB-Cl .....	118
Figure 4.44:	Optical photomicrograph of compound OBSB-OCH <sub>3</sub> exhibiting nematic phase during cooling cycle .....	119
Figure 4.45:	Optical photomicrograph of compound OBSB-Cl exhibiting nematic phase and smectic A phase during cooling cycle .....	120
Figure 4.46:	Structural formula of nAOTP .....	121
Figure 4.47:	Infrared spectrum of 16AOTP .....	123
Figure 4.48:	Molecular structure with atomic numbering scheme for 10AOTP .....	124
Figure 4.49:	$^1\text{H}$ NMR spectrum of compound 10AOTP .....	126
Figure 4.50:	$^{13}\text{C}$ NMR spectrum of compound 10AOTP .....	128
Figure 4.51:	DSC thermogram of 8AOTP .....	131
Figure 4.52:	DSC thermogram of 16AOTP .....	131
Figure 4.53:	Optical photomicrograph of compound 8AOTP exhibiting nematic phase during cooling cycle .....	133
Figure 4.54:	Optical photomicrograph of compound 18AOTP exhibiting SmC phase upon further cooling from nematic phase .....	133
Figure 4.55:	Plot of transition temperatures of nAOTP during heating cycle as a function of the number of carbon atoms .....	135
Figure 4.56:	Plot of transition temperatures of nAOTP during cooling cycle as a function of the number of carbon atoms .....	135



## LIST OF TABLES

Table 1.1:	Structure and phase transition of biphenyl analogous compounds with different terminal groups (Demus <i>et al.</i> , 1998) .....	8
Table 1.2:	Linking groups and their common names .....	11
Table 1.3:	Phase transition temperature of 6-decyloxy-2-(4-octyloxyphenyl-azo)-benzothiazoles (8), N-[2-(6-decyloxybenzothiazolyl)]-4-octyloxy-benzamides (9) and 6-decyloxy-2-(4-octyloxybenzylidene-aminobenzothiazoles (10).....	12
Table 1.4:	Example effect of lateral substituent of naphthanoic acid derivatives (Demus <i>et al.</i> , 1998).....	14
Table 1.5:	Effect of aromatic core and alicyclic core changes on transition temperatures.....	15
Table 2.1:	Phase variant of some liquid crystal compounds in nO.m, n.Om, nO.Om and n.m homologues series (Shanker & Pisipati, 2011) .....	22
Table 2.2:	Transition temperature and mesomorphic properties of 2-octyl-5-[4-(ω-hexyloxy)]phenylpyridines.....	31
Table 2.3:	Transition temperatures data of 2-[4-(4- <i>n</i> -alkoxybenzoyloxy)benzylideneamino] 3-cyano thiophene .....	35
Table 4.1:	Percentage yields of nSB-CH <sub>3</sub> , nSB-OCH <sub>3</sub> and nSB-NDEA .....	51
Table 4.2:	Micro-elemental analytical data of nSB-CH <sub>3</sub> , nSB-OCH <sub>3</sub> and nSB-NDEA.....	53
Table 4.3:	FTIR spectral analysis data of nSB-CH <sub>3</sub> .....	56
Table 4.4:	FTIR spectral analysis data of nSB-OCH <sub>3</sub> .....	57
Table 4.5:	FTIR spectral analysis data of nSB-NDEA.....	58
Table 4.6:	<sup>1</sup> H NMR spectral data of 12SB-CH <sub>3</sub> in CDCl <sub>3</sub> .....	61
Table 4.7:	<sup>13</sup> C NMR spectral data of compound 12SB-CH <sub>3</sub> in CDCl <sub>3</sub> .....	64
Table 4.8:	<sup>1</sup> H NMR data of 10SB-OCH <sub>3</sub> .....	66
Table 4.9:	<sup>13</sup> C NMR data of 10SB-OCH <sub>3</sub> .....	69
Table 4.10:	<sup>1</sup> H NMR data of 14SB-NDEA.....	71

Table 4.11:	$^{13}\text{C}$ NMR data of 14SB-NDEA.....	74
Table 4.12:	Phase transition temperatures and associated enthalpy changes of series nSB-CH <sub>3</sub> .....	78
Table 4.13:	Phase transition temperatures and associated enthalpy changes of series nSB-OCH <sub>3</sub> .....	83
Table 4.14:	Phase transition temperatures and associated enthalpy changes of series nSB-NDEA.....	87
Table 4.15:	Molecular structure of mesomorphic properties of 12SB-CH <sub>3</sub> , 12SB-OCH <sub>3</sub> , compound A, B and C.....	88
Table 4.16:	Percentage yields for nSHB-OCH <sub>3</sub> .....	90
Table 4.17:	Micro-elemental analytical data of nSHB-OCH <sub>3</sub> .....	91
Table 4.18:	FTIR spectral data of nSHB-OCH <sub>3</sub> .....	93
Table 4.19:	$^1\text{H}$ NMR spectral data of compound 10SHB-OCH <sub>3</sub> in CDCl <sub>3</sub> .....	96
Table 4.20:	$^{13}\text{C}$ NMR spectral data of compound 10SHB-OCH <sub>3</sub> in CDCl <sub>3</sub> .....	99
Table 4.21:	Phase transition temperatures and associated enthalpy changes of series nSHB-OCH <sub>3</sub> .....	102
Table 4.22:	Percentage yields OBSB-R.....	107
Table 4.23:	Micro-elemental analytical data of OBSB-R.....	108
Table 4.24:	FTIR spectrum data of OBSB-Br .....	109
Table 4.25:	$^1\text{H}$ NMR spectral data of compound OBSB-OCH <sub>3</sub> in CDCl <sub>3</sub> .....	112
Table 4.26:	$^{13}\text{C}$ NMR spectral data of compound OBSB-OCH <sub>3</sub> in CDCl <sub>3</sub> .....	115
Table 4.27:	Phase transition temperatures and associated enthalpy changes of series OBSB-R.....	118
Table 4.28:	Percentage yields of nAPTP .....	121
Table 4.29:	Micro-elemental analytical data of nAPTP .....	122
Table 4.30:	FTIR spectral analysis data of nAPTP .....	123
Table 4.31:	$^1\text{H}$ NMR spectral data of compound 10APTP in CDCl <sub>3</sub> .....	126

Table 4.32:	$^{13}\text{C}$ NMR spectra data of compound 10AFTP in $\text{CDCl}_3$ .....	129
Table 4.33:	Phase transition temperatures and associated enthalpy changes of series nAFTP .....	132

University of Malaya

## LIST OF SYMBOLS AND ABBREVIATIONS

<b><math>^{13}\text{C}</math> NMR</b>	: Carbon-13 Nuclear Magnetic Resonance
<b>Cr</b>	: Crystal
<b>d</b>	: Doublet
<b>DCC</b>	: N,N-Dicyclohexylcarbodiimide
<b>DCM</b>	: Dichloromethane
<b>dd</b>	: Double of Doublet
<b>DMAP</b>	: 4-Dimethylaminopyridine
<b>DMF</b>	: Dimethylformamide
<b>DSC</b>	: Differential Scanning Calorimetry
<b>FTIR</b>	: Fourier Transform Infrared Spectrometry
<b><math>^1\text{H}</math> NMR</b>	: Proton Nuclear Magnetic Resonance
<b>I</b>	: Isotropic Liquid
<b>LC</b>	: Liquid Crystal
<b>LCD</b>	: Liquid Crystal Display
<b>m</b>	: Multiplet
<b>MBBA</b>	: N-(4-Methoxybenzylidene)4-butaniline
<b>N</b>	: Nematic
<b>n.m</b>	: 4-n-Alkylbenzylidene-4'-alkylaniline
<b>n.Om</b>	: 4-n-Alkylbenzylidene-4'-alkoxyaniline
<b>nAPTP</b>	: 4-n-Alkanoyloxyphenylimino-4-methylphenyl thiophene-2-carboxylate
<b>nCB</b>	: 4-n-Alkylcyanobiphenyl
<b>nO.m</b>	: 4-n-Alkoxybenzylidene-4'-alkylaniline
<b>nO.Om</b>	: 4-n-Alkoxybenzylidene-4'-alkoxyaniline

<b>nSHB-OCH<sub>3</sub></b>	:	4-n-Alkanoyloxy-2-hydroxybenzylidene-4'-methoxyaniline
<b>nSB-CH<sub>3</sub></b>	:	4-n-Alkanoyloxybenzylidene-4'-methylaniline
<b>nSB-NDEA</b>	:	4-n-Alkanoyloxybenzylidene-4'-(N,N-diethylamino)aniline
<b>nSB-OCH<sub>3</sub></b>	:	4-n-Alkanoyloxybenzylidene-4'-methoxyaniline
<b>OBSB-R</b>	:	4-n-11-Bromoundecanoyloxybenzylidene-4'-substituted aniline
<b>POM</b>	:	Polarized Optical Microscopy
<b>ppm</b>	:	Part Per Million
<b>q</b>	:	Quintet
<b>qt</b>	:	Quartet
<b>s</b>	:	Singlet
<b>SmA</b>	:	Smectic A
<b>SmB</b>	:	Smectic B
<b>SmC</b>	:	Smectic C
<b>SmF</b>	:	Smectic F
<b>SmG</b>	:	Smectic G
<b>SmI</b>	:	Smectic I
<b>t</b>	:	Triplet
<b>TLC</b>	:	Thin Layer Chromatography
<b>TMS</b>	:	Tetramethylsilane
<b>&amp;</b>	:	And

## LIST OF APPENDICES

Appendix A: Retardation factor of series 1 – 4 compounds .....	148
Appendix B: FTIR spectra of series 1 – 4 compounds .....	149
Appendix C: $^1\text{H}$ & $^{13}\text{C}$ NMR spectra of series 1 – 4 compounds .....	167
Appendix D: DSC thermogram of Series 1 – 4 compounds .....	214

University of Malaya

## CHAPTER 1: INTRODUCTION

### 1.1 General Aspect of Liquid Crystals

Matter is generally thought to exist in one of the three basic states: solid, liquid and gas. But, not all compounds directly transform from solid into liquid state when temperature increase (Singh & Dunmur, 2002). In 1888, an unusual behavior was observed for cholesteryl benzoate (Figure 1.1) by Austrian botanist, Friedrich Reinitzer. As temperature increased, the crystal was first melted at 145.5 °C into an opaque solution before turned into transparent liquid at 178.5 °C and some iridescent color had been encountered upon cooling (Collings & Hird, 1997). This gave a significant attribution to the liquid crystal research.

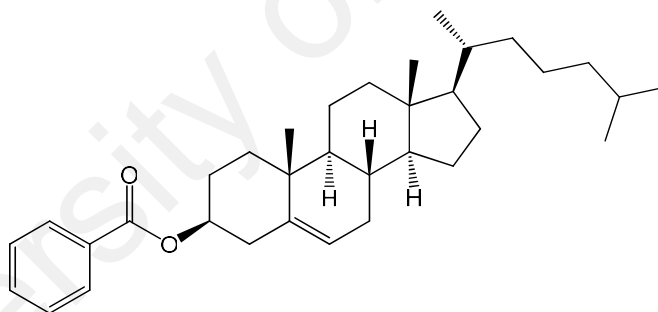


**Figure 1.1: Molecular structure of cholesteryl benzoate**

Later, German physicist, Otto Lehmann conducted experiments and concluded that there was a new state of matter which exhibited characteristics of crystal and liquid after the first approach of Reinitzer. This change of state is termed as “*Liquid Crystal*”. A systematic classification scheme had been proposed by George Friedal in 1922 and eventually it was used until nowadays.

Liquid crystal, LC is a class of fascinating material which has optical properties that lead to many applications. The usage of liquid crystal in display unit was among the earliest application. A stable liquid crystal compound, 4-cyano-4'-pentylbiphenyl (Figure 1.2), with low melting point was used as the new material which could produce result in the rapid adoption of small area liquid crystal displays, LCDs within electronic products (Gray *et al.*, 1973).

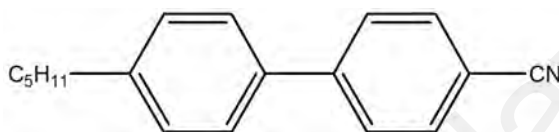


**Figure 1.2: Molecular structure of 4-cyano-4'-pentylbiphenyl**

Technologically, LCs have become part of our daily life, first showing up in small devices such as wristwatches and pocket calculators. and eventually being used as displays in all sorts of instrumentations such as portable computers and televisions. The low power consumption and smaller in size, give good advantages for LCs to be competing with other technologies.

Generally, LC material can be classified based on the interaction between the molecules and its surrounding environment either thermotropic or lyotropic liquid crystals, see Figure 1.3. This dissertation focuses only thermotropic LCs as they may have potential applications in electro-optic displays, temperature and pressure sensors.



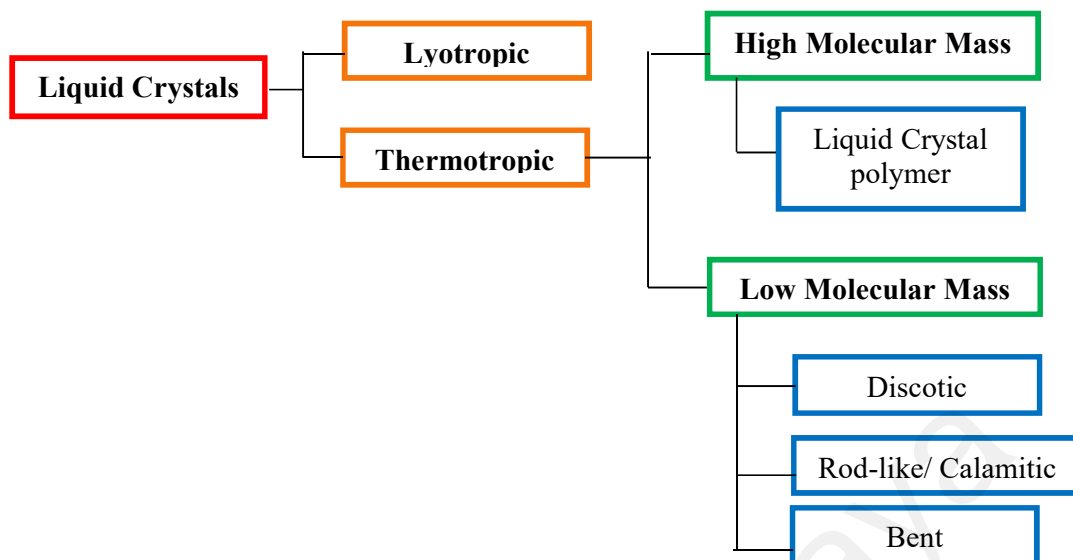


**Figure 1.3: General classification of liquid crystals**

Thermotropic LCs are temperature dependent and easily affect by the changes on surrounding energy to induce the optical properties. They can be either high or low molecular masses. The essential features are consisting of a rigid core center and a flexible chain. Basically, low molecular mass liquid crystals are classified into three main structural groups based on their shape of the mesogenic molecules as show in Figure 1.3, and their structures were illustrated in Figure 1.4.

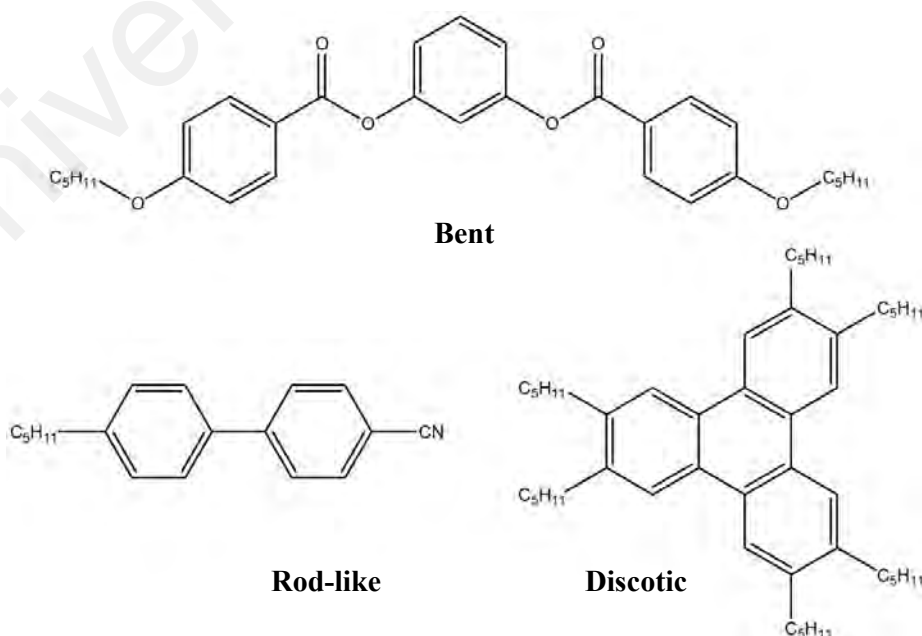


**Figure 1.4: Structure of thermotropic liquid crystal**

There were many mesophases which had been discovered, the most common mesophases showed by rod-like molecules were nematic and smectic. These phases were different in the way of the molecules aligned in the liquid crystalline mesophase (Kumar, 2001). Normally, the nematic phase is exhibited at the higher temperature compared to the smectic phase, it is due to the molecules in the nematic phase are arranged similar to the liquid phase, whilst the molecules in the smectic phase are arranged similar to the crystal phase. (Collings & Hird, 1997).

Nematic phase is the simplest liquid crystal phase exhibited by rod-like or calamitic LCs. The molecules in nematic phase are diffused randomly with some orientational order (have preferred direction), as shown in Figure 1.5, whereas the smectic phase possesses additional positional order which the molecules tend to arrange in layer-like or lamellar packing.

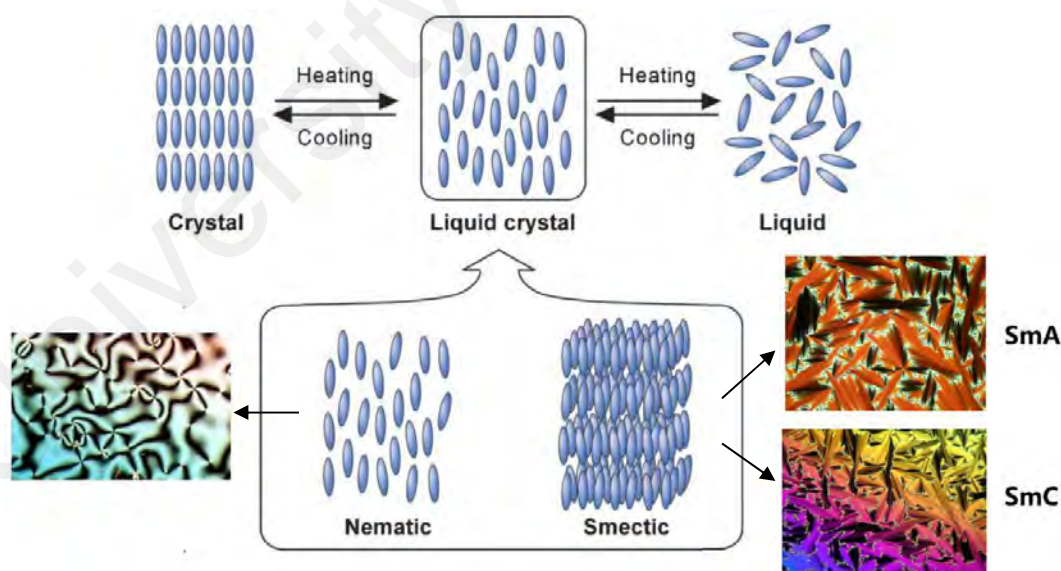
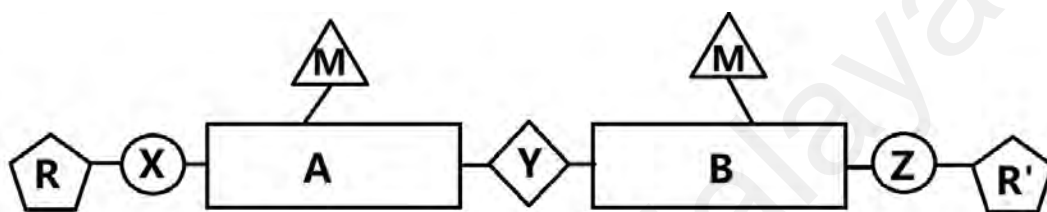


**Figure 1.5: Molecular structure and mesophase of liquid crystal (Kato *et al.*, 2007)**

## 1.2 Structure of Calamitic Liquid Crystals

An enormous number of liquid crystals had been prepared, although many were similar, but each had its own specific structural moieties which conferred certain phase morphology. Hence, a general template had been proposed (Collings & Hird, 1997), see Figure 1.6.



Given that,

X, Y, Z	= Linking group	M	= Lateral substituent
A, B	= Core central	R, R'	= Terminal substituent

**Figure 1.6: General structural templates for calamitic mesogens**

The rod-like structures consist of a rigid rod unit formed by two or more core units (A and B) which connected with or without linking group (Y). The terminal substituents (R and R') can be linked to the core through X and Z but usually directly linked to the core. Lateral substituents (M and N) are often used to modify the mesophase morphology and the physical properties exhibited by the compounds.

### 1.2.1 Terminal Substituents (R and R')

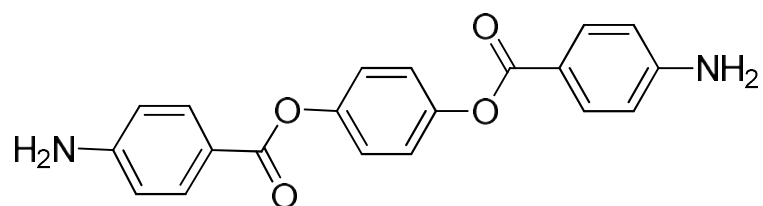
To a rigid core, it is rarely produced mesophase due to the shape of the molecules are rigid. Terminal groups other than hydrogen atom always employed in liquid crystal system to balance the rigidity with some flexible groups such as alkoxy or alkyl chains. It helped to moderately lowering the melting point and allowed liquid

crystal phase to be exhibited (Collings & Hird, 1997). Although, this flexible chain was lowered the melting or clearing temperature of the liquid crystal, but it still increased the melting or clearing temperature as the carbon chain was excessive long. This may be due to the excessive van der Waals forces (Singh & Dunmur, 2002).

Terminal groups are commonly used in synthesize LC compounds. A small polar substituent (CN, F and NO<sub>2</sub>) or a long, straight or branch hydrocarbon (usually alkyl and alkoxy) able to create dipoles along or across the molecular axis which able to enhance the preference for a specific mesophase (for example, short alkyl chain favors nematic phase). These are important in designing the desire compounds (Singh & Dunmur, 2002).

#### **1.2.1.1 Polar Groups**

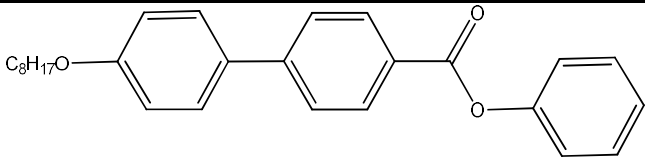
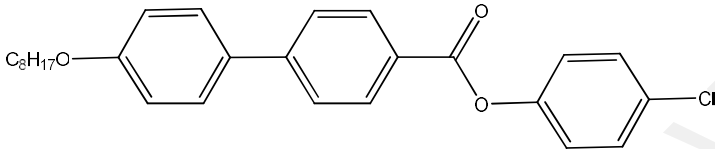
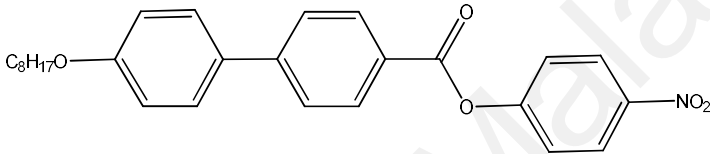
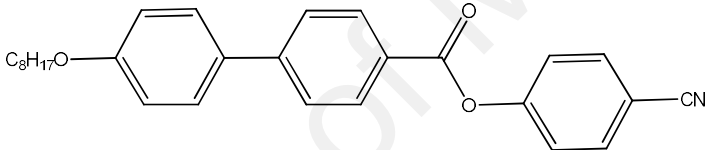
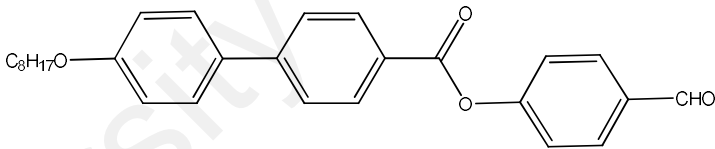
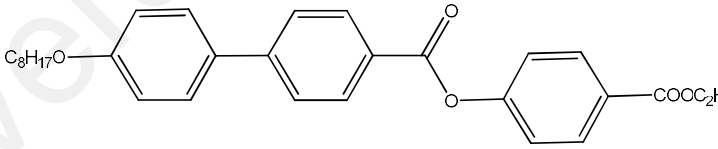
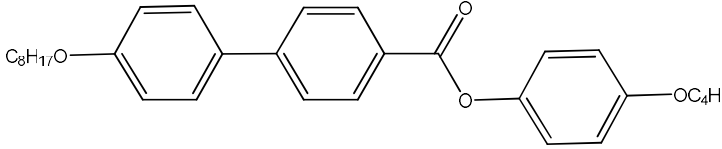
Although a terminal polar group can permanently increase the dipole moment among molecules, but it is not necessary for the mesogens to be mesomorphic. For the group, such as **OH** and **NH<sub>2</sub>** tend to form polymeric hydrogen bondings that will increase the melting point of the structure and depress the formation of liquid crystal phase. But, it had been rejected by Schroder and Schroder in 1974 which were the first examples of a liquid crystalline with primary amine and phenol groups that were incapable of intra-molecular hydrogen bonding, they suggested that three ring systems with both terminal ends of either OH or NH<sub>2</sub> groups exhibited mesomorphic properties (Figure 1.7).



**Figure 1.7:** Structure of *p*-phenylenedi-*p*-aminobenzoate

Normally, polar terminal groups able to conjugate with the aromatic core units and form nematic phases, whereas non-polar unconjugated group lean toward SmA and SmB phases. In Table 1.1, compound **1** - **7** differed in one of their end with different terminal group. The substituents were varied from being polar to apolar and its length was altered from hydro-, chloro- to butyloxy group. Tilted mesophase only occurred when the substituents exceed a certain length or size (equivalent to butyloxy). Nematic phases were exhibited for the cyano and carbaldehyde derivatives.

**Table 1.1: Structure and phase transition of biphenyl analogous compounds with different terminal groups (Demus *et al.*, 1998)**

Compound	Structure	Mesophase present
1		SmA SmB
2		SmA SmB
3		SmA
4		N, SmA SmB
5		N
6		SmA SmB
7		SmA SmC SmB

### 1.2.1.2 Straight Alkyl/ Alkoxy Chains

Straight alkyl or alkoxy chains were commonly reported by scientist of its homologous series. The length of the carbon chain was greatly affected the mesomorphic properties of liquid crystalline compounds. As the length of the methylene group increased, the lateral attraction force was also increased. But, the terminal attraction force becomes relatively weak or remains unchanged (Collings & Hird, 1997). It was due to the increased in length eventually blocked the interaction of the rigid core to each other and this was illustrated in Figure 1.8. Thus, the nematic property decreased, but the tendency of a compound to exhibit smectic phase increased for a homologous series as increased in number of carbons in the chain.

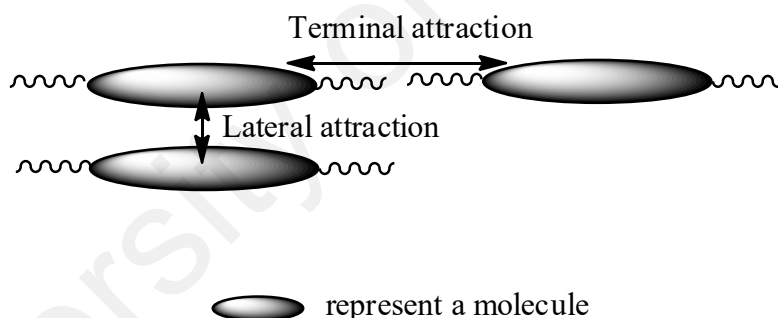


**Figure 1.8: Illustration of the terminal and lateral attraction between molecules**

For example, Prajapati and Bonde (2006) synthesized 2-(4'-*n*-alkoxyphenylazo)-6-methoxybenzothiazoles (Figure 1.16) which showed the nematic phase at lower alkoxy chain length ( $n = 4$  to  $10$ ) and higher member ( $n = 12$  to  $16$ ) showed both nematic and smectic phases.

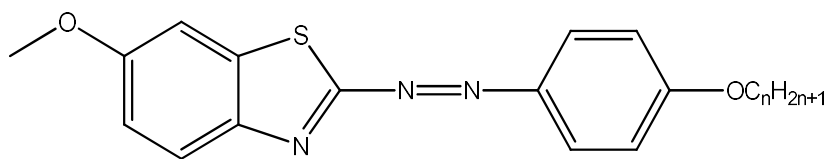


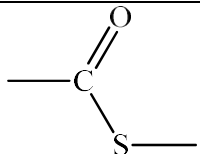
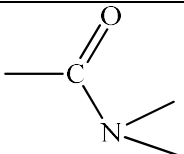
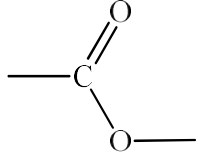
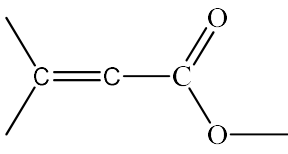
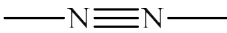
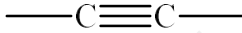
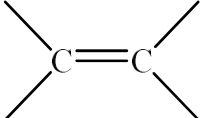
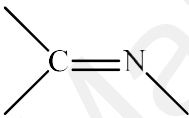
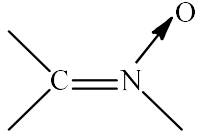
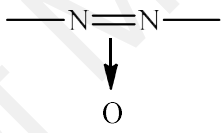
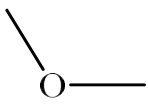
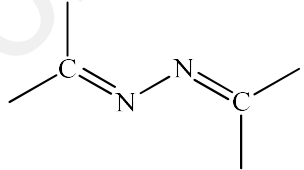
**Figure 1.9: Structure of 2-(4'-*n*-alkoxyphenylazo)-6-methoxybenzothiazoles**

### 1.2.2 Linking Groups

The linking groups are normally used to connect a few core units together. Several types of linking group are tabulated in Table 1.2. Linking group normally is needed to maintain the linearity of rigid core unit and ensured the mesophase has been generated successfully (Collings, 2002). For olefin compounds, it existed as a pair of geometrical isomer (*cis-trans* isomerism). However, only *trans*-isomer showed liquid crystalline properties due to *cis*-isomer had both bulky groups on the same side of the plane which tends to reduce the linearity of the structure. Generally, rigidity gave the best mesogens, but more flexible groups such as  $-\text{OCH}_2-$  and  $-\text{CH}_2\text{CH}_2-$  did show some mesomorphic properties.

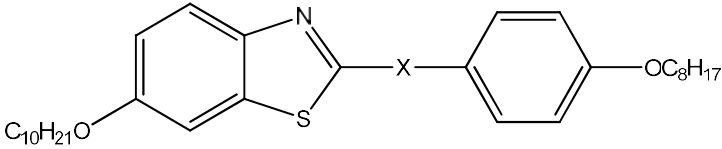


**Table 1.2: Linking groups and their common names**

Linking group	Common name	Linking group	Common name
	Thioester		Amide
	Ester		Cinnamate
	Azo		Alkyne/ Acetylene
	Olefin		Anils/ Schiff bases
	Nitro		Azoxy
	Ether		Azine

For examples, the influences of polar linking groups on the mesomorphic properties are best illustrated by the compound **8**, **9** and **10** with a benzothiazole unit reported by Belmar (1999). The structure and their phase transition temperature are tabulated in Table 1.3.

**Table 1.3: Phase transition temperature of 6-decyloxy-2-(4-octyloxyphenyl-azo)-benzothiazoles (8), N-[2-(6-decyloxybenzothiazolyl)]-4-octyloxybenzamides (9) and 6-decyloxy-2-(4-octyloxybenzylidene-aminobenzothiazoles (10)**

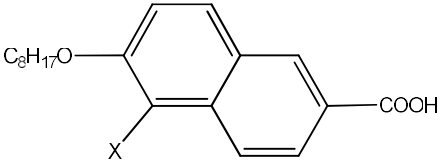
			
Compound	X	Transition	Temperature/ °C
<b>8</b>	-N=N-	Cr-SmC	70.7
		SmC-N	95.0
		N-I	123.8
<b>9</b>	-CONH-	Cr <sub>1</sub> -Cr <sub>2</sub>	88.0
		Cr <sub>2</sub> -SmC	100.5
		SmC-I	132.8
<b>10</b>	-C=N-	Cr-SmC	82.6
		SmC-N	112.1
		N-I	123.0

Compounds **8** and **10** showed very similar mesomorphic behavior wherein these compounds and their homologous series exhibited both nematic and smectic phases. However, only smectic phase was observed for the compound **9** and its homologous series. These observations could explain by taking into the account of the formation of intermolecular hydrogen bonding by amide group (CONH). The hydrogen bonding occurred at the side of the mesogens and able to attract the mesogens side by side. Hence, the molecules able to arrange in a parallel order and this had encouraged the formation of smectic mesomorphism.

### 1.2.3 Lateral Substituent

A wide range of lateral substituents were reported by incorporating atom such as F, Cl, CN, NO<sub>2</sub>, CH<sub>3</sub>, and CF<sub>3</sub> (Demus *et al.*, 1998). A lateral substituent is an atom/ a group of atoms that attached off the linear axis of the molecule, it is usually located at the side of center core. This atom/ group of atoms tend(s) to disrupt the molecular packing and therefore reduced the liquid crystal phase stability. But, it is also an advantage for certain compounds that require different criteria in their mesomorphic and physical properties based on the purpose of application. Lateral substitution is important in both nematic and smectic systems. For example, the lateral effect on the LC properties can be illustrated by the example in Table 1.4. Large lateral substituents caused an increase of the clearing point because it enhanced the intermolecular attraction. The smectic tendency was higher in compounds **12** and **13** compared to **11**. This high smectic tendency was due to the compounds favored in lamellar packing which promoted by the polar lateral substituent with the space filling effect.

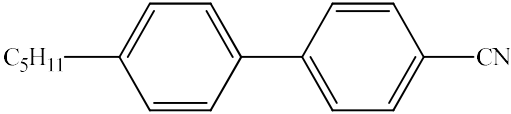
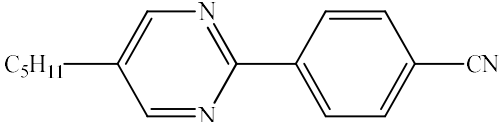
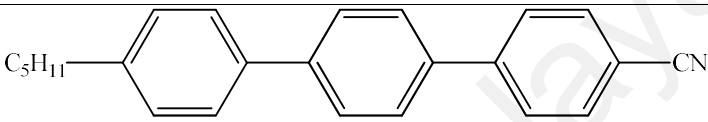
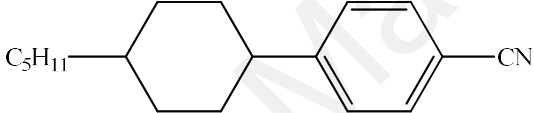
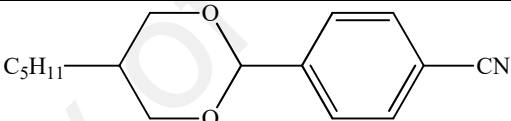
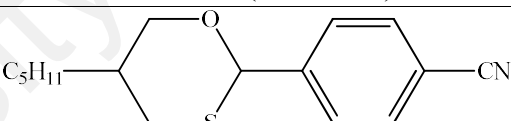
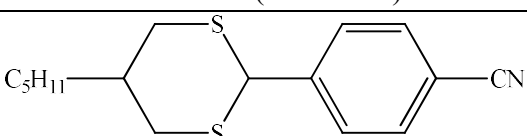
**Table 1.4: Example effect of lateral substituent of naphthanoic acid derivatives (Demus *et al.*, 1998)**

			
Compound	X	Transition	Temperature/ °C
11	H	Cr–N	161.5
		N–I	190.0
12	Cl	Cr–SmC	169.0
		SmC–N	183.0
		N–I	199.0
13	Br	Cr–SmC	164.0
		SmC–N	174.5
		N–I	196.0

#### 1.2.4 Center Core

Upon changing the core structure of the liquid crystal compounds, the transition temperature and phase stability were varied. Given in Table 1.5, an addition of extra aromatic ring (**16**) into cyanobiphenyl compound (**14**) had extended the linearity of the core structure. This had been given a much higher length to breadth ratio and increased the polarizability anisotropy. It resulted in a very large increment in the nematic phase stability and melting point (Collings & Hird, 1997).

**Table 1.5: Effect of aromatic core and alicyclic core changes on transition temperatures**

Compound	Structure & transition temperatures
14	 <p>Cr 24.0 °C N 35.0 °C I</p>
15	 <p>Cr 71.0 °C (N 52.0 °C) I</p>
16	 <p>Cr 130.0 °C N 239.0 °C I</p>
17	 <p>Cr 31.0 °C N 55.0 °C I</p>
18	 <p>Cr 56.0 °C (N 52.0 °C) I</p>
19	 <p>Cr 74.0 °C (N 19.0 °C) I</p>
20	 <p>Cr 98.0 °C I (supercool to 28.0 °C)</p>

A heteroatom can cause a large change in the kind of mesophase present or the physical properties of the mesophases (Prajapati & Bonde, 2006). Substitution of a heterocyclic pyrimidine ring (**15**) into the cyano biphenyl structure caused a moderate increase in the nematic phase stability (19.0 °C). This was due to the pyrimidine ring added had been reduced or removed the steric hindrance effect in the inter-ring. This enabled the two aromatic rings able to adopt a planar arrangement without inter-annular twisting of the parent system and enhanced the longitudinal polarizability which resulted increased in nematic phase stability. However, a nitrogen atom increased the polarity and generated higher melting point (Collings & Hird, 1997).

Different heteroatom will cause different changes to the physical properties of the liquid crystal compounds. This can be shown by the differences in the nematic phase stability of the compound **18** and **19**. The use of two oxygen atoms (dioxane) gave a small nematic stability (4.0 °C) compare to the parent cyclohexane (**17**) (24 °C). By substituted one of the oxygen atom to sulfur atom, the nematic stability enhanced by a larger difference (45.0 °C) compared to the dioxane compound. The size of the oxygen was not sufficiently large enough to disrupt the molecular packing that required to generate the nematic phase but sulfur atom did. Hence, introduction of a sulfur atom had enhanced the nematic stability (Collings & Hird, 1997).

When two oxygen atoms in the dioxane compound were substituted to sulfur atoms (**20**), the compound did not show any liquid crystalline properties. This was due to the size of the sulfur atom was large enough to disrupt the molecular packing until the molecules unable to arrange in the orientation of the liquid crystal phase. (Collings & Hird, 1997).

### 1.3 Research Objective

This project aims to prepare few homologous series of Schiff base esters with liquid crystal properties. The homologous series are varied either their terminal substituent groups such as methoxy, methyl and diethylamino or lateral substituent, hydroxy to study on the effect of liquid crystal properties due to the minor changes on the Schiff base ester structures. Besides that, a thiophene ring is incorporated into the Schiff base ester to study the effect of heterocyclic compound toward the liquid crystal properties.

### 1.4 Scope of Study

The scope of this work covers the synthesis and characterization aspects of new mesogens for thermotropic liquid crystals through modification on several aspects of liquid crystal science as summarized as below:

1. To synthesis four series of Schiff base liquid crystal with the modification terminal groups (methyl, methoxy and diethylamino), lateral hydroxy group and heterocyclic ring to center core group.
2. To elucidate the structures of the prepared compounds through Fourier transform infrared (FTIR), proton nuclear magnetic resonance ( $^1\text{H}$  NMR), carbon-13 nuclear magnetic resonance ( $^{13}\text{C}$  NMR) and CHN elemental analysis.
3. To study the liquid crystal properties of prepared compound using differential scanning calorimetry (DSC) and polarized optical microscopy (POM).

## **1.5 Significance of Study**

Schiff base liquid crystals have been extensively investigated for different terminal groups which showed nematic and smectic phases. There are still more researchable potentials as slight changes in structures may greatly influence the mesomorphic properties such as phase range and stability. This may use to determine the potential applications of newly synthesized materials. For examples, fast switching devices, liquid crystal thermometer or temperature sensor devices. In light of the previous discovery, it is interesting to study the co-relationship between an alkanoyloxy group with various types of terminal groups such as methyl, methoxy and dialkylamino.

## **1.6 Thesis Outline**

The dissertation is organized into five chapters. Chapter 1 gives an introduction to the background of liquid crystals, research objectives and scope of the dissertation. An in-depth description of Schiff base compounds and their liquid crystal properties are presented in Chapter 2. Chapter 3 is described the preparation of desirable molecules from the start of synthesis of the molecules till the characterization methods. Subsequently, in Chapter 4, detail discussion of the results of each homologous series obtained by their characterization techniques ( $^1\text{H}$  NMR,  $^{13}\text{C}$  NMR and FTIR) with the help of the elemental analysis on the percentage compositions. Their liquid crystalline properties of the homologous series are studied by POM and DSC to confirm the structural and mesomorphic properties relationship on the investigated molecules. Finally, Chapter 5 concludes the research output and recommends the potential research works on the application. The appendices are provided in the last part of the dissertation as the supplementary data related to the experimental work.



## CHAPTER 2: LITERATURE REVIEW

### 2.1 Rod-like Liquid Crystals

Research activities on rod-like liquid crystals increases dramatically after the discovery of **MBBA** in 1969 (Yuksel *et al.*, 2007). A vast number of calamitic liquid crystals were reported either without (Gray, 1998; Gray *et al.*, 1973) or with linkage units such as azo, -N=N- (Du *et al.*, 2018; Korbecka *et al.*, 2017; Ahmed *et al.*, 2016; Prajapati & Varia, 2008; Jadav *et al.*, 2003; Prajapati & Pandya, 2003, Prajapati, 2001; Prajapati, 2000; Vora & Prajapati, 1998), azomethine or Schiff base, -CH=N- (Mohammad *et al.*, 2018; Ong *et al.*, 2018; Ha & Lee, 2014; Ha *et al.*, 2010; Ha *et al.*, 2009; Yeap *et al.*, 2006; Yeap *et al.*, 2006; Sakagami *et al.*, 2002; Yeap *et al.*, 2002; Vora *et al.*, 2001; Galewski & Coles, 1999; Gandolfo *et al.*, 1988; Sakagami & Nakamizo, 1980), ester, -COO- (Jia *et al.*, 2016; Krishnan *et al.*, 2006; Prajapati, 2001; Haramoto & Kamogawa, 1989; Sakurai *et al.*, 1989), chalcone, -C=C-CO- (Kotadiya & Bhoya, 2015; Thaker & Kanojiya, 2011; Thaker *et al.*, 2009), cinnamate, -C=C-COO- (Rosa *et al.*, 2016; Thaker *et al.*, 2013; Prajapati *et al.*, 2003, Haramoto *et al.*, 1993,) and olefin (Buchs *et al.*, 2018; McAllister *et al.*, 2013; Wong *et al.*, 2012). Schiff base had been given more attention due to it has good stability and anisotropy properties (Ha *et al.*, 2010). In this work, Schiff base liquid crystals with two aromatic rings are focused as it contains a group which provide a step-wise structure to the central core of the liquid crystal system and enable the compound to exhibit optical and electrochemical properties. The effects of terminal and lateral substitution on mesomorphic properties of the Schiff base liquid crystal are studied. Besides, an extra heterocyclic ring (thiophene) will be added to mesogenic core group to investigate the possibility of thermal and optical properties of the thiophene liquid crystal.

### 2.1.1 Schiff Base Liquid Crystals

Most of the rod-like liquid crystals that had previously published have either one or two central linkage units within the rigid core composed by either two or more phenyl rings with terminal flexible chains. Schiff base is also known as imine, a linkage unit which is used in connecting the aromatic rings together in a rigid core group. It provides a step-wise structure with good molecular linearity and exhibits higher stability. It helped in the formation of mesophases (Ha *et al.*, 2010; Jber *et al.*, 2014).

In the early stage of liquid crystal research, the lengths of alkyl and alkoxy chains, as well as their derivatives were being studied in detail. A review had been done and discussed across all the four classes of the compounds (Shankar & Pisipati, 2011). The reported structures are shown in Figure 2.1.

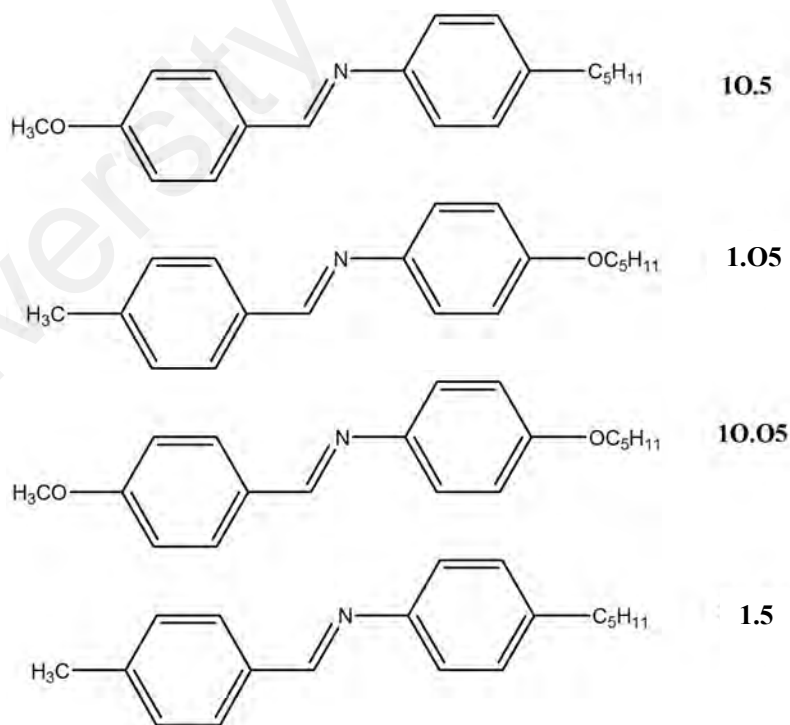


**Figure 2.1: Structures of Schiff Base Liquid Crystals (Shankar & Pisipati, 2011)**

**nO.m** series showed tremendous properties and these series of compounds tend to show polymorphism (present of more than one type of mesophase). The mesophases observed for **nO.m** series included N, SmA, SmC, SmB, SmF and SmG. This group of compounds showed about 21 types of phase transition sequences either mono-, di-, tri-, tetra-, penta or hexa-variant (Shanker & Pisipati, 2011). The richest polymorphism compound with the present of 6 variants of mesophases was **5O.6**. Although the variation of alkyl chain group tends to influence the mesomorphic properties, but the major effect was brought by the alkoxy chain group. When the chain of alkoxy group was short ( $n = 1, 2$  and  $3$ ), most of the compounds showed either non-mesogenic or nematic phase only. It was rare for smectic phase to present. When the alkoxy group was long ( $n = 15, 16$  and  $18$ ), only smectic phases (either A, B, F or G) were observed. This suggested that the alkoxy chain had more prominent effect toward the mesomorphic properties. The role of heteroatom, oxygen presents in the molecular structure was found to reduce the strength of lateral dipole and caused a depression in phase transition temperature, this can be shown by the differences in the results of the four series of compounds (Ajeetha *et al.* 2005; Ajeetha & Pisipati, 2003).

By changing the position of oxygen atom on either side of the rigid core (either benzylidene or aniline group), it tends to affect the present of mesophase. When the oxygen atom was located on benzaldehyde side, the compound exhibited rich polymorphism. Whereas, if the oxygen atom located on aniline side, the intermediate smectic phases were disappeared. However, there was no considerable changed in the clearing temperatures. When comparing **nO.m** and **n.Om**, the reverse of the orientation on central linkage showed a peculiar behavior by altogether quenching the nematic phase (Ajeetha *et al.* 2005).

**Table 2.1: Phase variant of some liquid crystal compounds in nO.m, n.Om, nO.Om and n.m homologues series (Shanker & Pisipati, 2011)**

Phase	I	°C	N	°C	A	°C	C	°C	B	°C	F	°C	G	°C	Cr
10.5	●	62.6	●	39.7	○	-	○	-	○	-	○	-	○	-	●
1.O5	●	Non mesogenic													●
10.O5	●	92.1	●	83.5	○	-	○	-	○	-	○	-	○	-	●
1.5	●	Liquid crystal below room temperature													●
20.5	●	90.4	●	63.3	○	-	○	-	○	-	○	-	○	-	●
2.O5	●	Non mesogenic													●
20.O5	●	119.3	●	88.5	○	-	○	-	○	-	○	-	○	-	●
2.5	●	Liquid crystal below room temperature													●
50.5	●	77.8	●	54.5	●	53.1	●	49.9	○	-	●	47.0	●	28.0	●
5.O5	●	76.8	●	51.6	○	-	○	-	○	-	○	-	●	40.7	●
50.O5	●	108.9	●	108.8	○	-	○	-	○	-	○	-	○	-	●
5.5	●	40.8	●	23.9	○	-	○	-	○	-	○	-	●	-	●
10.16	●	Non mesogenic													●
10.O16	●														●
1.16	●														●
20.16	●	70.1	●	52.2	●	-	○	-	○	-	○	-	○	-	●
20.O16	●	Non mesogenic													●
2.O16	●														●
2.16	●														●
40.16	●	69.2	●	68.5	●	-	○	51.3	●	<sup>a</sup>	○	-	○	-	●
40.O16	●	Non mesogenic													●
4.16	●	38.1	○	-	●	35.0	○	-	○	-	○	-	○	-	●
50.16	●	68.8	●	67.4	●	55.1	○	-	○	-	○	-	○	-	●
5.O16	●	79.2	○	-	●	72.3	○	-	●	51.3	○	-	○	-	●
50.O16	●	87.4	●	87.0	○	-	○	-	○	-	○	-	○	-	●
5.16	●	52.9	○	-	●	40.2	○	-	○	-	○	-	○	-	●
80.16	●	75.5	○	-	●	71.5	○	-	●	<sup>b</sup>	○	-	○	-	●
80.O16	●	: Non mesogenic													●
8.O16	●														●
8.16	●														●

● : phase present

○ : phase absent

**I: Isotropic; N: Nematic; A: SmA; B: SmB; C: SmC; F: SmF; G: SmG; Cr: Crystal**

<sup>a</sup> 40.16: no reported data on B → Cr

<sup>b</sup> 80.16: no reported data on B → Cr

The presence of oxygen atoms in both sides of the rigid core tends to increase the clearing temperature and the compound was almost lost its liquid crystalline nature. For **nO.Om** series, it showed a higher clearing temperature than **nO.m** series. Alkoxy derivatives were considered to have higher polarizability (due to the presence of oxygen atom) than the corresponding alkyl compounds (Ajeetha & Ohja, 2010). It was suggested that the presence of polarizable alkoxy group in both chains by replacing the alkyl group in **nO.m** improved the appearance of nematic phases for large region (Shanker & Pisipati, 2011). On absence of oxygen in the liquid crystal moiety, the clearing temperature decreased and showed the liquid crystal nature at ambient temperature. It was clearly showed by comparing compounds **5O.5** and **5.5**, the difference in the clearing temperature (isotropic phase  $\leftrightarrow$  liquid crystal phase) of **5O.5** and **5.5** is about 30 °C (Table 2.1).

The electronegative atom such as oxygen when incorporates into the side chain (alkoxy chain) of the liquid crystals tends to influence and alters the mesomorphic properties of the liquid crystal compounds. The work reported later was then started to focus on the terminal polar substituents such as halogen groups (**F**, **Cl** and **Br**) and nitro group (**NO<sub>2</sub>**) (Galewski, 1987; Galewski, 1990; Galewski, 1994). Typical terminal substituents that exhibited liquid crystalline properties were those with electronegative atoms such as halogen groups. Some of the examples are shown in Figure 2.2.

Halogen groups were polar substituents which tend to give a strong dipole moment to the molecular structure due to their high electronegative nature. Thus, the halogen substituted liquid crystal compounds could promote mesomorphic properties. The increase in dipole moment not only enhances the strength of the lattice and melting temperature properties, it also helps in the orientation of molecules in a parallel

arrangement. This parallel arrangement enabled the present of smectic mesomorphism to be frequently observed in terminal halogenated liquid crystals as the length of the alkyl or alkoxy chains increased (Ha *et al.*, 2011; Ha *et al.*, 2014).

By comparing halogens or nitro groups derivatives with their respective compounds in alkylated or alkoxyated derivatives, the results of the transition temperatures from DSC and their liquid crystal textures from POM showed that the present of high dipole moment group as terminal substituents tend to increase the dielectric properties of the molecules (Galewski, 1994). Based on the However, the variant of mesophases was also reduced with the present of polar groups. This showed by only N, SmA and SmB were generated by the polar substituent series instead of a total of 6 variants (including SmC, SmF and SmG) present in the respectively series. The polar terminal substituent was less favored towards the rich polymorphism, but the polar terminal substituent helped to increase the lateral interaction between the molecules and allowed the molecules to favor the parallel arrangement and led to the formation of smectic phases and suppressed the nematic phase (Mingos, 1999).

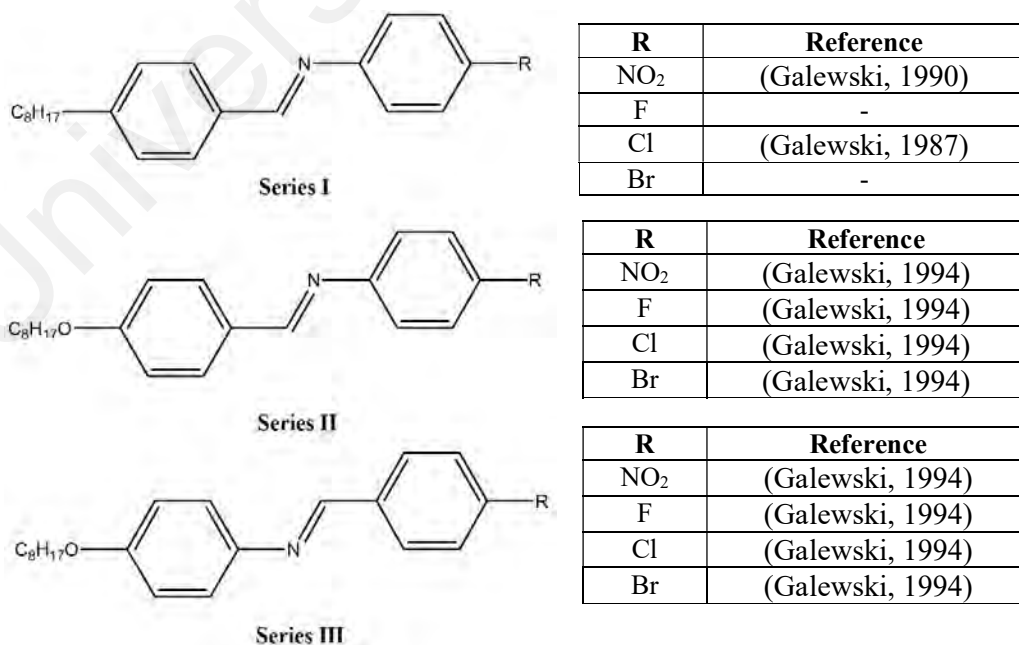


**Figure 2.2: Schiff base liquid crystal with different polar substituent**

Most studies on benzylidene-anilines moieties before 21<sup>th</sup> century were focused on alkoxy or alkyl chain as the terminal flexible chains for Schiff base liquid crystals. The first series of benzylidene-aniline moiety liquid crystal with alkanoyloxy (RCOO-) terminal flexible unit was reported by replacing one of the alkyl or alkoxy chains into alkanoyloxy group. The structure is showed in Figure 2.3. All of the three compounds, **10.5**, **10.05** and **10.OOC5** showed the presence of N phase. Based on the result given by the DSC and POM analysis, it was found that the present of extra alkoxy chain on in **10.05** has increased the clearing point from 62.6 °C (**10.5**) to 92.1 °C and depressed the nematic phase stability from 22.9 °C to 8.6 °. Both structures **10.05** and **10.OOC5** (Figure 2.3) were showing nematic phase under POM, when the alkoxy chain replaced by the alkanoyloxy chain, it was clearly showed that the nematic phase stability was about the same as seen in **10.5** from the DSC result. The present of ester linkage, COO- group in **10.OOC5**, it still maintained the molecules linearity and yet increased the breath of the rod-like shape. Hence, it was said that the ester group tends to increase the breath to length ratio which helps in enhanced the nematic phase stability ( $T_{N-I}$ ) (Collings and Hird, 1997).

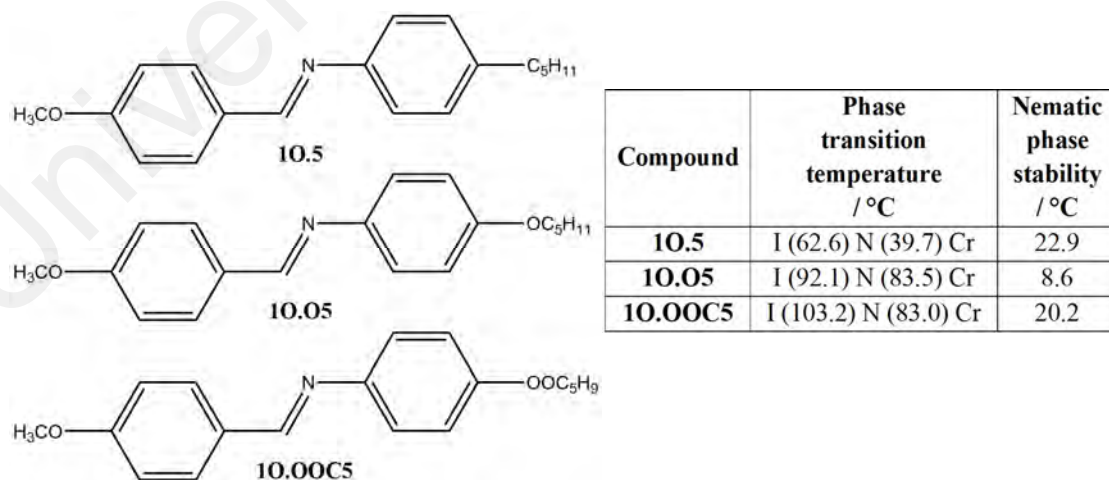


**Figure 2.3:** Molecular structure and their phase transition temperature of **10.5**, **10.05** and **10.OOC5** (Taylor & Francis, 1984)

There is no similar structure reported after **10.OOC5** till year 2002 where Yeap and his co-worker reported a series of octadecanoyloxy chain benzyldeneaniline compounds with polar terminal groups (**CN**, **NO<sub>2</sub>**, **COOH** and **OH**) (Yeap *et al.*, 2002). A detail studied on mesomorphic temperature was carried out explicitly using DSC and POM method. In their finding, they discovered that the compound with nitro group showed non-mesogenic properties whereas others exhibited transition from crystal to liquid crystal phase then isotropic over different temperatures.

Texture observations for the liquid crystal mesophase were examined under POM. They focused on the first and second cooling processes for the captured of textures. Under POM, compound with cyano group showed the presence of broken fan-shaped texture and this was unique for the SmA phase and confirmed by previous reported literature. They also found that schlieren textures have been observed in compounds with hydroxy group and carboxylic acid group. Through further investigation, the schlieren texture in carboxylic acid group derivative was lie to the nematic phase, which was confirmed later by the presence of “two or four *brushes*” in their texture. Both the hydroxy and carboxylic acid group exhibited schlieren smectic C phase (Yeap *et al.*, 2002).

For the DSC analysis, they also found that the clearing temperature of compounds with hydroxy and carboxylic acid were higher than cyano derivative. It was about 20 °C different between the hydroxy derivative and the cyano derivative. Moreover, a greater different in clearing temperature was found about 130 °C for the carboxylic acid derivative. The unusual behavior on the clearing temperature was due to the present of lateral intermolecular H-bonding and gave rise to the formation of linear dimeric molecules in the solid and liquid phases (Yeap *et al.*, 2002).



Later, this work was further investigated on the effect of lateral hydroxy group and polar terminal groups such as halogens (**F**, **Cl** & **Br**), methoxy (**OCH<sub>3</sub>**), methyl (**CH<sub>3</sub>**), and ethyl (**C<sub>2</sub>H<sub>5</sub>**) on the liquid crystal properties (Yeap *et al.*, (2006); Ha *et al.*, (2014). The reported structures are given in Figure 2.4. By comparing reported Schiff base ester bearing terminal bromo substituent (Ha *et al.*, 2014) with their respective alkoxy chain derivative (Galewski, 1994), it was found that both compounds had similar melting and clearing points but different in the phase range. Alkoxy derivative present a large phase stability in SmB phase compared to the SmA phase, whereas alkanoyloxy derivative tends to give higher SmA phase stability than SmB. It was suggested that ester group in terminal flexible chain tend to disrupt the orderly arrangement of the molecules in smectic phase such as hexatic arrangement in SmB phase and led to a least order SmA phase. A further comparison was made with the lateral hydroxy substituted compound (Yeap *et al.*, 2006), the SmB phase was diminished after the introduction of a lateral hydroxy group. It was suggested that the present of lateral bulky group such as hydroxy group eventually blocked the molecules to arrange closely in an orderly manner. The steric hindrance effect also helped in repelled the molecules and forced it to arrange randomly. The present of the lateral hydroxy group had been lowered the melting point of the compound than other respectively compounds (Galewski, 1994) and higher in clearing point. A huge phase stability was observed for lateral hydroxy compound with about 59 °C of phase range of the SmA phase.

Hence, ester group tends to increase the breath to length ratio which helps in enhanced the nematic phase stability. However, it tends to diminish the polymorphism properties and reduced the possibilities for the compound to arrange orderly (Collings and Hird, 1997).

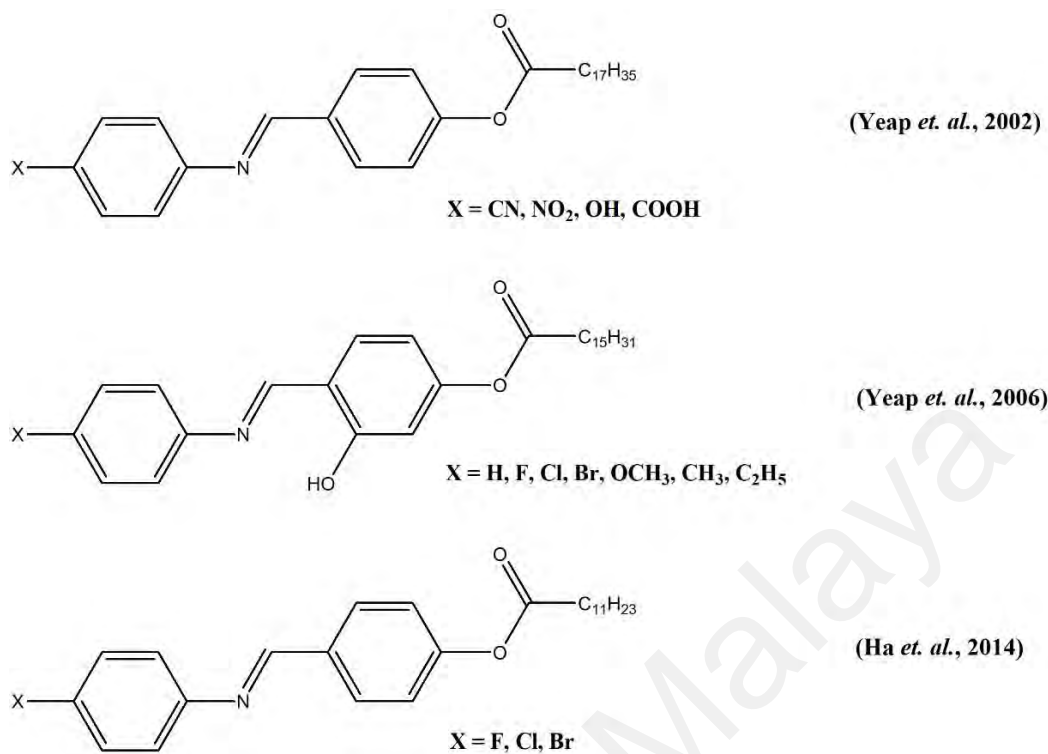


**Figure 2.4:** Molecular structure of Schiff base esters by Yeap and co-worker

Usually, an odd-even effect was able to be illustrated by the liquid crystals. In 2003, Taki and his co-workers (Taki *et al.*, 2003) have studied on the odd-even effect presents in the molecular alignment of *n*-alkyloxy-cyanobiphenyl (Figure 2.5).

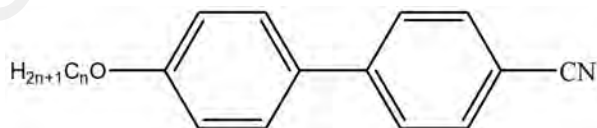


**Figure 2.5:** Structure of nCB

The result revealed that the odd and even members of the homologous will show different kinds of anti-parallel molecular alignment due to the dipole-dipole interaction between the side of the molecules (Taki *et al.*, 2003). Odd membered is to be said difficult to give mesomorphic properties as it showed a bend conformation which experience better packing into a crystalline structure as compared to even members

which structures are more elongated. In this project will be focused in even parity homologous series instead of odd parity.

### 2.1.2 Terminal Substituted Flexible Alkyl Chain Liquid Crystals

Most of the liquid crystalline materials reported previously were focused on the substituent either laterally or terminally. There were still some of the literature reported on the terminally substituted flexible alkyl chain liquid crystal compounds. Functional terminal groups such as hydroxy- (Griffin & Vaidya, 1989), amino- (Chien *et al.*, 1992), carboxylate- (Lunkwitz *et al.* 2001) and thiol- (Kumar & Pal, 2005)  $\omega$ -substituted alkoxy cyanobiphenyls were reported previously. The reported series of  $\omega$ -terminally substituted alkoxy cyanobiphenyls are shown in Figure 2.6.

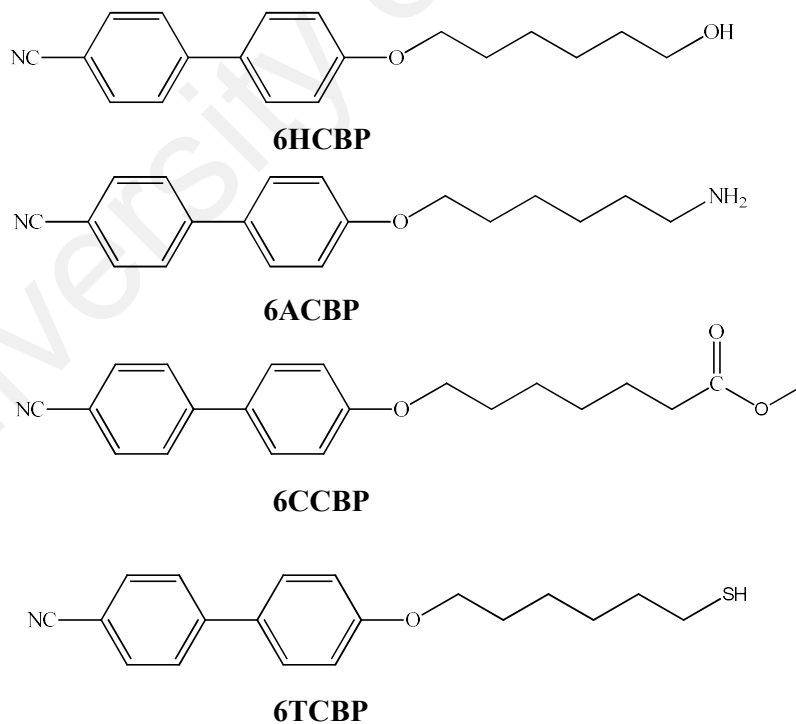


**Figure 2.6: Molecular structure of  $\omega$ -substituted alkoxy cyanobiphenyls**

All the reported mesogens possessed only nematic properties either enantiotropically or monotropically where the homologues family of 4-alkoxycyanobiphenyls exhibited smectic phase at higher homologues members. It was suggested that the absence of smectic phase in longer alkoxy chain for thiol-, amine-, hydroxy- and carboxylate-substituted mesogens was due to the anti-parallel ordering in the  $\omega$ -substituted alkoxy cyanobiphenyls which could increase the effective molecular length, thus enhanced the nematic order and weakening the smectic behavior (Chien *et al.*, 1992).

Another few homologues series of  $\omega$ -substituted alkoxy chain mesogens were reported based on the 2-alkoxy-5-phenylpyrimidines family (Starkulla *et al.*, 2009). The reported structure is shown in Figure 2.7.

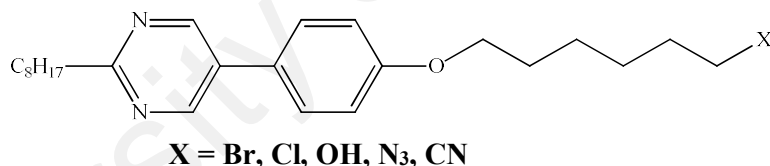


**Figure 2.7: Molecular structure of  $\omega$ -substituted 2-alkoxy-5-phenylpyrimidines**

According to Starkulla *et al.* (2009), the mesomorphic properties of the compounds were relied on the terminal group that attached to the flexible alkoxy chain. Based on the result, the formation of smectic A mesophase was observed for the chloro-, bromo- and azido- derivatives whereas the stronger latent dipole moment group such as hydroxy and cyano derivatives seemed to completely suppress the formation of mesophase. The results are shown in Table 2.2.

**Table 2.2: Transition temperature and mesomorphic properties of 2-octyl-5-[4-( $\omega$ -hexyloxy)]phenylpyridines**

X	Cr <sub>1</sub>	°C	Cr <sub>2</sub>	°C	SmA	°C	I	Cycle
Br	•	64	-	-	-	-	•	Heating
	•	35	-	-	•	58	•	Cooling
Cl	•	55	-	-	•	64	•	Heating
	•	42	-	-	•	59	•	Cooling
OH	•	75	-	-	-	-	•	Heating
	Reported data did not disclosed							Cooling
CN	•	41	-	-	•	58	•	Heating
	•	22	•	25	•	53	•	Cooling
N <sub>3</sub>	•	68	-	-	-	-	•	Heating
	Reported data did not disclosed							Cooling

Cr<sub>1</sub>: Crystal phase 1; Cr<sub>2</sub>: Crystal phase 2

Later on, Yeap *et al.* also researched on the effect of bromoalkyloxy chain on various mesogenic core structure such as isoflavone (Yeap *et al.*, 2011), benzylidene-aniline (Yeap *et al.*, 2012) and benzothiazole (Alshargabi *et al.*, 2013). The representative compounds of the reported structures were given in Figure 2.8.

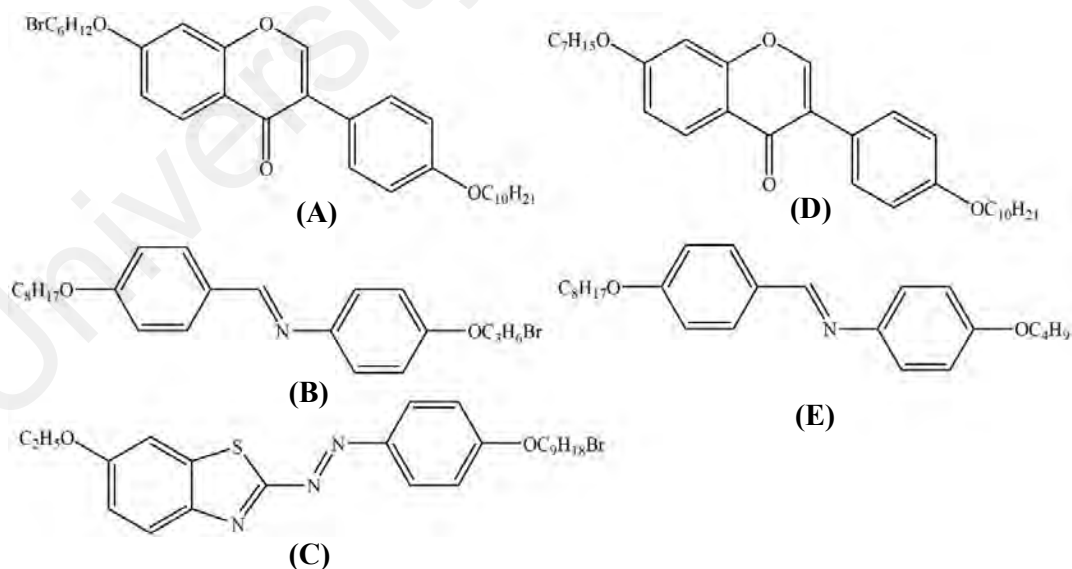


**Figure 2.8: Molecular structure of bromoalkyloxy chain derivatives and their related compounds**

When compared the structure **A** with its corresponded structure **D**, which replaced the methyl group at the end of alkoxy chain into a Br atom, both structures were showed SmA phase with structure **D** presents with extra SmC phase. However, smectic phase range of structure **A** was higher than structure **D** by 37.6 °C (Belmer *et al.*, 1999, Yeap *et al.*, 2011) with similar clearing temperature. This suggested that the replacement of Br atom has enhanced the mesophase range but induced a stronger steric hindrance effect to the molecules. This can be illustrated by a tilted angle mesophase (SmC phase) was diminished by the introduction of Br atom (Yeap *et al.*, 2011).

For structure **B**, it showed only dimorphism properties with SmA and SmC phases (Yeap *et al.*, 2012). Whereby, structure **E** showed trimorphic properties with N, SmC and SmI phase (Godwin *et al.*, 2009). It reveals that the present of the Br atom had greatly affected the types of mesomorphism. It helped in promoting the lamellar packing structure which has diminished the N phase in structure **E**. Meanwhile, the smectic arrangement that occurred become less orderly which showed by the suppress of a more orderly smectic phase such as SmI phase (Yeap *et al.*, 2012). This was due to the steric hindrance effect of the Br atom. A higher smectic phase range was observed for the structure **B** (57.5 °C) compared to the structure **E** (11.6 °C), this showed the Br atom will help in lowering the melting temperature (Godwin *et al.*, 2009, Yeap *et al.*, 2012) and create a bigger phase stability.

Yeap and his co-workers suggested that the presence of Br atom in terminal alkoxy chain gives rise to the lamellar packing which required by the smectic phase. But, due to the Br atom is a large polar atom which rich in electrons, it will create a stronger repulsion force. This will hinder the molecules to arrange in a more orderly arrangement such as SmB, SmE, SmI or SmF (Yeap *et al.*, 2012).

## 2.2 Heterocyclic Liquid Crystals

Recently, heterocyclic liquid crystal has received the greatest attention from the scientist due to its unique properties that able to change the physical properties and mesophases of the liquid crystal compounds (Prajapati & Bonde, 2006). It was found to be an interesting strategy to design a new class of liquid crystalline compounds due to the greater possibility in the variation of direction of magnitude on their permanent dipole moment, mesomorphism and potential electro-optical properties (Belmer *et al.*, 1999). The heterocyclic compounds used for this work was thiophene. Thiophene consists of sulfur atom, S as the heteroatom in a five-membered cyclic ring (Figure 2.9). Thiophene moiety liquid crystal compounds were still rarely reported nowadays and it will be a good potential material for enhance the nematic phase properties.

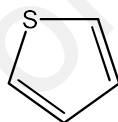


**Figure 2.9:** Structural formula of thiophene

Five-membered heterocycles show some potential applications such as bistable nematic displays due to the flexoelectric properties (Thaker *et al.*, 2012). A vast number of thiophenes were already studied. The insertion of thiophene in the central core of the mesogenic compound is not only help in generating the mesophases, it is also enhanced the transition temperatures considerably. This had been contributed for some interesting properties such as dielectric anisotropy and dielectric biaxiality so that enabled them to be classified as functional materials (Reddy *et al.*, 2014).

### 2.2.1 Thiophene-based Liquid Crystals

A homologous series of thiophene-based liquid crystal compounds, 2-[4-(4'-n-alkoxybenzoyloxy)benzylideneamino]-3-cyano thiophene was studied by Thaker *et al.* (2012). The molecular structure of the thiophene liquid crystal is given in Figure 2.10.

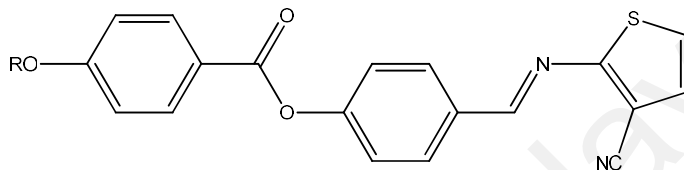


**Figure 2.10: Molecular structure of 2-[4-(4'-n-alkoxybenzoyloxy) benzylidene-amino]-3-cyano thiophene**

The entire members of the homologous exhibited an enantiotropic nematic phase. When going down the homologous series, enantiotropic smectic C phase started to appear from tetradecanoyloxy derivative. However, the smectic phase was first observed as the monotropic phase upon cooling for the dodecanoyloxy derivative (Thaker *et al.*, 2012). This showed that the present of heterocyclic ring as the terminal core ring tended to increase the molecular anisotropy properties of the mesogen. This may increase the mesogen-to-mesogen interaction and enhance the parallel arrangement of molecules that similar to the smectic phase layer arrangement (Ha *et al.*, 2009; Foo *et al.*, 2015). Besides that, the thiophene ring presented in the end of the center core was also lowered the transition temperatures due to its highly electronegative atom, S. Although the cyano group, CN presented at the lateral position in the heterocyclic ring, but there was not much effect had been observed on the transition temperature (Thaker *et al.*, 2012).



**Table 2.3: Transition temperatures data of 2-[4-(4-*n*-alkoxybenzoyloxy)benzylideneamino] 3-cyano thiophene**

Transition Temperature (°C)							
R	Cr		SmC		N		I
Methyl	•	—	—	126	•	165	•
Ethyl	•	—	—	118	•	162	•
Propyl	•	—	—	121	•	160	•
Butyl	•	—	—	114	•	156	•
Pentyl	•	—	—	110	•	153	•
Hexyl	•	—	—	105	•	150	•
Heptyl	•	—	—	94	•	127	•
Octyl	•	—	—	78	•	110	•
Decyl	•	—	—	69	•	94	•
Dodecyl	•	(49)*	•	72	•	91	•
Tetradecyl	•	47	•	74	•	88	•
Hexadecyl	•	52	•	67	•	86	•
Octadecyl	•	54	•	64	•	83	•

\* monotropic

## CHAPTER 3: MATERIALS AND METHODS

### 3.1 Chemicals

All chemicals and solvents were commercially purchased and used without further purification. Decanoic acid, lauric acid, myristic acid, palmitic acid, stearic acid, aniline, 4-chloroaniline, 4-bromoaniline, *p*-anisidine, *p*-toluidine, N,N-diethyl-*p*-phenylenediamine, 4-dimethylaminopyridine were purchased from Merck Chemical, Malaysia. Hexanoic acid, octanoic acid, 4-hydroxybenzaldehyde, 2,4-dihydroxybenzaldehyde, 4-aminophenol, 2-thiophenecarbonyl chloride, 11-bromoundecanoic acid, N,N-dicyclohexylcarbodiimide and dimethylformamide were purchased from Sigma Aldrich, Malaysia. Acetic acid, ethanol, dichloromethane, hexane, chloroform, methanol and benzene were purchased from R & M Chemicals, Malaysia.

### 3.2 Synthesis

In this section, the detail procedures for preparing the desired compounds will be discussed. The desired products were synthesized using well-known Steglich esterification and imination which had described previously by Yeap and his co-worker in literature (Yeap *et al.*, 2009; Ha *et al.*, 2010; Ha *et al.*, 2014).

#### 3.2.1 Synthesis of Series 1

There were three sub-series in series 1 with different terminal substituents, namely methyl, methoxy and N,N-diethylamino groups. The synthesis route for the

intermediates and final compounds are illustrated in Figure 3.1 and their synthetic methods are stated as follows.

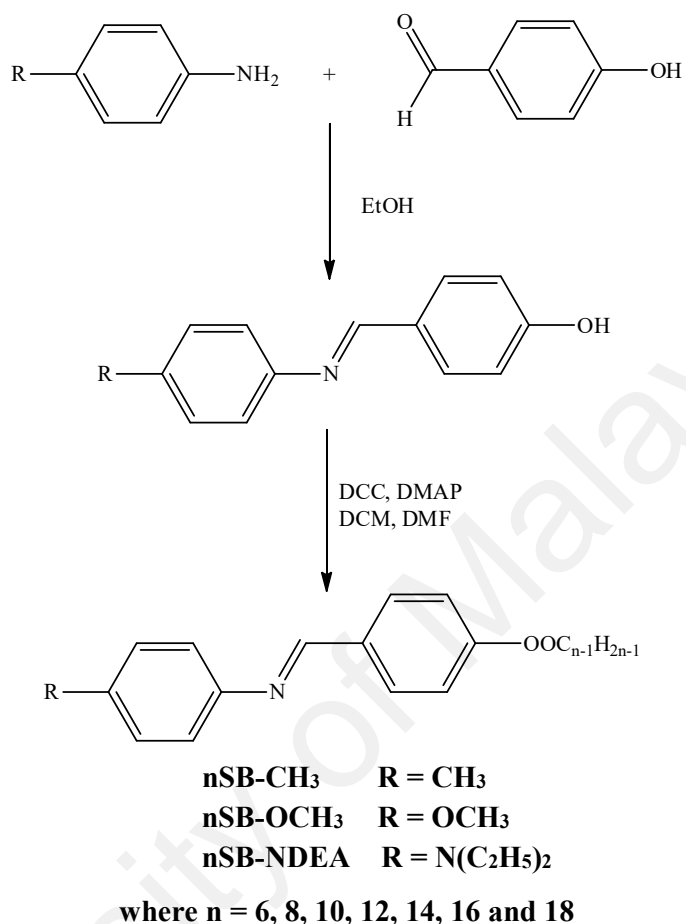


**Figure 3.1:** Synthetic route towards the formation of the intermediate and the compounds named as nSB-CH<sub>3</sub>, nSB-OCH<sub>3</sub> and nSB-NDEA

### 3.2.1.1 Synthesis of 4-hydroxybenzylidene-4'-methyl, 4'-methoxy, 4'-(N,N-diethyl-amino)aniline

**Synthesis of 4-hydroxybenzylidene-4'-methylaniline:** 4-methyl-aniline (4.29 g, 40 mmol) was dissolved in 30 mL of ethanol into a 250 mL round bottom flask. In a 100 mL beaker, 4-hydroxybenzaldehyde (4.88 g, 40 mmol) was dissolved in 20 mL of ethanol. The ethanolic solution of 4-hydroxybenzaldehyde was then mixed together with ethanolic solution of 4-methylaniline in the round bottom flask. Three drops of acetic acid were added into round bottom flask as catalyst. The mixture was stirred and

heated under reflux at 70 – 80 °C three hours. The reaction mixture was filtered while hot and the filtrate was cooled to room temperature and this allowed the precipitation of yellowish solid. The solution was further stored at refrigerator for further precipitation and filtered afterward. The dry yellowish solid thus obtained was recrystallized several times with hexane and ethanol. Similar reactions to make **4-hydroxybenzylidene-4'-methoxyaniline** and **4-hydroxybenzylidene-4'-(N,N-diethylamino)aniline** are following the same procedure by substituting the 4-methylaniline to 4-methoxyaniline (4.93 g, 40 mmol) or 4-(N,N-diethylamino)aniline (6.57 g, 40 mmol).

### 3.2.1.2 Synthesis of Series 1A (nSB-CH<sub>3</sub>)

**Synthesis of 4-n-hexanoyloxybenzylidene-4'-methylaniline:** 4-hydroxybenzylidene-4'-methylaniline (1.06 g, 5 mmol) was dissolved in 5 mL of DMF in a 250 mL round bottom flask and DMAP (0.61 g, 0.5 mmol) was added into the round bottom flask to dissolve together. In another 100 mL beaker, DCC (1.03 g, 5 mmol) and hexanoic acid (0.58 g, 5 mmol) were dissolved in 45 mL of DCM. Chlorinated mixture of DCC and hexanoic acid was then added into the round bottom flask dropwise. The resulted mixture was first stirred at 0 °C. Then the mixture was continued to stir at room temperature for another 24 hours before it was filtered. The residue was washed with several portions of DCM and all filtrates were combined. The filtrate was then evaporated to dryness. The crude solid thus obtained was recrystallized once with hexane and twice with ethanol to obtain the pure product. Similar reactions to make **4-n-octanoyloxybenzylidene-4'-methylaniline**, **4-n-decanoyloxybenzylidene-4'-methylaniline**, **4-n-dodecanoyloxybenzylidene-4'-methylaniline**, **4-n-tetradecanoyloxybenzylidene-4'-methylaniline**, **4-n-hexadecanoyloxybenzylidene-4'-methylaniline** and **4-n-octadecanoyloxybenzylidene-4'-methylaniline** are following the same

procedure by substituting the hexanoic acid to octanoic acid (0.72 g, 5 mmol), decanoic acid (0.86 g, 5 mmol), dodecanoic acid (1.00 g, 5 mmol), tetradecanoic acid (1.14 g, 5 mmol), hexadecanoic acid (1.28 g, 5 mmol) or octa-decanoic acid (1.42 g, 5 mmol).

### 3.2.1.3 Synthesis of Series 1B (nSB-OCH<sub>3</sub>)

**Synthesis of 4-n-hexanoyloxybenzylidene-4'-methoxyaniline:** 4-hydroxybenzylidene-4'-methoxyaniline (1.14 g, 5 mmol) was dissolved in 5 mL of DMF in a 250 mL round bottom flask and DMAP (0.61 g, 0.5 mmol) was added into the round bottom flask to dissolve together. In another 100 mL beaker, DCC (1.03 g, 5 mmol) and hexanoic acid (0.58 g, 5 mmol) were dissolved in 45 mL of DCM. Chlorinated mixture of DCC and hexanoic acid was then added into the round bottom flask dropwise. The resulted mixture was first stirred at 0 °C. Then the mixture was continued to stir at room temperature for another 24 hours before it was filtered. The residue was washed with several portions of DCM and all filtrates were combined. The filtrate was then evaporated to dryness. The crude solid thus obtained was recrystallized once with hexane and twice with ethanol to obtain the pure product. Similar reactions to make **4-n-octanoyloxybenzylidene-4'-methoxyaniline**, **4-n-decanoyloxybenzylidene-4'-methoxyaniline**, **4-n-dodecanoyloxybenzylidene-4'-methoxyaniline**, **4-n-tetradecanoyloxybenzylidene-4'-methoxyaniline**, **4-n-hexadecanoyloxybenzylidene-4'-methoxyaniline** and **4-n-octadecanoyloxybenzylidene-4'-methoxyaniline** are following the same procedure by substituting the hexanoic acid to octanoic acid (0.72 g, 5 mmol), decanoic acid (0.86 g, 5 mmol), dodecanoic acid (1.00 g, 5 mmol), tetradecanoic acid (1.14 g, 5 mmol), hexadecanoic acid (1.28 g, 5 mmol) or octa-decanoic acid (1.42 g, 5 mmol).

### 3.2.1.4 Synthesis of Series 1C (nSB-NDEA)

#### **Synthesis of 4-n-hexanoyloxybenzylidene-4'-(N,N-diethylamino)aniline:**

4-hydroxybenzylidene-4'-(N,N-diethylamino)aniline (1.44 g, 5 mmol) was dissolved in 5 mL of DMF in a 250 mL round bottom flask and DMAP (0.61 g, 0.5 mmol) was added into the round bottom flask to dissolve together. In another 100 mL beaker, DCC (1.03 g, 5 mmol) and hexanoic acid (0.58 g, 5 mmol) were dissolved in 45 mL of DCM. Chlorinated mixture of DCC and hexanoic acid was then added into the round bottom flask dropwise. The resulted mixture was first stirred at 0 °C. Then the mixture was continued to stir at room temperature for another 24 hours before it was filtered. The residue was washed with several portions of DCM and all filtrates were combined. The filtrate was then evaporated to dryness. The crude solid thus obtained was recrystallized once with hexane and twice with ethanol to obtain the pure product. Similar reactions to make 4-n-octanoyloxybenzylidene-4'-(N,N-diethylamino)aniline, 4-n-decanoyloxybenzylidene-4'-(N,N-diethylamino)aniline, 4-n-dodecanoyloxybenzylidene-4'-(N,N-diethylamino)aniline, 4-n-tetradecanoyloxybenzylidene-4'-(N,N-diethylamino)aniline, 4-n-hexadecanoyloxybenzylidene-4'-(N,N-diethylamino)aniline and 4-n-octadecanoyloxybenzylidene-4'-(N,N-diethylamino)aniline are following the same procedure by substituting the hexanoic acid to octanoic acid (0.72 g, 5 mmol), decanoic acid (0.86 g, 5 mmol), dodecanoic acid (1.00 g, 5 mmol), tetradecanoic acid (1.14 g, 5 mmol), hexadecanoic acid (1.28 g, 5 mmol) or octadecanoic acid (1.42 g, 5 mmol).

### 3.2.2 Synthesis of Series 2

The synthesis route for the intermediates and final compounds are illustrated in Figure 3.2 and their synthetic methods are stated as follows.

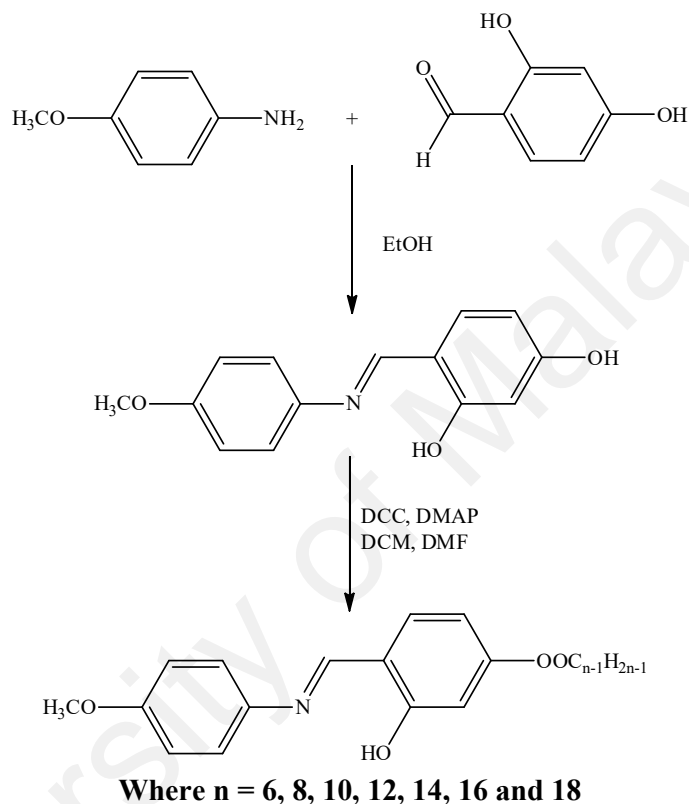


**Figure 3.2:** Synthetic route towards the formation of the intermediate and the compound named as nSHB-OCH<sub>3</sub>

#### 3.2.2.1 Synthesis of 2,4-dihydroxybenzylidene-4'-methoxyaniline

**Synthesis of 2,4-dihydroxybenzylidene-4'-methoxyaniline:** 4-methoxyaniline (4.93 g, 40 mmol) and 2,4-dihydroxybenzaldehyde (5.52 g, 40 mmol) were dissolved in 50 mL of ethanol in a 250 mL round bottom flask. Three drops of acetic acid were added into round bottom flask as catalyst. The mixture was allowed to stir and heat under reflux at 70 – 80 °C for three hours. The reaction mixture was subjected

to hot filtration. Then, the filtrate was cooled to room temperature and allowed the precipitation of yellowish intermediate solid. The solution was further stored at refrigerator for further precipitation and filtered. The dry yellowish solid thus obtained was recrystallized several times with hexane and ethanol.

### 3.2.2.2 Synthesis of Series 2 (nSHB-OCH<sub>3</sub>)

#### Synthesis of 4-n-hexanoyloxy-2-hydroxybenzylidene-4'-methoxyaniline:

2,4-dihydroxybenzylidene-4'-methoxyaniline (1.22 g, 5 mmol) was dissolved in 5 mL of DMF in a 250 mL round bottom flask and DMAP (0.61 g, 0.5 mmol) was added into the round bottom flask to dissolve together. In another 100 mL beaker, DCC (1.03 g, 5 mmol) and hexanoic acid (0.58 g, 5 mmol) were dissolved in 45 mL of DCM. Chlorinated mixture of DCC and hexanoic acid was then added into the round bottom flask dropwise. The resulted mixture was first stirred at 0 °C. Then the mixture was continued to stir at room temperature for another 3 hours before it was filtered. The residue was washed with several portions of DCM and all filtrates were combined. The filtrate was then evaporated to dryness. The crude solid thus obtained was recrystallized once with hexane and twice with ethanol to obtain the pure product. Similar reactions to make 4-n-octanoyloxy-2-hydroxybenzylidene-4'-methoxyaniline, 4-n-decanoyloxy-2-hydroxybenzylidene-4'-methoxyaniline, 4-n-dodecanoyloxy-2-hydroxybenzylidene-4'-methoxyaniline, 4-n-tetradecanoyloxy-2-hydroxybenzylidene-4'-methoxyaniline, 4-n-hexadecanoyloxy-2-hydroxybenzylidene-4'-methoxyaniline and 4-n-octadenoyloxy-2-hydroxybenzylidene-4'-methoxyaniline are following the same procedure by substituting the hexanoic acid to octanoic acid (0.72 g, 5 mmol), decanoic acid (0.86 g, 5 mmol), dodecanoic acid (1.00 g, 5 mmol), tetradecanoic acid (1.14 g, 5 mmol), hexadecanoic acid (1.28 g, 5 mmol) or octadecanoic acid (1.42 g, 5 mmol).



### 3.2.3 Synthesis of Series 3

The synthesis route for the intermediates and final compounds are illustrated in Figure 3.3 and their synthetic methods are stated as follows.

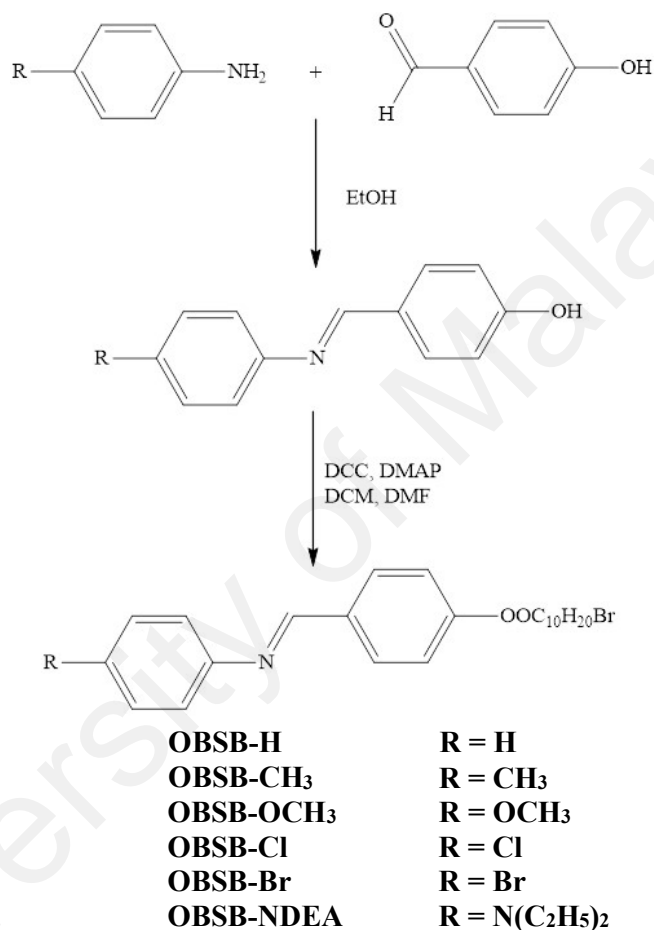


Figure 3.3: Synthetic route towards the formation of OBSB-H, OBSB-CH<sub>3</sub>, OBSB-OCH<sub>3</sub>, OBSB-Cl, OBSB-Br and OBSB-NDEA

#### 3.2.3.1 Synthesis of 4-hydroxybenzylidene-4'-substituted aniline

**Synthesis of 4-hydroxybenzylidene-4'-methylaniline:** 4-methylaniline (4.29 g, 40 mmol) and 4-hydroxybenzaldehyde (4.88 g, 40 mmol) were dissolved in 50 mL of ethanol in a 250 mL round bottom flask. Three drops of acetic acid were added into

round bottom flask as catalyst. The mixture was stirred and heated under reflux at 70 – 80 °C for three hours. The reaction mixture was subjected to hot filtration. Then, the filtrate was cooled to room temperature allowing yellowish intermediate solid to form. The solution was further stored at refrigerator for further precipitation and filtered. The dry yellowish solid thus obtained was recrystallized several times with hexane and ethanol. Similar reactions to **4-hydroxybenzylidene-4'-methoxyaniline**, **4-hydroxybenzylidene-4'-chloroaniline**, **4-hydroxybenzylidene-4'-bromoaniline**, **4-hydroxybenzylidene-4'-(N,N-diethylamino)aniline** and **4-hydroxybenzylidene-4'-aniline** are following the same procedure by substituting the 4-methylaniline to 4-methoxyaniline (4.93 g, 40 mmol), 4-chloroaniline (5.10 g, 40 mmol), 4-bromoaniline (6.88 g, 40 mmol), 4-(N,N-diethylamino)aniline (6.57 g, 40 mmol) and aniline (3.73 g, 40 mmol).

### 3.2.3.2 Synthesis of Series 3 (OBSB-R)

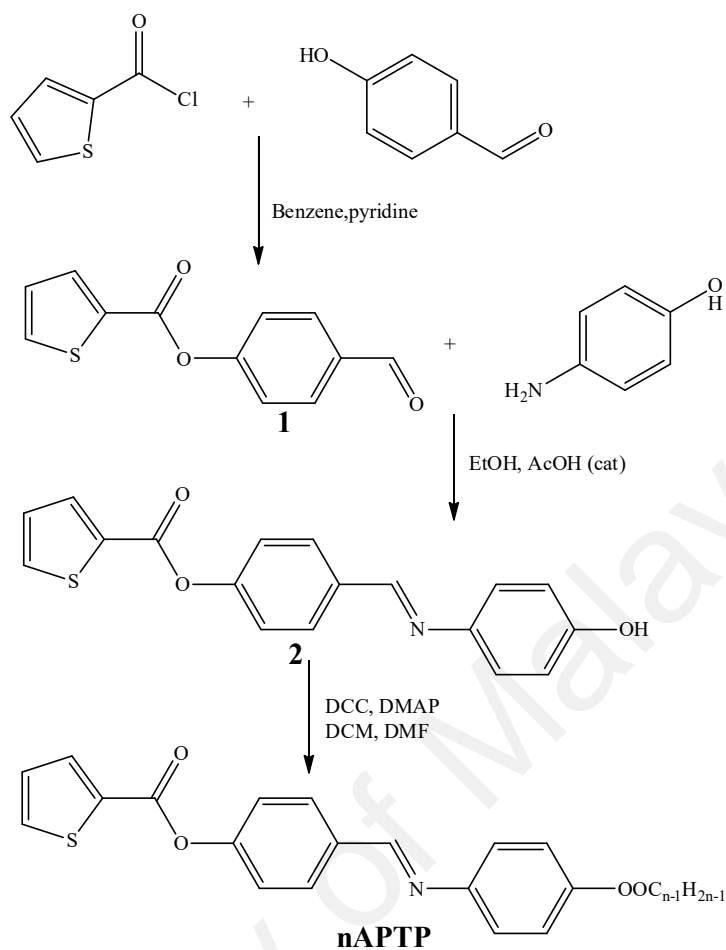
#### Synthesis of **4-(11-bromoundecanoyloxy)benzylidene-4'-methylaniline**:

4-hydroxybenzylidene-4'-methylaniline (1.06 g, 5 mmol) and DMAP (0.61 g, 0.5 mmol) were dissolved in 5 mL of DMF in a 250 mL round bottom flask. In another beaker, 11-bromoundecanoic acid (1.33 g, 5 mmol) and DCC (1.03 g, 5 mmol) were dissolved in 45 mL of DCM. Chlorinated mixture of 11-bromoundecanoic acid and DCC were then added into round bottom flask dropwise. The resulted mixture was first stirred at 0 °C. Then, the mixture was continued to stir at room temperature for another 24 hours before it was filtered. The residue was washed with several portions of DCM and all filtrates were combined. The filtrate was evaporated to dryness. The crude solid thus obtained was recrystallized once with hexane and twice with ethanol to obtain the pure product. Similar reactions to **4-(11-bromoundecanoyloxy)benzylidene-4'-**

**methylaniline, 4-(11-bromoundecanoyloxy)benzylidene-4'-methoxyaniline, 4-(11-bromoundecanoyloxy)benzylidene-4'-chloroaniline, 4-(11-bromoundecanoyloxy)benzylidene-4'-bromoaniline, 4-(11-bromoundecanoyloxy)benzylidene-4'-(N,N-diethylamino)aniline and 4-(11-bromo-undecanoyloxy)benzylidene-4'-aniline** by substituted the **4-hydroxybenzylidene-4'-methylaniline** to **4-hydroxybenzylidene-4'-methoxyaniline** (1.14 g, 5 mmol), **4-hydroxybenzylidene-4'-chloroaniline** (1.16 g, 5 mmol), **4-hydroxybenzylidene-4'-bromoaniline** (1.38 g, 5 mmol), **4-hydroxybenzylidene-4'-(N,N-diethylamino)aniline** (1.34 g, 5 mmol) and **4-hydroxybenzylidene-4'-aniline** (0.99 g, 5 mmol).

#### **3.2.4 Synthesis of Series 4**

The synthesis route for the intermediates and final compounds are illustrated in Figure 3.4 and their synthetic methods are stated as follows.



Where n = 6, 8, 10, 12, 14, 16 and 18

**Figure 3.4:** Synthetic route towards the formation of the intermediate and the compound named as nAFTP

#### 3.2.4.1 Synthesis of intermediate 1 for series 4

**Synthesis of 4-formylphenyl thiophene-2-carboxylate:** 4-Hydroxybenzaldehyde (2.44 g, 20 mmol) was dissolved in 8 mL of pyridine in a 250 mL round-bottom flask prior to the addition of 50 mL benzene. 2-thiophenecarbonyl chloride (2.93 g, 20 mmol) was then added in slowly to the stirring solution. The mixture was subjected to reflux 80 °C for 2 hours. The undesired precipitate was immediately filtered off and the filtrate was evaporated to dryness. The product was washed with

absolute ethanol and subsequently recrystallized from a mixture of chloroform and hexane.

#### 3.2.4.2 Synthesis of intermediate 2 for series 4

**Synthesis of 4-(((4-hydroxyphenyl)imino)methyl)phenyl thiophene-2-carboxylate:** 4-formylphenyl thiophene-2-carboxylate (9.29 g, 40 mmol) and 40 mmol of 4-aminophenol (4.37 g, 40 mmol) were added in a 250 mL round bottom flask. The mixture was dissolved in 50 mL of ethanol and three drops of acetic acid was added in as catalyst. The mixture was stirred and heated under refluxed at 70 – 80 °C for three hours. The reaction mixture was subjected to hot filtration. Then, the filtrate was cooled to room temperature and allowed the precipitation of yellowish solid. The solution was further stored at refrigerator for further precipitation and filtered. The dry yellowish solid thus obtained was recrystallized several times with hexane and ethanol.

#### 3.2.4.3 Synthesis of Series 4 with different alkyl chain (nAFTP)

**Synthesis of 4-hexanoyloxyphenylimino-4-methylphenyl thiophene-2-carboxylate:** 4-(((4-hydroxyphenyl)imino)methyl)phenyl thiophene-2-carboxylate (1.62 g, 5 mmol) and DMAP (0.61 g, 0.5 mmol) were dissolved in 5 mL of DMF in a round bottom flask. In another beaker, hexanoic acid (0.58 g, 5 mmol) and DCC (1.03 g, 5 mmol) were dissolved in 45 mL of DCM and then the mixture was added into the round bottom flask dropwise. The resulted mixture was first stirred at 0 °C. Then, the mixture was continued to stir at room temperature for another 24 hours before it was filtered. The residue was washed with several portions of DCM and all filtrates were combined. The filtrate was then evaporated to dryness. The desired crude solid thus obtained was recrystallized once with hexane and twice with ethanol to obtain the pure

product. Similar reactions to make **4-octanoyloxyphenylimino-4-methylphenyl thiophene-2-carboxylate**, **4-decanoyloxyphenylimino-4-methylphenyl thiophene-2-carboxylate**, **4-dodecanoyloxyphenylimino-4-methylphenyl thiophene-2-carboxylate**, **4-tetra-decanoyloxyphenylimino-4-methylphenyl thiophene-2-carboxylate**, **4-hexadeca-noyloxyphenylimino-4-methylphenyl thiophene-2-carboxylate** and **4-octadeca-noyloxyphenylimino-4-methylphenyl thiophene-2-carboxylate** are following the same procedure by substituting the hexanoic acid to octanoic acid (0.72 g, 5 mmol), decanoic acid (0.86 g, 5 mmol), dodecanoic acid (1.00 g, 5 mmol), tetradecanoic acid (1.14 g, 5 mmol), hexadecanoic acid (1.28 g, 5 mmol) or octadecanoic acid (1.42 g, 5 mmol).

### 3.3 Characterization Method

Several microscopic techniques were used to elucidate the structures and study their LC properties.

#### 3.3.1 Fourier Transform Infrared (FTIR)

Infrared spectroscopy is a tool which allowed to identify the functional groups in a molecule based on the absorption bands. The FT-IR analysis were performed on a Perkin Elmer 2000-FTIR spectrometer. The powder samples were first mixed homogenously with potassium bromide and subsequently compressed into pellets form. The samples were then run to scan in the range of  $4000 - 400 \text{ cm}^{-1}$  with 16 scanning numbers at a resolution of  $4 \text{ cm}^{-1}$  at room temperature

### **3.3.2 Nuclear Magnetic Resonance (NMR)**

The chemical structure and purity of the liquid crystal compounds were investigated by NMR spectroscopy.  $^1\text{H}$  NMR and  $^{13}\text{C}$  NMR analysis were conducted using the Bruker Avance III series with a magnetic field strength of 400 MHz, equipped with an auto-charger. Each sample was dissolved in deuterated chloroform with an internal standard, tetramethylsilane (TMS) to obtain viscous solution in NMR tube. The  $^1\text{H}$  NMR spectrum was run for 16 scans and  $^{13}\text{C}$  NMR spectrum was run for 1024 scans to obtain an optimized resolution. The data obtained from the NMR analysis was then subjected to be analyzed with ACD/NMR Processor Academic Edition.

### **3.3.3 Differential Scanning Calorimetry (DSC)**

The thermal properties of the liquid crystals were investigated via differential scanning calorimetry (DSC) and the analyses were carried out using TA Instruments DSC Q20 series. The sample was first measured in the range of 1 – 2 mg on tin sample holder and compressed to close the holder with the hematic lid. The sample was placed in the instrumental with iridium as the reference cell. The experiment was conducted in nitrogen gas environment. The heating and cooling rates of the differential scanning calorimeters were set to  $10\text{ }^{\circ}\text{C min}^{-1}$ . The experiments were run for 2 cycles of heating and cooling. The results of the second heating and cooling were used to analyze.

#### **3.3.4 Polarized Optical Microscope (POM).**

The liquid crystalline texture for the compounds were observed using a Olympus BX50 polarizing optical microscope equipped with a temperature controlled by Mettler Toledo FP 82 hot stage and Mettler FP 90 Central Processor. A video camera was installed on the polarizing optical microscope to allow real-time video capture and image saving. Melt-recrystallization method was used to prepare the liquid crystal sample for POM analysis. About 1 – 2 mg of sample was placed on top of a glass slide. The sample was carefully sandwiched between a microscope slide and coverslip. The sample was started to heat slowly until melted. After the sample completely melted, the microscope was removed from heating immediately into a heat-proof mat. The cover slip was dragged from one end of the slide to another end. This created a flat sheet of crystals when cooled. The sample is now ready for analyze.

#### **3.3.5 Elemental CHN Analysis.**

The analysis was carried out on Perkin Elmer CHNS/O 2400 Series II. Analyze and calibration standard acetanilide were packed with pre-cleaned tin capsule and folded.

#### **3.3.6 Thin Layer Chromatography.**

Thin layer chromatography analyses were performed using aluminum-backed silica gel plates (Merck 60 F254) and were examined under UV light with the wavelength of 254 nm.



## CHAPTER 4: RESULTS AND DISCUSSION

### 4.1 Series 1

The chemical structure of **nSB-CH<sub>3</sub>**, **nSB-OCH<sub>3</sub>** and **nSB-NDEA** are given in Figure 4.1 and the percentage yields are summarized in Table 4.1.

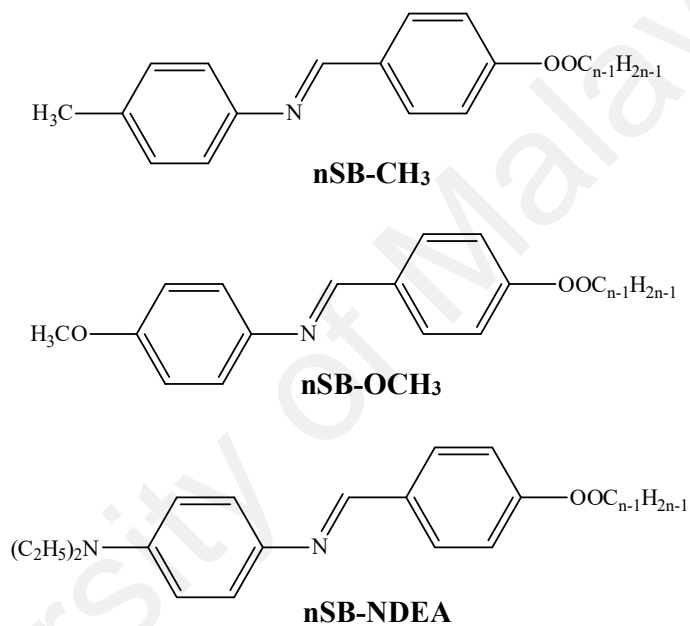


**Figure 4.1:** Structural formula of **nSB-CH<sub>3</sub>**, **nSB-OCH<sub>3</sub>** and **nSB-NDEA**

**Table 4.1:** Percentage yields of **nSB-CH<sub>3</sub>**, **nSB-OCH<sub>3</sub>** and **nSB-NDEA**

n	Yield (%)		
	nSB-CH <sub>3</sub>	nSB-OCH <sub>3</sub>	nSB-NDEA
6	40	40	45
8	45	43	53
10	44	45	54
12	42	43	52
14	48	47	56
16	50	50	61
18	52	54	60

#### 4.1.1 Structural Elucidation

Various spectroscopic techniques were used to elucidate the structural information of **nSB-CH<sub>3</sub>**, **nSB-OCH<sub>3</sub>** and **nSB-NDEA**. The techniques used for elucidation were **FTIR**, **<sup>1</sup>H NMR**, **<sup>13</sup>C NMR** and micro-elemental analysis. The purities of **nSB-CH<sub>3</sub>**, **nSB-OCH<sub>3</sub>** and **nSB-NDEA** were monitored by TLC analysis. The TLC  $R_f$  value for **nSB-CH<sub>3</sub>**, **nSB-OCH<sub>3</sub>** and **nSB-NDEA** are tabulated in Appendix A.

Elemental analysis was carried out for all the synthesized compounds and the data are tabulated in Table 4.2. The analytical data are quite agreeable with the calculated values (within 0.5%). The molecular formulae obtained are similar to those obtained from elemental analysis and spectra analysis.

**Table 4.2: Micro-elemental analytical data of nSB-CH<sub>3</sub>, nSB-OCH<sub>3</sub> and nSB-NDEA**

n	Experimental analysis: found ( <i>calculated</i> ) / %					
	C		H		N	
<b>6SB-CH<sub>3</sub></b>	77.25	(77.64)	7.59	(7.49)	4.44	(4.53)
<b>8SB-CH<sub>3</sub></b>	77.92	(78.30)	8.2	(8.06)	4.03	(4.15)
<b>10SB-CH<sub>3</sub></b>	78.51	(78.86)	8.65	(8.55)	3.73	(3.83)
<b>12SB-CH<sub>3</sub></b>	79.02	(79.35)	9.04	(8.96)	3.48	(3.56)
<b>14SB-CH<sub>3</sub></b>	79.73	(79.76)	9.41	(9.32)	3.24	(3.32)
<b>16SB-CH<sub>3</sub></b>	80.17	(80.13)	9.68	(9.64)	3.07	(3.11)
<b>18SB-CH<sub>3</sub></b>	80.64	(80.45)	9.96	(9.92)	2.89	(2.93)

n	Experimental analysis: found ( <i>calculated</i> ) / %					
	C		H		N	
<b>6SB-OCH<sub>3</sub></b>	73.53	(73.82)	7.22	(7.12)	4.18	(4.30)
<b>8SB-OCH<sub>3</sub></b>	74.53	(74.76)	7.76	(7.70)	3.92	(3.96)
<b>10SB-OCH<sub>3</sub></b>	75.33	(75.56)	8.24	(8.19)	3.64	(3.67)
<b>12SB-OCH<sub>3</sub></b>	76.05	(76.25)	8.71	(8.61)	3.34	(3.42)
<b>14SB-OCH<sub>3</sub></b>	76.57	(76.85)	9.11	(8.98)	3.11	(3.20)
<b>16SB-OCH<sub>3</sub></b>	77.17	(77.38)	9.40	(9.31)	2.94	(3.01)
<b>18SB-OCH<sub>3</sub></b>	77.63	(77.85)	9.69	(9.60)	2.81	(2.84)

n	Experimental analysis: found ( <i>calculated</i> ) / %					
	C		H		N	
<b>6SB-NDEA</b>	75.17	(75.41)	8.30	(8.20)	7.52	(7.65)
<b>8SB- NDEA</b>	75.77	(76.14)	8.75	(8.63)	7.00	(7.11)
<b>10SB- NDEA</b>	76.74	(76.78)	9.06	(9.01)	6.63	(6.64)
<b>12SB- NDEA</b>	77.25	(77.33)	9.46	(9.33)	6.10	(6.22)
<b>14SB- NDEA</b>	77.61	(77.82)	9.78	(9.62)	5.69	(5.86)
<b>16SB- NDEA</b>	78.47	(78.26)	10.02	(9.88)	5.43	(5.53)
<b>18SB- NDEA</b>	78.53	(78.60)	10.25	(10.18)	5.11	(5.24)

The infrared spectra of **10SB-CH<sub>3</sub>**, **12SB-OCH<sub>3</sub>** and **16SB-NDEA** are shown in Figures 4.2 – 4.4 and selected bond absorption data for **nSB-CH<sub>3</sub>**, **nSB-OCH<sub>3</sub>** and **nSB-NDEA** are summarized in Tables 4.3 – 4.5. The remaining spectra are given in Appendix B.

The Schiff base group (C=N) is indicated by the presence of sharp peaks at 1623 cm<sup>-1</sup> (**10SB-CH<sub>3</sub>**), 1623 cm<sup>-1</sup> (**12SB-OCH<sub>3</sub>**) and 1624 cm<sup>-1</sup> (**16SB-NDEA**). These values confirmed those reported in the literature (Ha *et al.* 2011) that involve benzylidene aniline moieties (–C<sub>6</sub>H<sub>5</sub>CH=NC<sub>6</sub>H<sub>5</sub>–). These results indicated that imination reaction between the amino group of 4-substituted aniline and the carbonyl group of 4-hydroxybenzaldehyde had successfully taken place and yielded the intermediate compounds for the **nSB-CH<sub>3</sub>**, **nSB-OCH<sub>3</sub>** and **nSB-NDEA**.

The absorption peaks appeared at 3060 & 3027 cm<sup>-1</sup> (**10SB-CH<sub>3</sub>**), 3071 & 3027 cm<sup>-1</sup> (**12SB-OCH<sub>3</sub>**) and 3067 & 3041 cm<sup>-1</sup> (**16SB-NDEA**) are attributed to the sp<sup>2</sup> hybridized C–H stretch of two aromatic rings. The presence of peaks at 1601 & 1469 cm<sup>-1</sup> in **10SB-CH<sub>3</sub>**, 1601 & 1469 cm<sup>-1</sup> in **12SB-OCH<sub>3</sub>** and 1594 & 1469 cm<sup>-1</sup> in **16SB-NDEA** are due to the C=C stretch of aromatic rings. This indicates that the aromatic rings are found within the structures of **nSB-CH<sub>3</sub>**, **nSB-OCH<sub>3</sub>** and **nSB-NDEA**.

From the spectra of **10SB-CH<sub>3</sub>**, **12SB-OCH<sub>3</sub>** and **16SB-NDEA**, the absorption peaks appeared at 2949, 2924 & 2854 cm<sup>-1</sup> (**10SB-CH<sub>3</sub>**), 2957, 2920 & 2850 cm<sup>-1</sup> (**12SB-OCH<sub>3</sub>**) and 2968, 2924 & 2854 cm<sup>-1</sup> (**16SB-NDEA**) and all were assigned to the symmetrical and asymmetrical C–H stretch of the methylene (–CH<sub>2</sub>–) and methyl (–CH<sub>3</sub>) groups in the terminal long alkyl chain. The peak height of the compounds depends on the number of carbons present in the methylene group in the terminal

flexible chain. The stronger the absorption peak indicates a greater number of carbons present in the methylene group.

Characteristic strong absorption peaks at  $1756\text{ cm}^{-1}$  (**10SB-CH<sub>3</sub>**),  $1752\text{ cm}^{-1}$  (**12SB-OCH<sub>3</sub>**) and  $1756\text{ cm}^{-1}$  (**16SB-NDEA**) are ascribed to the carbonyl group (C=O) of an ester linkage. The two strong peaks at  $1201\text{ cm}^{-1}$  &  $1135\text{ cm}^{-1}$  (**10SB-CH<sub>3</sub>**),  $1208\text{ cm}^{-1}$  &  $1167\text{ cm}^{-1}$  (**12SB-OCH<sub>3</sub>**) and  $1197\text{ cm}^{-1}$  &  $1131\text{ cm}^{-1}$  (**16SB-NDEA**) represented the C–O stretching of the ester group which one peak will be broader and stronger than another one. These observations indicated the presence of the ester bond in the structure of the compound and further ascertained that the esterification of the carboxylic acid group with the alcohol group was successful and led to the formation of **nSB-CH<sub>3</sub>**, **nSB-OCH<sub>3</sub>** and **nSB-NDEA**.

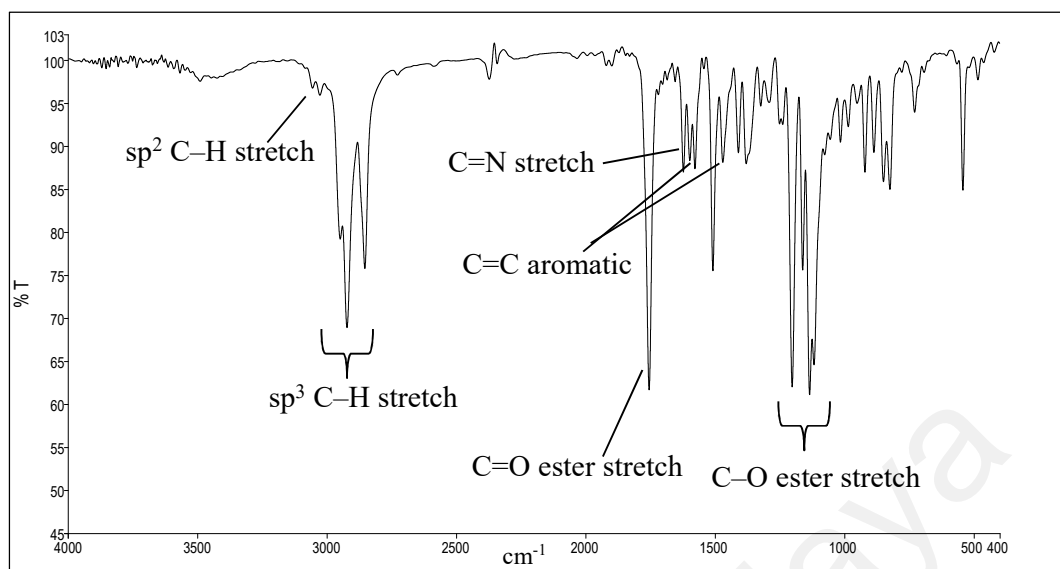


**Figure 4.2: FTIR spectrum of 10SB-CH<sub>3</sub>**

**Table 4.3: FTIR spectral analysis data of nSB-CH<sub>3</sub>**

Functional group	IR v (cm <sup>-1</sup> )					
	sp <sup>2</sup> C-H stretch Aromatic	sp <sup>3</sup> C-H stretch Aliphatic	C=O Ester	C=N Schiff base	C=C Aromatic	C-O Ester
<b>6SB-CH<sub>3</sub></b>	3052 3030	2953 2927 2867	1756	1623	1598 1469	1201 1135
<b>8SB-CH<sub>3</sub></b>	3060 3030	2949 2924 2854	1756	1623	1598 1473	1201 1135
<b>10SB-CH<sub>3</sub></b>	3060 3027	2949 2924 2854	1756	1623	1601 1469	1201 1135
<b>12SB-CH<sub>3</sub></b>	3060 3030	2946 2924 2854	1756	1623	1598 1469	1201 1131
<b>14SB-CH<sub>3</sub></b>	3060 3027	2946 2924 2854	1756	1623	1598 1469	1201 1131
<b>16SB-CH<sub>3</sub></b>	3060 3030	2946 2924 2858	1756	1623	1598 1469	1205 1131
<b>18SB-CH<sub>3</sub></b>	3060 3027	2953 2920 2850	1752	1627	1598 1469	1212 1153

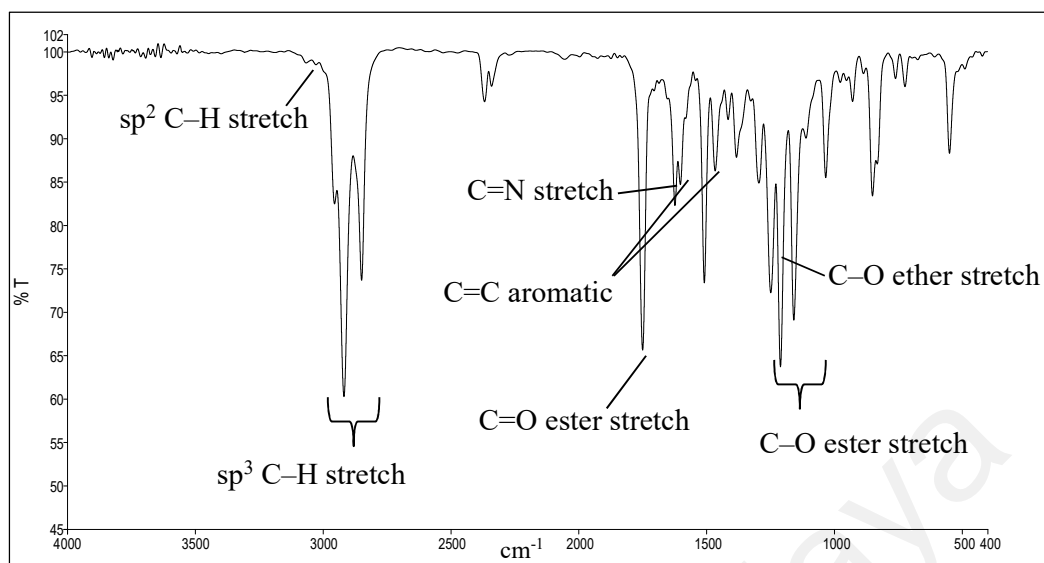


**Figure 4.3: FTIR spectrum of 12SB-OCH<sub>3</sub>**

**Table 4.4: FTIR spectral analysis data of nSB-OCH<sub>3</sub>**

Functional group	IR v (cm <sup>-1</sup> )						
	sp <sup>2</sup> C-H stretch Aromatic	sp <sup>3</sup> C-H stretch Aliphatic	C=O Ester	C=N Schiff base	C=C Aromatic	C-O Ester	C-O Ether
<b>6SB-CH<sub>3</sub></b>	3063	2953 2927 2869 2839	1756	1623	1601 1465	1198 1135	1249
<b>8SB-CH<sub>3</sub></b>	3060	2953 2924 2854	1756	1623	1598 1465	1201 1135	1252
<b>10SB-CH<sub>3</sub></b>	3067 3030	2957 2920 2850	1748	1623	1605 1465	1212 1160	1252
<b>12SB-CH<sub>3</sub></b>	3071 3027	2957 2920 2850	1752	1623	1601 1469	1208 1157	1249
<b>14SB-CH<sub>3</sub></b>	3071 3034	2957 2920 2850	1752	1623	1601 1469	1212 1160	1252
<b>16SB-CH<sub>3</sub></b>	3067 3020	2953 2916 2847	1752	1623	1605 1465	1212 1160	1252
<b>18SB-CH<sub>3</sub></b>	3071 3030	2957 2920 2850	1752	1623	1601 1469	1212 1157	1252

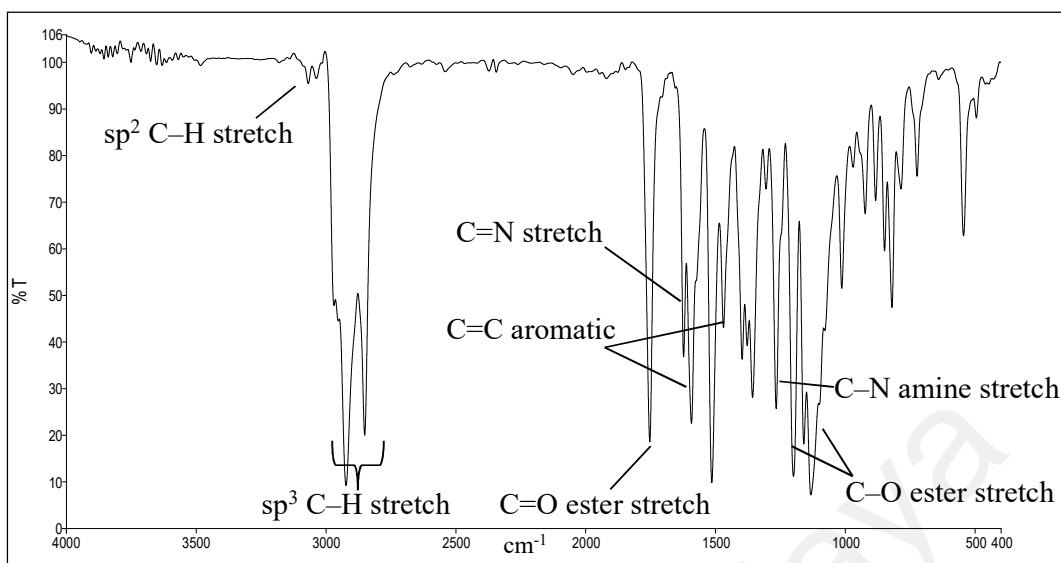


**Figure 4.4: FTIR spectrum of 16SB-NDEA**

**Table 4.5: FTIR spectral analysis data of nSB-NDEA**

Functional group	IR $\nu$ (cm <sup>-1</sup> )						
	sp <sup>2</sup> C-H stretch Aromatic	sp <sup>3</sup> C-H stretch Aliphatic	C=O Ester	C=N Schiff base	C=C Aromatic	C-O Ester	C-N Amine
<b>6SB-CH<sub>3</sub></b>	3064 3038	2960 2931 2854	1756	1627	1594 1469	1205 1138	1267
<b>8SB-CH<sub>3</sub></b>	3071 3038	2969 2949 2931 2867	1752	1623	1591 1469	1197 1135	1267
<b>10SB-CH<sub>3</sub></b>	3063 3034	2979 2949 2924 2854	1756	1620	1601 1469	1205 1138	1256
<b>12SB-CH<sub>3</sub></b>	3071 3038	2971 2927 2854	1756	1623	1594 1469	1197 1138	1267
<b>14SB-CH<sub>3</sub></b>	3067 3038	2968 2927 2854	1756	1623	1594 1469	1197 1135	1267
<b>16SB-CH<sub>3</sub></b>	3067 3041	2968 2924 2854	1756	1623	1594 1469	1197 1131	1267
<b>18SB-CH<sub>3</sub></b>	3071 3038	2971 2924 2854	1756	1623	1594 1469	1201 1131	1267



The  $^1\text{H}$  and  $^{13}\text{C}$  NMR spectra of **12SB-CH<sub>3</sub>**, **10SB-OCH<sub>3</sub>** and **14SB-NDEA** are given in Figures 4.6 – 4.11 and the  $^1\text{H}$  and  $^{13}\text{C}$  NMR spectra data for **nSB-CH<sub>3</sub>**, **nSB-OCH<sub>3</sub>** and **nSB-NDEA** are summarized in Tables 4.6 – 4.11. The spectra of the remaining members in the series are given in Appendix C.  $^1\text{H}$  &  $^{13}\text{C}$  NMR spectral analysis were performed on representative compounds **12SB-CH<sub>3</sub>**, **10SB-OCH<sub>3</sub>** and **14SB-NDEA**. The molecular structures with an atomic numbering scheme for **12SB-CH<sub>3</sub>**, **10SB-OCH<sub>3</sub>** and **14SB-NDEA** are depicted in Figure 4.5.

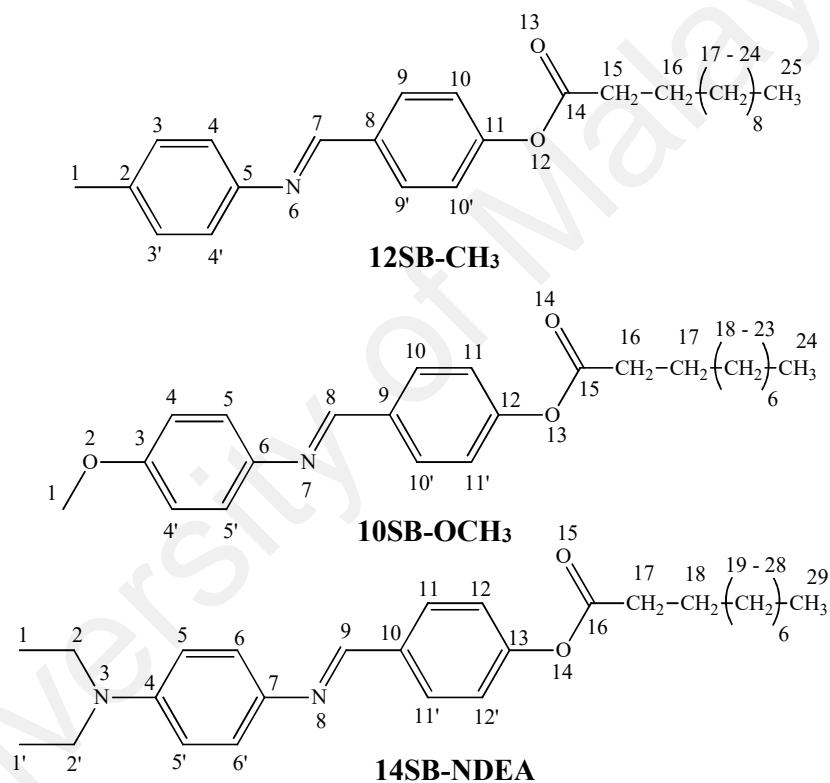


**Figure 4.5: Atomic numbering scheme for 12SB-CH<sub>3</sub>, 10SB-OCH<sub>3</sub> and 14SB-NDEA**

In the  $^1\text{H}$  NMR spectrum of **12SB-CH<sub>3</sub>** (Figure 4.6), a sharp peak appeared as a singlet at chemical shift,  $\delta = 8.37$  ppm can be assigned to the **H7** proton which is located at the carbon atom in the Schiff base linkage ( $-\text{CH}=\text{N}-$ ) (Hagar *et al.*, 2018). This served as an evidence for the successful synthesis of the Schiff base. This peak was located at the most deshielded region due to some local diamagnetic shielding that

caused by the electronegative atom (N) and magnetic anisotropy effect, triggered by the conjugation between the double bond (C=N) and aromatic ring.

In the higher chemical shift region range from chemical shift,  $\delta = 6.50 - 8.00$  ppm, there were a total of four peaks assigned to the hydrogen atoms located at two aromatic rings. The doublet appeared at chemical shift,  $\delta = 7.04 - 7.06$  ppm with an integral of 2 protons assigned to **H4** & **H4'** as it is closer to an electronegative atom, N. The doublet appeared at chemical shift,  $\delta = 7.10 - 7.13$  ppm with an integral of 4 protons was assigned to **H10** & **H10'** to **H3** & **H3'**. This was due to the two doublet peaks were too close and hard to be identified. The remaining doublet appeared at chemical shift,  $\delta = 7.82 - 7.85$  ppm was assigned to **H9** & **H9'** as the proton experienced a stronger electron withdrawing effect from the imine linkage (C=N) and ester linkage (COO).

For the lower chemical shift region, it can be noticed a sharp singlet at chemical shift  $\delta = 2.29$  ppm which was due to a strong magnetic anisotropy effect by aromatic rings toward the methyl group in **H1**. For a triplet present at chemical shift,  $\delta = 2.48 - 2.52$  ppm, it was assigned to **H15** as it was closer to the C=O which experienced a stronger diamagnetic effect. The quintet located at  $\delta = 1.65 - 1.73$  ppm was assigned to **H16** as it is located one bond further from C=O compared to **H15**. Hence, it experienced less diamagnetic effect from the ester linkage. The multiplet at  $\delta = 1.20 - 1.35$  ppm was ascribed to the protons of the long chain alkyl group (**H17** – **H24**). Lastly, the triplet which appeared at the most shielded region,  $\delta = 0.78 - 0.83$  ppm was assigned to the methyl group in the long alkyl chain, **H25**.

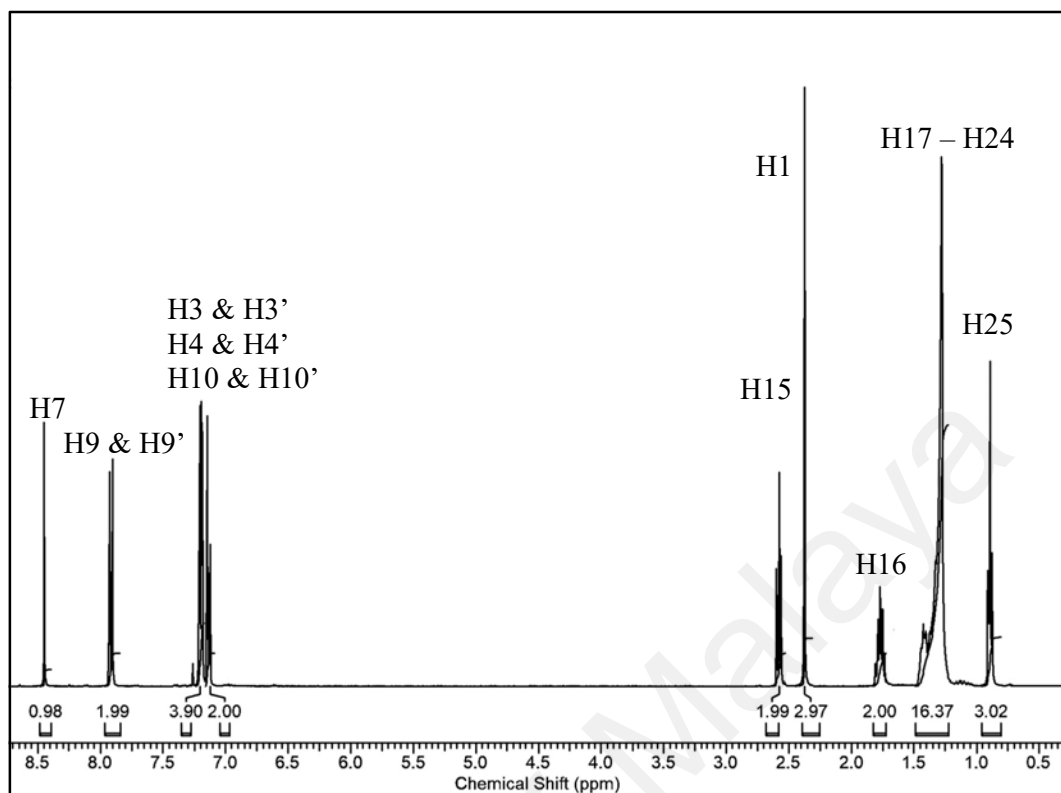


Figure 4.6:  $^1\text{H}$  NMR spectrum of 12SB-CH<sub>3</sub>

Table 4.6:  $^1\text{H}$  NMR spectral data of 12SB-CH<sub>3</sub> in CDCl<sub>3</sub>

Proton number	Chemical shift, $\delta$ ppm	No. of Proton	Multiplicity	Coupling constant, $J$ (Hz)
H7	8.37	1	s	-
H9 & H9'	7.82 – 7.85	2	d	8.6
H3 & H3' <sup>a</sup>	7.11 – 7.13	2	d	8.1
H10 & H10' <sup>a</sup>	7.10 – 7.13	2	d	8.6
H4 & H4'	7.04 – 7.06	2	d	8.3
H15	2.48 – 2.52	2	t	7.5
H1	2.29	3	s	-
H16	1.65 – 1.73	2	q	7.5
H17 – H24	1.20 – 1.35	16	m	-
H25	0.79 – 0.83	3	t	6.8

Note:

<sup>a</sup> the signals attributed to H3 & H3' and H10 & H10' overlap

In the  $^{13}\text{C}$  NMR spectrum of **12SB-CH<sub>3</sub>** (Figure 4.7), deuterated solvent peaks were located at chemical shift,  $\delta = 76.72 - 77.35$  ppm. **C14** atom is an ester carbon bonded with two electronegative oxygen atoms and showed the highest chemical shift peak at  $\delta = 171.98$  ppm following by a resonance signal at chemical shift,  $\delta = 158.34$  ppm which corresponded to the carbon of Schiff base ( $-\text{C}=\text{N}-$ ), **C7**. Eight peaks located between chemical shift,  $\delta = 110.34 - 153.01$  ppm were attributed to the carbon atoms of two aromatic rings. There was a total of four peaks which have higher intensities ( $\delta = 120.80 - 129.86$  ppm) than four other peaks assigned to the four aromatic carbons, **C3 & 3'**, **C4 & 4'**, **C9 & 9'** and **C10 & 10'** atoms. Electron withdrawing effect was greatly influenced the chemical shift and led to higher chemical shift. The peak observed at chemical shift,  $\delta = 153.01$  ppm was assigned to **C11** and carbon with chemical shift,  $\delta = 149.31$  ppm was attributed to **C5**. **C11** possessed a higher chemical shift because it is attached to a more electronegative atom, O bonded to a carbonyl group. The remaining peaks at chemical shift,  $\delta = 135.90$  and  $133.96$  ppm were assigned to **C2 & C8**.

The peak with the chemical shift,  $\delta = 21.01$  ppm was attributed to the **C1** as it is directly attached to an aromatic ring. The peak with the chemical shift  $\delta = 34.45$  ppm was attributed to the **C15** in the dodecanoyloxy chain. It showed the highest chemical shift among all the  $\text{sp}^3$  hybridized carbon atom in the dodecanoyloxy chain due to it being directly attached to the carbonyl group which experienced a strong  $\text{sp}^2$  hybridization effect. **C16** atom was assigned to the chemical shift,  $\delta = 24.95$  ppm. It may due to the hyperconjugation effect with the carbonyl group of the ester linkage. For **C21 – C26** atoms, methylene group along the long chain alkyl groups ( $-\text{CH}_2-$ ) showed several signals in the chemical shift,  $\delta = 22.70 - 31.92$  ppm. The peak at chemical shift,  $\delta = 14.09$  ppm was attributed to the methyl group, **C25** at the end of the long alkanoyloxy chain.

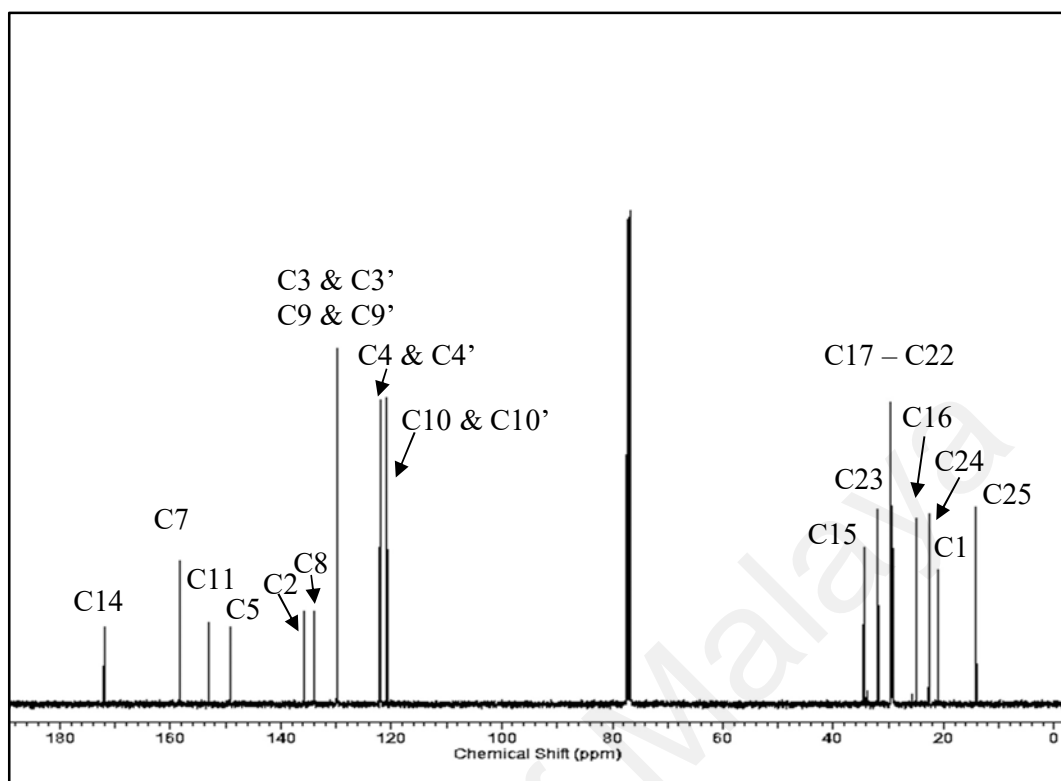


Figure 4.7:  $^{13}\text{C}$  NMR spectrum of 12SB- $\text{CH}_3$

**Table 4.7:**  $^{13}\text{C}$  NMR spectral data of compound 12SB-CH<sub>3</sub> in CDCl<sub>3</sub>

Carbon number	Chemical Shift, $\delta$ ppm
C14	171.98
C7	158.34
C11	153.01
C5	149.31
C2	135.90
C8	133.96
C9 & C9'	129.86
C3 & C3'	129.78
C4 & C4'	122.01
C10 & C10'	120.80
C13	34.45
C23	31.92
	29.61
	29.47
C17 – C22 <sup>a</sup>	29.35
	29.27
	29.12
C16	24.91
C24	22.70
C1	21.02
C25	14.13

<sup>a</sup> some of the signals attributed to C17 – C22 appeared in the same column in the  $^{13}\text{C}$  NMR spectrum which resulted in less than 6 signals observed in the  $^{13}\text{C}$  NMR spectrum

In the  $^1\text{H}$  NMR spectrum of **10SB-OCH<sub>3</sub>** (Figure 4.8), a singlet peak at chemical shift,  $\delta = 8.38$  ppm assigned to proton in Schiff base linkage ( $-\text{CH}=\text{N}-$ ), **H8** (Hagar *et al.*, 2018). This indicated the successful synthesis of the Schiff base.

In the region of chemical shift,  $\delta = 6.50 - 8.00$  ppm, a total of four peaks with a total integral of 8 protons appeared. They can be assigned to the two aromatic rings. The doublet at chemical shift,  $\delta = 6.85 - 6.87$  ppm was assigned to **H4 & H4'** as it is closer to an electronegative oxygen atom of methoxy group. It is less deshielded than other aromatic protons. The doublet at chemical shift,  $\delta = 7.10 - 7.12$  ppm was assigned to **H11 & H11'**. For the doublet with a chemical shift,  $\delta = 7.14 - 7.16$  ppm was ascribed to **H5 & H5'**. The remaining doublet which appeared at chemical shift,  $\delta = 7.82 - 7.84$  ppm was assigned to **H10 & H10'** as the proton experienced a stronger electron withdrawing effect from the imine linkage ( $\text{C}=\text{N}$ ) and ester linkage ( $\text{COO}$ ).

For the lower chemical shift region range from chemical shift,  $\delta = 0.00 - 5.00$  ppm, it can be noticed a sharp singlet at chemical shift,  $\delta = 3.76$  ppm due to strong magnetic anisotropy effect by the aromatic ring toward the methoxy group that attached with an oxygen atom in **H1**. For the triplet present at chemical shift,  $\delta = 2.48 - 2.52$  ppm, it was assigned to **H16** as it is closer to the  $\text{C}=\text{O}$  which experienced a stronger diamagnetic effect. The quintet at chemical shift,  $\delta = 1.65 - 1.73$  ppm was assigned to **H17** as it is located one bond further from the  $\text{C}=\text{O}$  compared to **H15**. Hence, it experienced less diamagnetic effect from the ester linkage. The multiplet at chemical shift,  $\delta = 1.21 - 1.35$  ppm was ascribed by the protons of the long alkyl chain (**H18 - H23**). Lastly, the triplet appeared at the most shielded chemical shift region,  $\delta = 0.80 - 0.83$  ppm was assigned to the methyl group in the long alkyl chain, **H24** (Ha *et al.*, 2014).

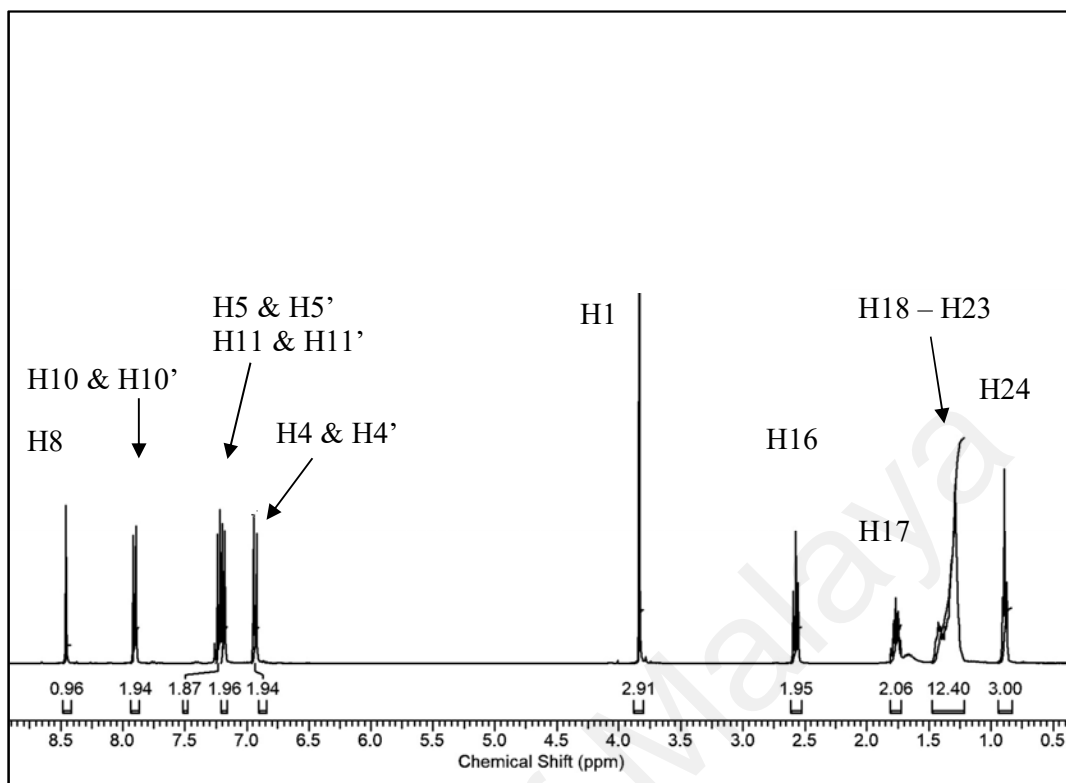


Figure 4.8:  $^1\text{H}$  NMR spectrum of 10SB- $\text{OCH}_3$

Table 4.8:  $^1\text{H}$  NMR data of 10SB- $\text{OCH}_3$

Proton number	Chemical shift, $\delta$ ppm	No. of proton	Multiplicity	Coupling constant, $J$ (Hz)
H8	8.38	1	s	-
H10 & H10'	7.82 – 7.84	2	d	8.6
H5 & H5' <sup>a</sup>	7.14 – 7.16	2	d	8.8
H11 & H11' <sup>a</sup>	7.10 – 7.12	2	d	8.6
H4 & H4'	6.85 – 6.87	2	d	8.8
H1	3.76	3	s	-
H16	2.48 – 2.52	2	t	7.5
H17	1.65 – 1.73	2	q	7.4
H18 – H23	1.21 – 1.35	12	m	-
H24	0.80 – 0.83	3	t	6.8

Note:

<sup>a</sup> the signals attributed to H5 & H5' and H11 & H11' are slightly overlapping each other



In the  $^{13}\text{C}$  NMR spectrum of **10SB-OCH<sub>3</sub>** (Figure 4.9), **C15** atom is an ester carbon that bonded with two electronegative atoms, oxygen, and showed the peak with the highest chemical shift at  $\delta = 172.00$  ppm. The following resonance signal at chemical shift,  $\delta = 157.34$  ppm corresponded to the carbon atom in Schiff base linkage, **C8**.

The remaining eight peaks appeared at chemical shift,  $\delta = 114.41 - 158.34$  ppm were attributed to the aromatic carbon in the two aromatic rings. There are four peaks which have higher intensities ( $\delta = 114.41 - 129.71$  ppm) than the four other peaks were assigned to the four aromatic carbons, **C4 & 4'**, **C5 & 5'**, **C10 & 10'** and **C11 & 11'** atoms. The impact of the electron withdrawing effect was greatly influenced and shifted the peaks to a higher chemical shift. The peak observed at chemical shift,  $\delta = 158.34$  ppm was assigned to **C3** and carbon with chemical shift,  $\delta = 152.87$  ppm was attributed to **C12** as it is directly attached to an electronegative atom O. **C3** has a higher chemical shift due to its direct attachment to the more electronegative atom O attributed to the methoxy group. The remaining peaks at chemical shift,  $\delta = 144.76$  and  $134.06$  ppm were assigned to **C6 & C9**.

The peak with the chemical shift,  $\delta = 55.51$  ppm was attributed to the **C1** as it is directly attached to an electronegative atom. The peak with the chemical shift  $\delta = 34.45$  ppm is attributed to the **C16** in the decanoyloxy chain. It showed the highest chemical shift among all the  $\text{sp}^3$  hybridized carbon atom in the decanoyloxy chain due to its direct attachment with the carbonyl group which experienced a strong  $\text{sp}^2$  hybridization effect. **C17** atom was assigned to the peak with chemical shift,  $\delta = 24.91$  ppm. It may have been due to the hyperconjugation effect with the carbonyl group of the ester linkage. For **C18 - C23** atoms, a long chain of methylene groups ( $-\text{CH}_2-$ )

showed several signals in the chemical shift,  $\delta = 22.70 - 31.92$  ppm. The peak at chemical shift,  $\delta = 14.09$  ppm was attributed to the methyl group, **C24** at the end of the long alkanoyloxy chain.

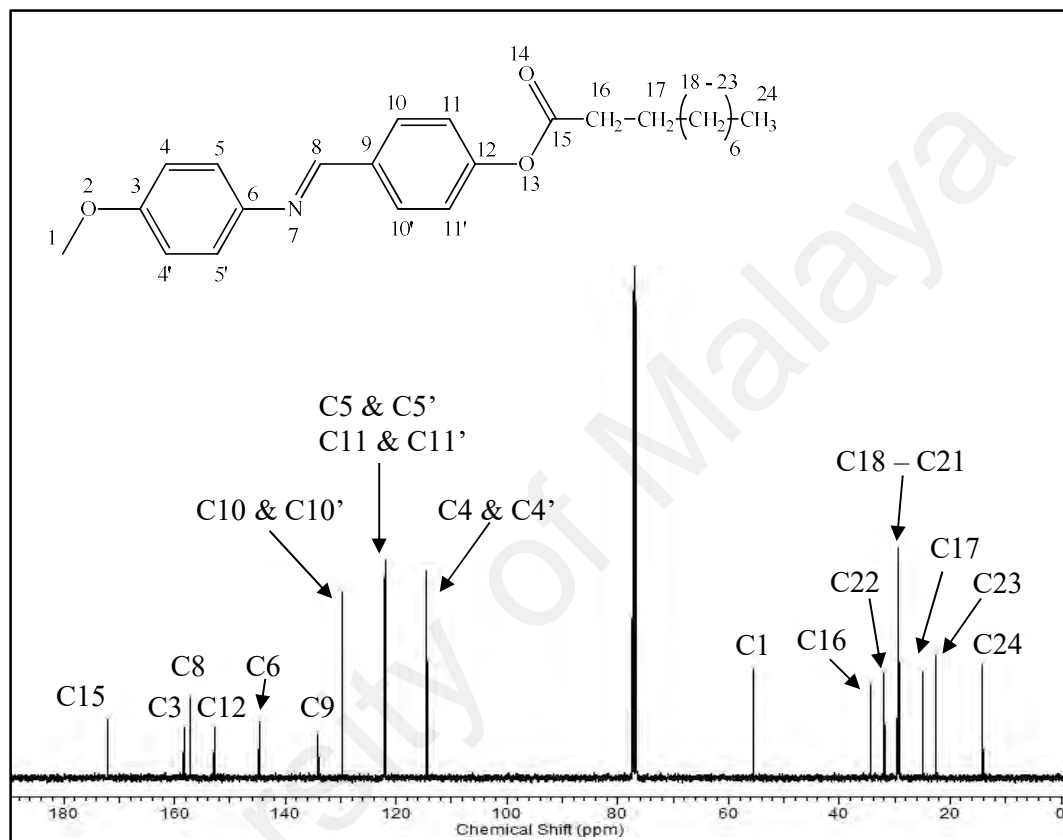


**Figure 4.9:**  $^{13}\text{C}$  NMR spectrum of 10SB-OCH<sub>3</sub>

**Table 4.9:**  $^{13}\text{C}$  NMR data of 10SB-OCH<sub>3</sub>

Carbon number	Chemical Shift, $\delta$ ppm
C15	172.00
C3	158.34
C8	157.16
C12	152.87
C6	144.76
C9	134.06
C10 & C10'	129.71
C5 & C5'	122.20
C11 & C11'	121.99
C4 & C4'	114.41
C1	55.51
C16	34.45
C22	31.86
	29.42
C18 – C21 <sup>a</sup>	29.26
	29.11
C17	24.91
C23	22.68
C24	14.12

<sup>a</sup> some of the signals attributed to C18 – C21 appear in the same column in the  $^{13}\text{C}$  NMR spectrum which resulted in less than 4 signals observed in the  $^{13}\text{C}$  NMR spectrum.

In the  $^1\text{H}$  NMR spectrum of **14SB-NDEA** (Figure 4.10), a sharp singlet peak which appeared at chemical shift,  $\delta = 8.38$  ppm can be assigned to the **H9** proton located at the carbon atom in the Schiff base linkage ( $-\text{CH}=\text{N}-$ ) (Hagar *et al.*, 2018). This suggested that the Schiff base group was successfully formed.

In the high chemical shift region range from chemical shift,  $\delta = 6.50 - 8.00$  ppm, there are four peaks with a total integral of 8 protons which can be assigned to the two aromatic rings. The doublet at chemical shift,  $\delta = 6.61 - 6.64$  ppm was assigned to **H5 & H5'** as it is closer with an electronegative atom, N, ascribed to the diethylamino group. It is less deshielded than other aromatic protons due to the electron donating effect from the diethylamino group. The doublet at chemical shift,  $\delta = 7.08 - 7.10$  ppm was assigned to **H12 & H12'**. For the doublet with a chemical shift,  $\delta = 7.16 - 7.18$  ppm was assigned to **H6 & H6'**. The remaining doublet appeared at chemical shift,  $\delta = 7.80 - 7.82$  ppm is assigned to **H11 & H11'** as the protons experienced a stronger electron withdrawing effect from the imine linkage ( $\text{C}=\text{N}$ ) and ester linkage ( $\text{COO}$ ).

For the lower chemical shift region, a quartet at chemical shift,  $\delta = 3.28 - 3.33$  ppm can be noticed due to a strong electronegative nitrogen atom, N onto **H2**. For the triplet present at chemical shift,  $\delta = 2.47 - 2.51$  ppm, it was assigned to **H17** as it is located closer to the  $\text{C}=\text{O}$  which experienced a stronger diamagnetic effect. The quintet at chemical shift,  $\delta = 1.65 - 1.72$  ppm was assigned to **H18** as it is one bond further from the  $\text{C}=\text{O}$  compared to **H17**. Hence, its experienced a less diamagnetic effect from the ester linkage. The multiplet at chemical shift,  $\delta = 1.19 - 1.35$  ppm was ascribed to the protons of the long alkyl chain (**H19 – H28**). Lastly, the triplet appeared at the most shielded chemical shift region,  $\delta = 0.79 - 0.83$  ppm was assigned to the methyl group in the long alkyl chain, **H29** (Ha *et al.*, 2014).

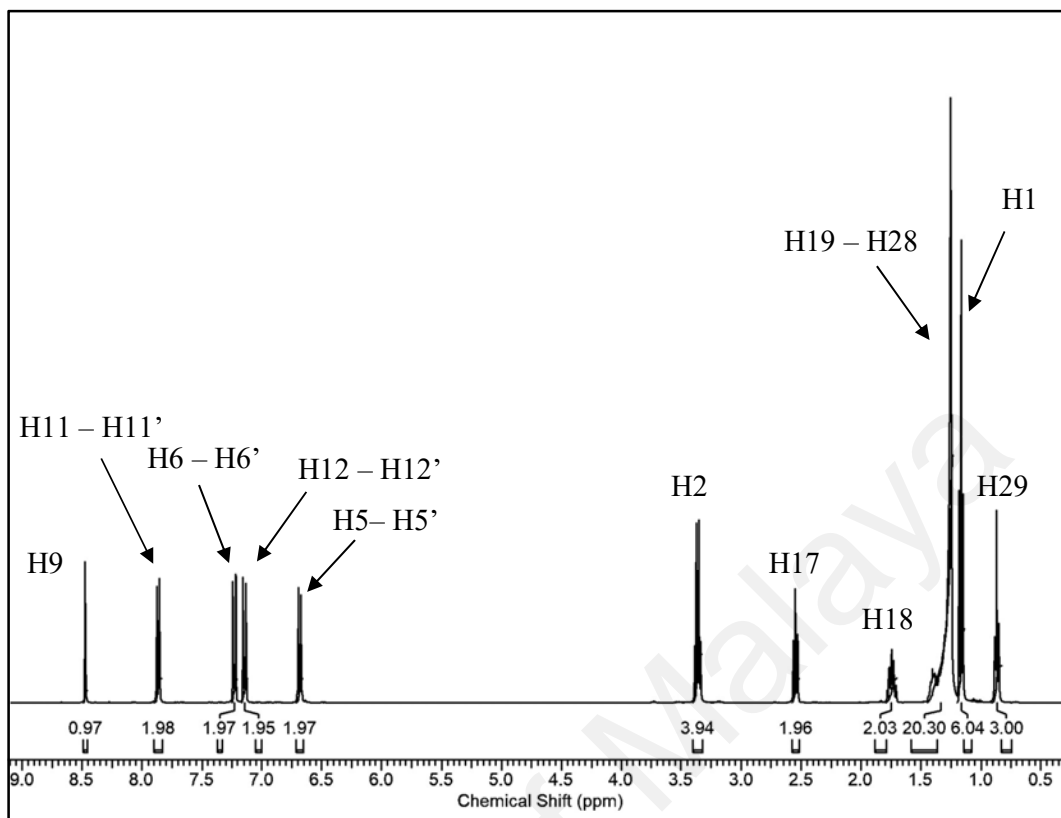


**Figure 4.10:**  $^1\text{H}$  NMR spectrum of 14SB-NDEA

**Table 4.10:**  $^1\text{H}$  NMR data of 14SB-NDEA

Proton number	Chemical shift, $\delta$ ppm	No. of proton	Multiplicity	Coupling constant, $J$ (Hz)
H9	8.42	1	s	-
H11 & H11'	7.80 – 7.82	2	d	8.6
H6 & H6'	7.16 – 7.18	2	d	8.9
H12 & H12'	7.08 – 7.10	2	d	8.6
H5 & H5'	6.61 – 6.64	2	d	9.0
H2	3.28 – 3.33	4	qt	7.1
H17	2.47 – 2.51	2	t	7.5
H18	1.65 – 1.72	2	q	7.4
H19 – H28	1.19 – 1.35	20	m	-
H1	1.09 – 1.13	6	t	7.0
H29	0.79 – 0.83	3	t	6.8

In the  $^{13}\text{C}$  spectrum of **14SB-NDEA** (Figure 4.11), **C16** atom is an ester carbon that is bonded with two electronegative oxygen atoms, O and showed a peak with the highest chemical shift at  $\delta = 172.04$  ppm. The subsequent resonance signal at chemical shift,  $\delta = 153.88$  ppm was corresponded to the carbon in a Schiff base linkage, **C9**.

The remaining eight peaks appeared between chemical shift,  $\delta = 114.41 - 158.34$  ppm were attributed to the aromatic carbons in the two aromatic rings. There are four peaks, which have higher intensities ( $\delta = 112.16 - 129.31$  ppm) than four other peaks, were assigned to the four aromatic carbons, **C5 & 5'**, **C6 & 6'**, **C11 & 11'** and **C12 & 12'**. The peak observed at chemical shift,  $\delta = 152.36$  ppm was assigned to **C13** and carbon with chemical shift,  $\delta = 146.94$  ppm was attributed to **C7** as its direct attachment to the electronegative atoms, O or N with the presence of an electron withdrawing effect. **C4** was directly attached to an electronegative N atom of the diethylamino group and observed at chemical shift,  $\delta = 139.57$  ppm. **C10** was assigned with a chemical shift,  $\delta = 134.66$  ppm.

The peak with the chemical shift,  $\delta = 44.57$  ppm was attributed to the **C2** as it is directly attached to an electronegative atom, N. The peak with the chemical shift  $\delta = 34.45$  ppm was attributed to **C17** in the tetradecanoyloxy chain. It showed the highest chemical shift among all the  $\text{sp}^3$  hybridized carbon atom in the tetradecanoyloxy chain due to its direct attachment to the carbonyl group which experienced a strong  $\text{sp}^2$  hybridization effect. **C18** atom was assigned to chemical shift,  $\delta = 24.92$  ppm. It may have been due to the hyperconjugation effect with the carbonyl group of the ester linkage. A long methylene chain, **C19 – C28** atoms showed several signals in the chemical shift,  $\delta = 22.70 - 31.93$  ppm. The peak at chemical shift,  $\delta = 14.09$  ppm was attributed to the methyl group, **C29** at the end of the long alkanoyloxy chain.

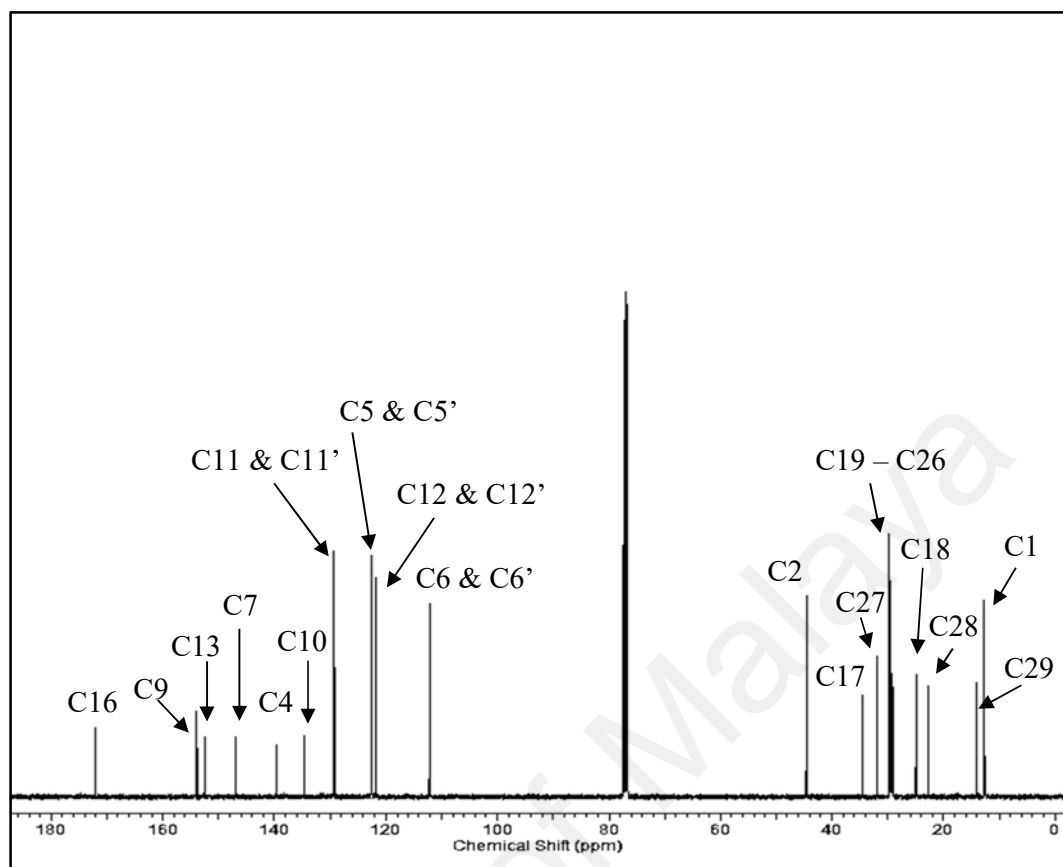


Figure 4.11:  $^{13}\text{C}$  NMR spectrum of 14SB-NDEA

**Table 4.11:**  $^{13}\text{C}$  NMR data of 14SB-NDEA

Carbon number	Chemical Shift, $\delta$ ppm
C16	172.04
C9	153.88
C13	152.36
C7	146.94
C4	139.67
C10	134.66
C11 & 11'	129.31
C5 & 5'	122.58
C12 & 12'	121.85
C6 & 6'	112.16
C2	44.57
C17	34.45
C27	31.93
	29.68
	29.66
	29.60
C19 – C26 <sup>a</sup>	29.47
	29.36
	29.26
	29.12
C18	24.92
C28	22.70
C29	14.12
C1	12.64

<sup>a</sup> some of the signals attributed to C19 – C26 appear in the same column in the  $^{13}\text{C}$  NMR spectrum which resulted in less than 8 signals observed in the  $^{13}\text{C}$  NMR spectrum.

Based on the results obtained from infrared and NMR spectroscopy together with elemental analysis, the structure of **nSB-CH<sub>3</sub>**, **nSB-OCH<sub>3</sub>** and **nSB-NDEA** were confirmed.



#### 4.1.2 Thermal Behavior and Mesomorphic Properties

The study of thermal and mesomorphic properties of **nSB-CH<sub>3</sub>**, **nSB-OCH<sub>3</sub>** and **nSB-NDEA** were carried out using DSC and POM.

##### 4.1.2.1 Series 1A

For the **nSB-CH<sub>3</sub>** series, representative DSC thermograms **10SB-CH<sub>3</sub>**, **14SB-CH<sub>3</sub>** and **18SB-CH<sub>3</sub>** are depicted in Figures 4.12 – 4.14. The phase transition temperatures and associated enthalpy changes ( $\Delta H$ ) obtained from DSC analysis during heating and cooling processes are tabulated in Table 4.12. The remaining DSC thermograms of **nSB-CH<sub>3</sub>** are given in Appendix D.

All synthesized compounds showed liquid crystalline characteristics based on the endotherms and/or exotherms that appeared in DSC thermograms which could be attributed to the crystal-mesophase and mesophase-isotropic transitions or vice versa. There was only an endotherm peak found in the **nSB-CH<sub>3</sub>** compounds which corresponding to the crystal-isotropic liquid phase during heating cycle. For the subsequent cooling cycle of compounds demonstrated exotherms characteristic of the isotropic-mesophase and mesophase-crystal transitions. This phenomenon was term as monotropic.

*N*-hexanoyloxy derivative is a non-mesogenic compound which displayed direct melting from crystal into isotropic liquid and vice versa. It may have been due to the *n*-hexanoyloxy chain being not enough long to provide significant flexibility to the mesogenic core, thereby reducing the possibility of generating a mesophase. *N*-

octanoyloxy, *n*-decanoyloxy, *n*-dodecanoyloxy and *n*-tetradecanoyloxy derivatives exhibited the monotropic nematic phase. The mesophase was identified through the existence of nematic droplets which coalesced to form a nematic phase with thread-like properties (Ha *et al.*, 2010). An interesting behavior was observed for *n*-dodecanoyloxy and *n*-tetradecanoyloxy in that they exhibited an additional focal-conic fan shaped textures which assigned as SmA after the formation of the nematic phase. Upon further cooling, the transition bars from SmA-SmB phase were observed for *n*-tetradecanoyloxy derivatives (Ha *et al.*, 2012).

The textures of the mesophase can be observed under a polarized optical microscope (POM). It was found that a nematic droplet was formed during cooling from isotropic liquid and show a thread-like texture. The longer member like the *n*-tetradecanoyloxy derivative showed the transition of the thread-like nematic phase into the fan-shaped texture of SmA. It is further transited into the mosaic texture of SmB (Dierking, 2003, Gray & Goodby, 1984) phase through a unique bar transition (Ha *et al.*, 2010, Ha *et al.*, 2012). The optical photomicrographs of **12SB-CH<sub>3</sub>** and **14SB-CH<sub>3</sub>** are depicted in Figures 4.15 – 4.16.

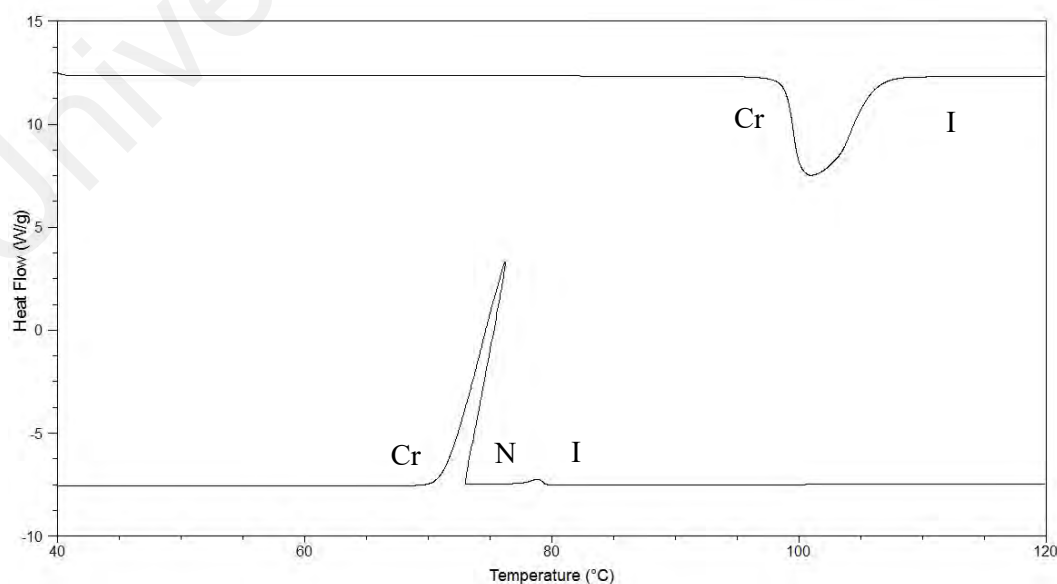


**Figure 4.12: DSC thermogram of 10SB-CH<sub>3</sub>**

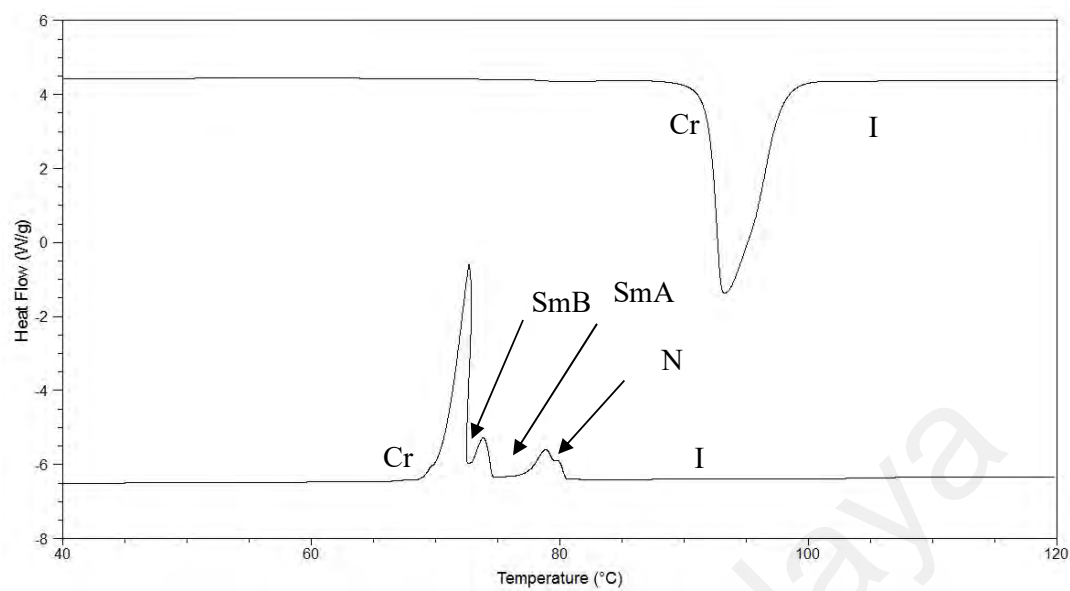


**Figure 4.13: DSC thermogram of 14SB-CH<sub>3</sub>**

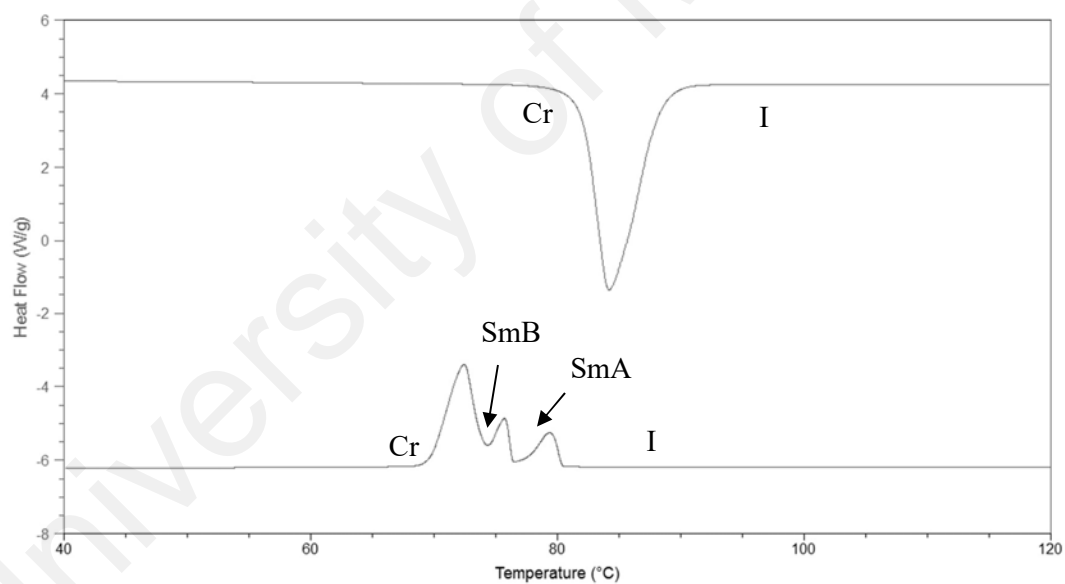


**Figure 4.14: DSC thermogram of 18SB-CH<sub>3</sub>**

**Table 4.12: Phase transition temperatures and associated enthalpy changes of series nSB-CH<sub>3</sub>**

Compound	Phase transition, °C
	(Corresponding enthalpy changes, kJ mol <sup>-1</sup> )
6SB-CH <sub>3</sub>	Cr 106.69 (37.82) I <i>I</i> 83.97 (36.52) <i>Cr</i>
8SB-CH <sub>3</sub>	Cr 100.58 (46.87) I <i>I</i> 83.50 <sup>a</sup> <i>N</i> 80.25 (42.60) <i>Cr</i>
10SB-CH <sub>3</sub>	Cr 100.97 (53.40) I <i>I</i> 79.51 (1.25) <i>N</i> 76.26 (46.99) <i>Cr</i>
12SB-CH <sub>3</sub>	Cr 84.03 (52.42) I <i>I</i> 80.53 (7.82) <i>N</i> 76.45 (6.77) <i>SmA</i> 74.04 (30.60) <i>Cr</i>
14SB-CH <sub>3</sub>	Cr 93.27 (58.21) I <i>I</i> 80.36 (0.34) <i>N</i> 79.48 (1.98) <i>SmA</i> 74.55 (4.66) <i>SmB</i> 72.72 (32.36) <i>Cr</i>
16SB-CH <sub>3</sub>	Cr 95.32 (59.88) I <i>I</i> 79.76 (5.29) <i>SmA</i> 77.90 <sup>a</sup> <i>SmB</i> 75.96 (42.36) <i>Cr</i>
18SB-CH <sub>3</sub>	Cr 84.21 (65.31) I <i>I</i> 80.33 (8.14) <i>SmA</i> 76.34 (5.93) <i>SmB</i> 73.81 (31.78) <i>Cr</i>

<sup>a</sup> denotes as data acquired from POM

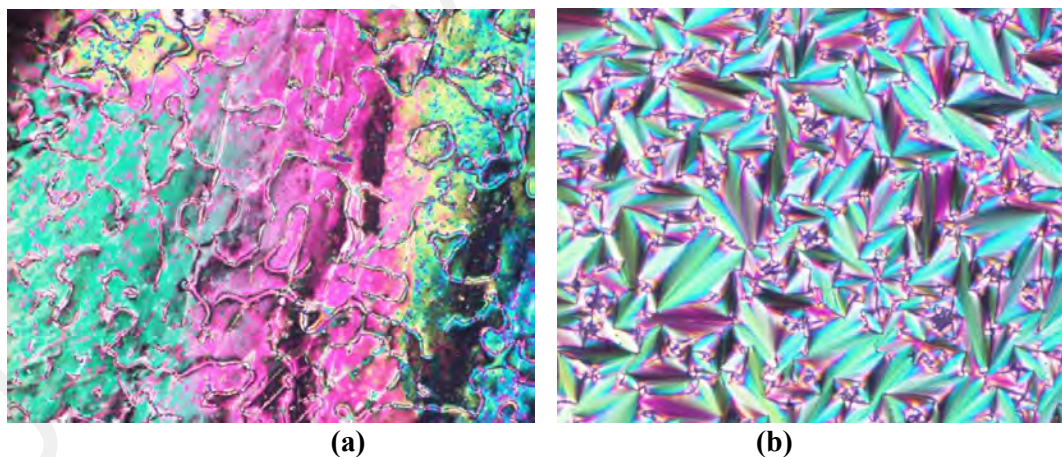


**Figure 4.15: Optical photomicrographs of compound 12SB-CH<sub>3</sub> exhibiting nematic phase during cooling cycle**

- (a) Nematic phase with thread-like texture at 78 °C
- (b) Smectic A phase with fan-shaped texture at 75 °C

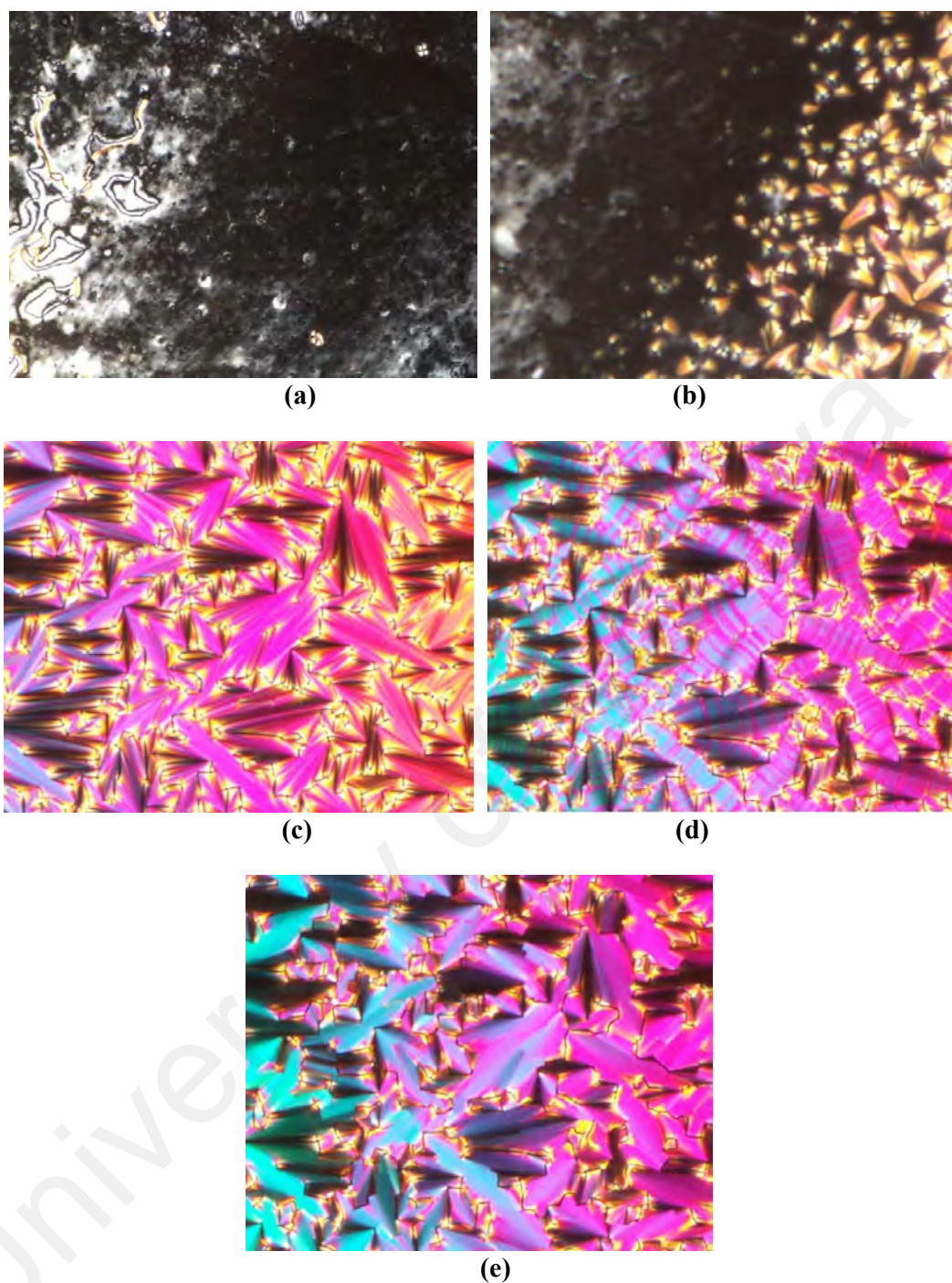


**Figure 4.16:** Optical photomicrographs of compound 14SB-CH<sub>3</sub> exhibiting nematic phase during cooling cycle

- (a) Nematic phase at 80 °C
- (b) Transition of nematic to SmA batonnet at 79 °C
- (c) SmA phase with fan-shaped texture at 75 °C
- (d) Bar transition to SmA-SmB at 74 °C
- (e) SmB phase with fan-shaped texture at 72 °C

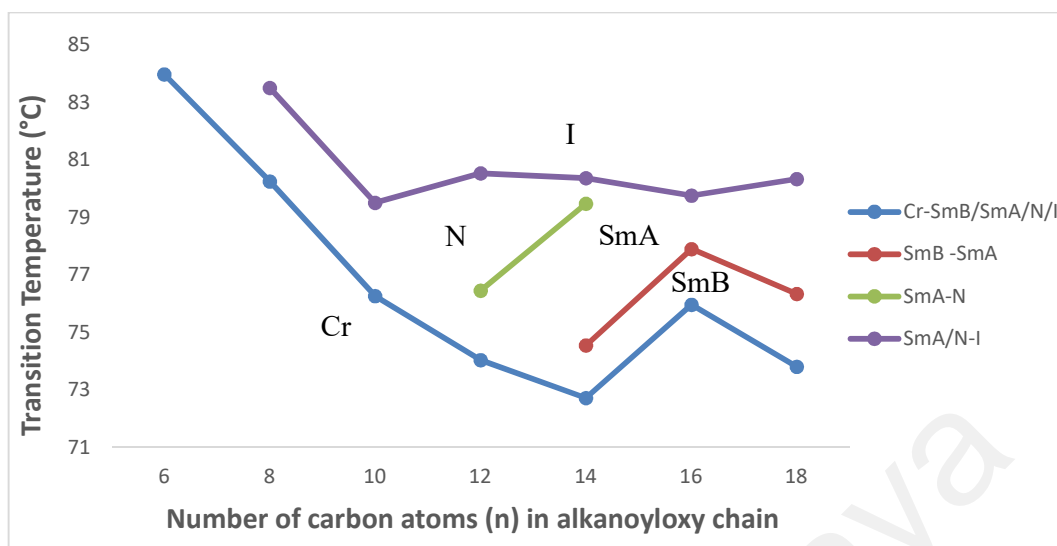


**Figure 4.17: Plot of transition temperatures of  $n\text{SB-CH}_3$  during cooling cycle as a function of the number of carbon atoms**

A graph of phase transition temperature during cooling cycle against number of carbon atoms in the chain is plotted. The cooling cycle is used to plot as the phase transition temperature and their range are more prominent comparing to the heating cycle. More information can be extracted from the cooling cycle.

The nematic phase was observed for  $n$ -hexanoyloxy to  $n$ -tetradecanoyloxy derivatives. As the number of carbon atoms in the chain increased, the nematic phase stability ( $T_N$ ) decreased. The flexibility of the molecules increased with the number of carbons. This excessive flexibility may have been due to the extra long alkanoyloxy chain which tended to disrupt the orientation of molecular packing required for nematic phase generation. In other words, a longer alkanoyloxy chain favoured in a lamellar packing which led to the presence of the smectic phase (Yeap *et al.*, 2006). Therefore, the SmA phase was observed in  $n$ -dodecanoyloxy and  $n$ -tetradecanoyloxy to  $n$ -octadecanoyloxy chains showed an additional SmB phase.



#### 4.1.2.2 Series 1B

For the **nSB-OCH<sub>3</sub>** series, representative DSC thermograms of **12SB-OCH<sub>3</sub>** and **16SB-OCH<sub>3</sub>** are depicted in Figures 4.18 and 4.19. The phase transition temperatures and associated enthalpy changes ( $\Delta H$ ) obtained from DSC analysis during the heating and cooling process of **nSB-OCH<sub>3</sub>** are tabulated in Table 4.13. The remaining DSC thermograms of **nSB-OCH<sub>3</sub>** are given in Appendix D.

All members of **nSB-OCH<sub>3</sub>** exhibited the nematic phase either in enantio- or monotropic. Early members ( $n = 6, 8, 10$  &  $12$ ) of the homologous series displayed enantiotropic behavior, there were one endotherm and exotherms each during heating and cooling cycles as illustrated by the DSC thermogram of **12SB-OCH<sub>3</sub>**. As for the subsequent members ( $n = 14, 16$  &  $18$ ), they showed only one endotherm for heating while remained two exotherms in cooling. This was well illustrated by the representative compound, **16SB-OCH<sub>3</sub>**.

The texture of the mesophase was observed via polarized optical microscopy (POM). It was found that the nematic droplets were formed during the cooling of isotropic liquid and showed a thread-like texture (Dierking, 2003) which has showed some similarity to the reported structures (Yeap *et al.*, 2006, Ha *et al.*, 2010). The optical micrograph of **nSB-OCH<sub>3</sub>** depicted in the Figure 4.20.

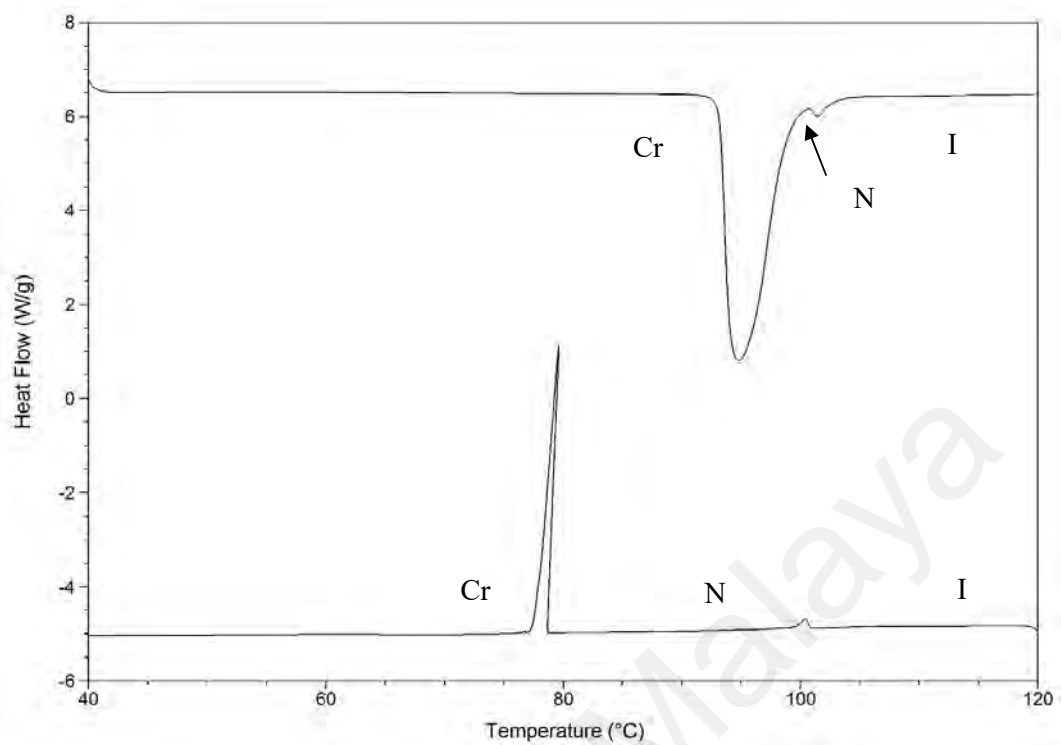


**Figure 4.18: DSC thermogram of 12SB-OCH<sub>3</sub>**

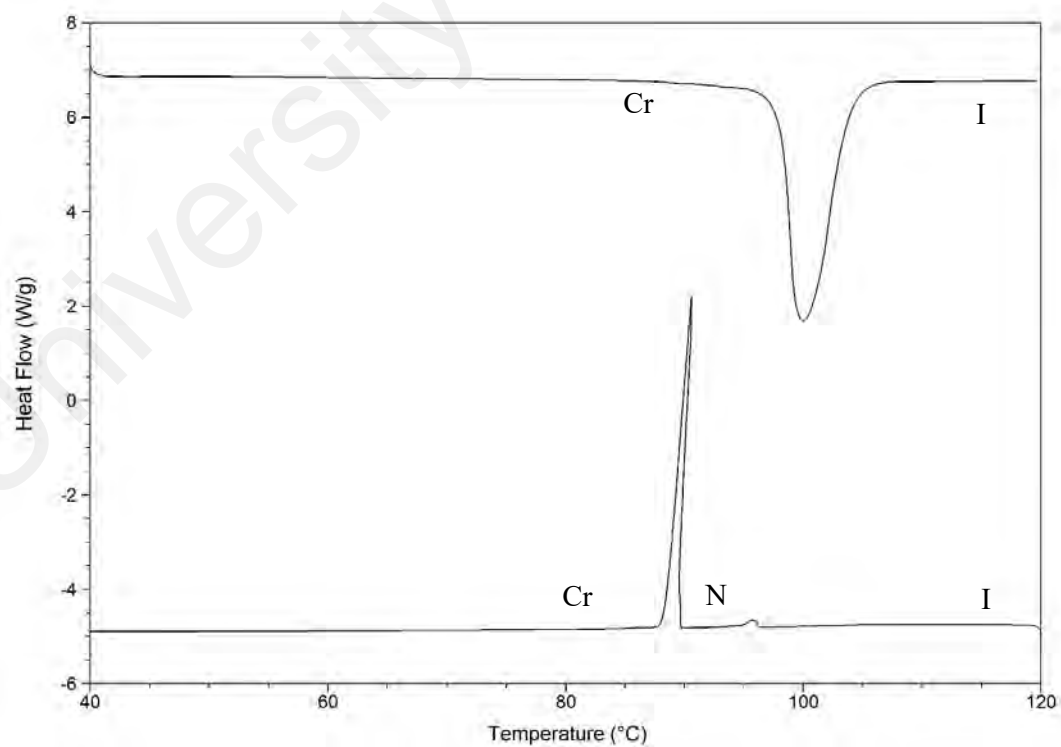


**Figure 4.19: DSC thermogram of 16SB-OCH<sub>3</sub>**



**Table 4.13: Phase transition temperatures and associated enthalpy changes of series nSB-OCH<sub>3</sub>**

Compound	Phase transition, °C
	(Corresponding enthalpy changes, kJ mol <sup>-1</sup> )
<b>6SB-OCH<sub>3</sub></b>	Cr 90.9 (40.10) N 98.2 (0.56) I <i>I 96.5 (0.12) N 64.8 (38.01) Cr</i>
<b>8SB-OCH<sub>3</sub></b>	Cr 97.7 (45.31) N 104.7 (0.69) I <i>I 103.7 (0.24) N 71.9 (44.22) Cr</i>
<b>10SB-OCH<sub>3</sub></b>	Cr 90.4 (35.56) N 101.0 (0.85) I <i>I 99.0 (0.72) N 73.6 (34.80) Cr</i>
<b>12SB-OCH<sub>3</sub></b>	Cr 94.8 (50.79) N 101.5 (1.12) I <i>I 100.8 (0.83) N 79.6 (50.62) Cr</i>
<b>14SB-OCH<sub>3</sub></b>	Cr 100.5 (54.09) I <i>I 99.1 (1.24) N 86.1 (50.54) Cr</i>
<b>16SB-OCH<sub>3</sub></b>	Cr 100.6 (57.14) I <i>I 96.2 (1.56) N 90.6 (54.58) Cr</i>
<b>18SB-OCH<sub>3</sub></b>	Cr 98.2 (63.34) I <i>I 95.9 (1.79) N 90.8 (58.80) Cr</i>

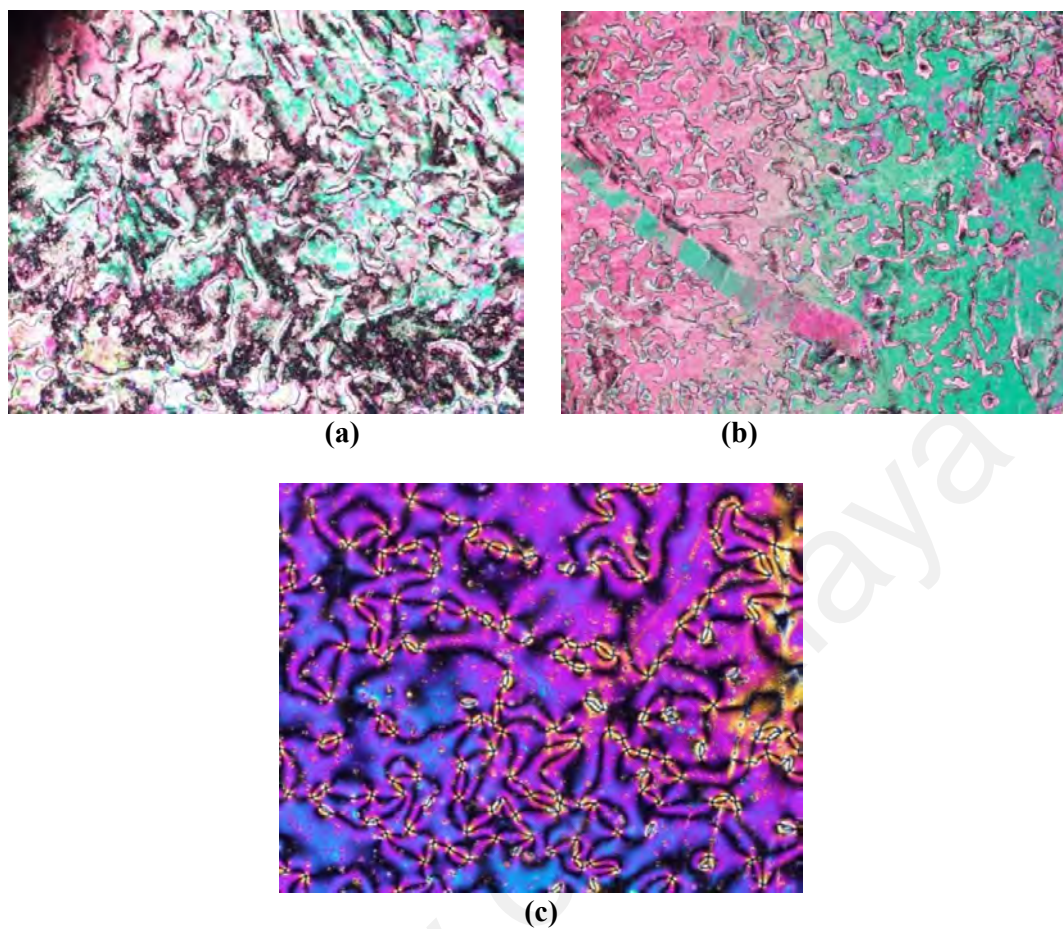


**Figure 4.20: Optical photomicrographs of compounds nSB-OCH<sub>3</sub> exhibiting nematic phase during cooling cycle**

- (a) Nematic phase for 10SB-OCH<sub>3</sub> at 93.5 °C
- (b) Nematic phase for 12SB-OCH<sub>3</sub> at 94.0 °C
- (c) Nematic phase for 16SB-OCH<sub>3</sub> at 92.5 °C

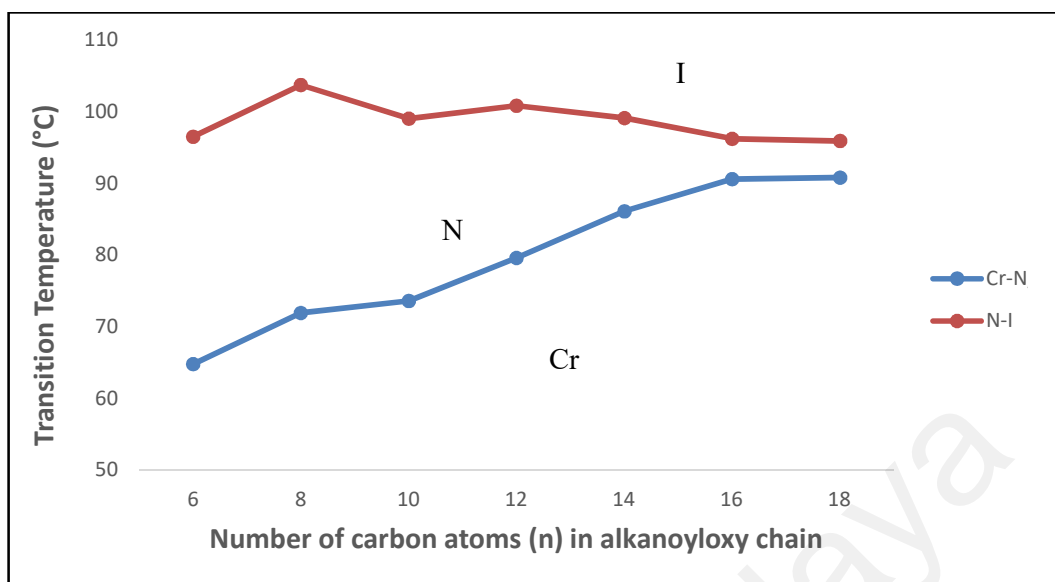


**Figure 4.21: Plot of transition temperatures of  $n\text{SB-OCH}_3$  during cooling cycle as a function of the number of carbon atoms**

As the carbon length increased in Figure 4.21, the clearing temperatures of  $n\text{SB-OCH}_3$  showed a decreasing trend. Due to the presence of methoxy group which serves as a blockage group to the mesogenic core group. Hence, it will reduce the rigidity of the core and lowering the interaction force between the molecules, as a similar behavior reported recently (Foo *et al.*, 2018). Increase flexibility in alkanoyloxy chain has reduced the interaction between molecules and, thus, reduced the isotropization temperature. However, the melting temperatures showed an increasing trend. This may have arisen due to the strength of the van der Waals force which held the molecules strongly and extra energy needed to separate the molecules (Ha *et al.*, 2010). As the length of carbon increase, the structure becomes longer and favorable in lamellar packing which has reduced the stability of nematic phase. This is illustrated in Figure 4.21 showing that the nematic phase stability is lower when the number of carbons increase. In conclusion, alkanoyloxy derivatives become more orderly in their packing when the chain is lengthened (Foo *et al.*, 2018).

### 4.1.2.3 Series 1C

For the **nSB-NDEA** series, representative DSC thermograms of **12SB-NDEA** and **16SB-NDEA** are depicted in Figures 4.22 – 4.23. The phase transition temperatures and associated enthalpy changes ( $\Delta H$ ) obtained from DSC analysis during heating and cooling processes of **nSB-NDEA** are tabulated in Table 4.14. The remaining DSC thermograms of **nSB-NDEA** are given in Appendix D.

All members of **nSB-NDEA** were found to be non-mesogenic compounds. They exhibited an endotherm peak and an exotherm peak during heating and cooling cycles in DSC thermograms. This observed by direct melting behavior of the crystal phase into the isotropic liquid phase from the DSC thermogram and further confirmed with polarizing optical microscopy. The crystal phase changed into dark isotropic region when heated and no liquid crystal texture detected during cooling.

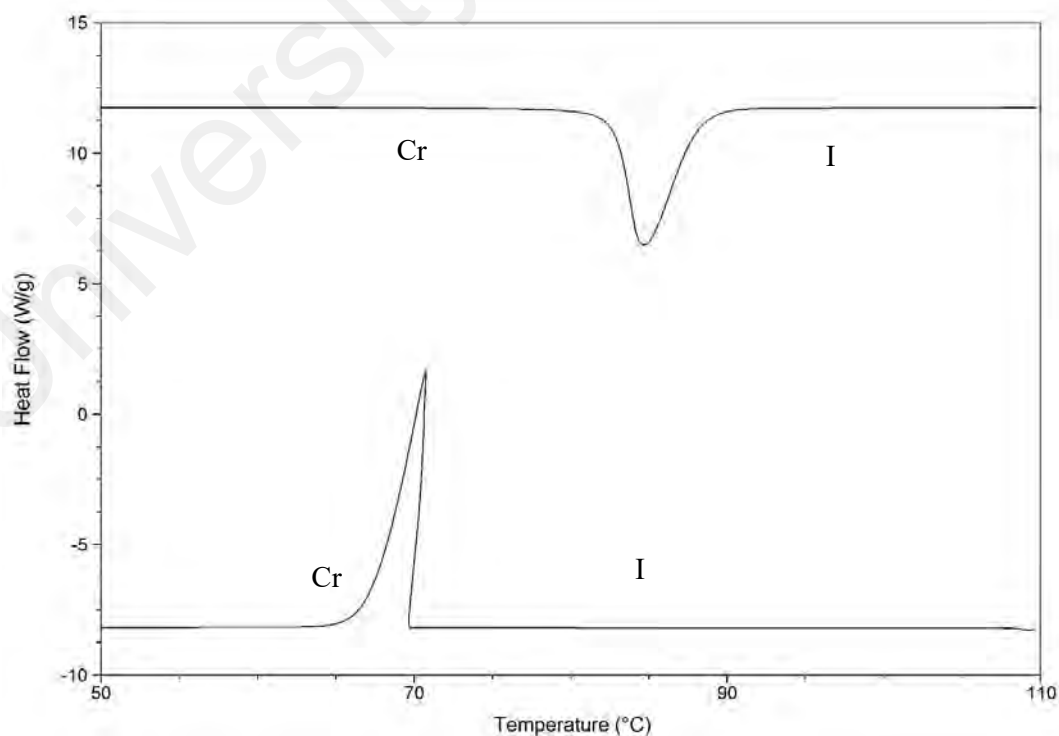


**Figure 4.22: DSC thermogram of 12SB-NDEA**

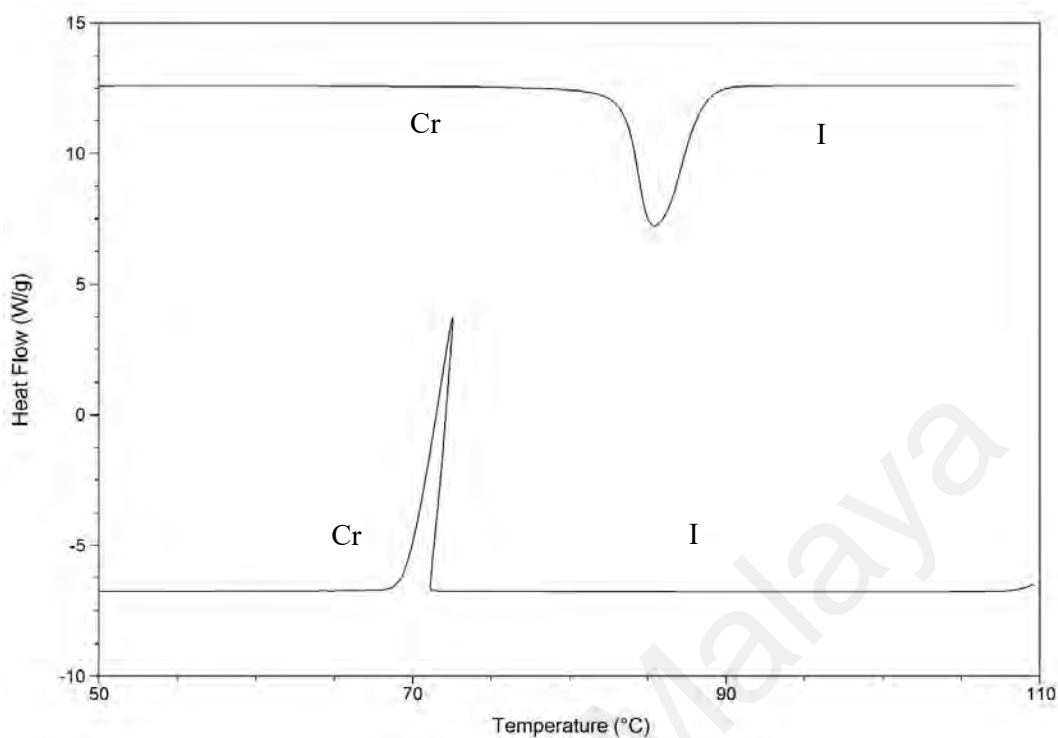


Figure 4.23: DSC thermogram of 14SB-NDEA

Table 4.14: Phase transition temperatures and associated enthalpy changes of series nSB-NDEA

Compound	Phase transition, °C
	(Corresponding enthalpy changes, kJ mol <sup>-1</sup> )
6SB- NDEA	Cr 80.3 (31.97) I
	I 58.7 (29.75) Cr
8SB- NDEA	Cr 85.6 (36.11) I
	I 57.9 (32.73) Cr
10SB- NDEA	Cr 76.0 (49.57) I
	I 62.5 (46.75) Cr
12SB- NDEA	Cr 84.7 (50.43) I
	I 70.7 (49.66) Cr
14SB- NDEA	Cr 85.4 (54.05) I
	I 72.5 (50.98) Cr
16SB- NDEA	Cr 87.8 (59.70) I
	I 72.2 (61.57) Cr
18SB- NDEA	Cr 85.2 (71.97) I
	I 73.2 (68.61) Cr

### 4.1.3 Chemical Structure-Liquid Crystal Property Relationship

The relationship between the chemical structure and liquid crystal property of **12SB-CH<sub>3</sub>** and **12SB-OCH<sub>3</sub>** can be compared with the compounds studied in the literature.

**Table 4.15: Molecular structure of mesomorphic properties of 12SB-CH<sub>3</sub>, 12SB-OCH<sub>3</sub>, compound A, B and C.**

Transition temperature	Reference
<p><b>I 80.5 °C N 76.5 °C SmA 74.0 °C Cr</b></p>	<b>12SB-CH<sub>3</sub></b>
<p><b>I 100.8 °C N 79.6 °C Cr</b></p>	<b>12SB-OCH<sub>3</sub></b>
<p><b>I 104.8 °C SmA 78.0 °C SmB 42.1 °C Cr</b></p>	<b>A</b> (Ha <i>et al.</i> , 2010)
<p><b>I 108.8 °C SmA 90.8 °C SmB 53.5 °C Cr</b></p>	<b>B</b> (Ha <i>et al.</i> , 2012)
<p><b>I 102.0 °C SmA 98.9 °C SmB 84.3 °C Cr</b></p>	<b>C</b> (Ha <i>et al.</i> , 2011)

There is close relation between mesomorphism and molecular structure. By comparing **12SB-CH<sub>3</sub>** and **12SB-OCH<sub>3</sub>** with compound **A**, **B** and **C**, it was found that the type of terminal substituent had great impact on the mesomorphism. In compound

**A**, **B** and **C**, halogen groups (**Cl**, **Br** and **I**) were used. They were considered as the electronegative groups which provide polarizability to the molecular structures. They were highly enhanced the anisotropy effect, which were later increased the lateral interaction. Hence, it is favor in lamellar packing (smectic arrangement). Even though, there was an electronegative oxygen, **O**, present in **12SB-OCH<sub>3</sub>**, the structure still favors in nematic phase. This can be explained by the methoxy group was bulky enough to disrupt the lamellar packing which required by the smectic arrangement. Unlike **12SB-OCH<sub>3</sub>**, the methyl group in **12SB-CH<sub>3</sub>** was small and less bulky compared to methoxy group but not as polar as halogen groups. Hence, **12SB-CH<sub>3</sub>** showed an intermediate properties whereby both nematic and smectic phase were existed in the compound.

By comparing structure **A**, **B** and **C** with **12SB-CH<sub>3</sub>**, both the four structures exhibited SmA phase. The clearing temperature of **12SB-CH<sub>3</sub>** was different from the other three structures. Structure **A**, **B** and **C** showed their clearing temperature at 104.8 °C, 108.8 °C and 102.0 °C, where **12SB-CH<sub>3</sub>** showed clearing temperature at 80.5 °C. A different of about 20 °C was given by the four structures. This may due to the anisotropy effect of the mesogenic core group which structure **A**, **B** and **C** having larger size with the stronger force of attraction. Hence, more energy is required to change the phases. Besides that, Table 4.15. SmA phase for structure **A**, **B** and **C** appeared at 104.8 °C, 108.8 °C and 102.0 °C, respectively, whereas SmA phase only started to form at 74.0 °C **12SB-CH<sub>3</sub>**. There is a different of about 30 °C on the transition temperature for the mesophase. This result revealed that liquid crystal properties is greatly affected by the types of group appeared in the structure.

## 4.2 Series 2

The chemical structure of **nSHB-OCH<sub>3</sub>** is given in Figure 4.24 and the percentage yields are summarized in Table 4.16.

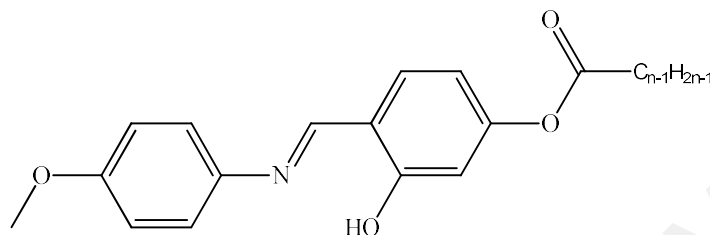


Figure 4.24: Structural formula of **nSHB-OCH<sub>3</sub>**

Table 4.16: Percentage yields for **nSHB-OCH<sub>3</sub>**

Compound	Yield (%)
<b>6SHB-OCH<sub>3</sub></b>	30
<b>8SHB-OCH<sub>3</sub></b>	38
<b>10SHB-OCH<sub>3</sub></b>	40
<b>12SHB-OCH<sub>3</sub></b>	43
<b>14SHB-OCH<sub>3</sub></b>	58
<b>16SHB-OCH<sub>3</sub></b>	56
<b>18SHB-OCH<sub>3</sub></b>	63

### 4.2.1 Structural Elucidation

Structural elucidation of compounds, **nSHB-OCH<sub>3</sub>** was established by using various spectroscopic techniques including FTIR, <sup>1</sup>H NMR, <sup>13</sup>C NMR and micro-elemental analysis. The purities of **nSHB-OCH<sub>3</sub>** were monitoring by TLC analysis. Elemental analysis was performed and the data are tabulated in Table 4.17. Overall, the analytical data were in agreed with calculated values (within 0.5%). The molecular



formula of **nSHB-OCH<sub>3</sub>** has been suggested according to the data mentioned above together with those obtained from the spectral analysis discussed later in this section.

**Table 4.17: Micro-elemental analytical data of nSHB-OCH<sub>3</sub>**

n	Experimental analysis found ( <i>calculated</i> ) / %					
	C		H		N	
<b>6</b>	70.09	<b>(70.36)</b>	6.90	<b>(6.79)</b>	4.01	<b>(4.10)</b>
<b>8</b>	71.31	<b>(71.52)</b>	7.49	<b>(7.37)</b>	3.70	<b>(3.79)</b>
<b>10</b>	72.15	<b>(72.52)</b>	7.94	<b>(7.86)</b>	3.46	<b>(3.52)</b>
<b>12</b>	73.14	<b>(73.38)</b>	8.32	<b>(8.29)</b>	3.27	<b>(3.29)</b>
<b>14</b>	73.84	<b>(74.14)</b>	8.73	<b>(8.67)</b>	3.03	<b>(3.09)</b>
<b>16</b>	74.63	<b>(74.81)</b>	9.05	<b>(9.00)</b>	2.87	<b>(2.91)</b>
<b>18</b>	75.45	<b>(75.40)</b>	9.35	<b>(9.29)</b>	2.70	<b>(2.75)</b>

The infrared spectrum of **12SHB-OCH<sub>3</sub>** is given in Figure 4.25 and the selected data for **nSHB-OCH<sub>3</sub>** are summarized in Table 4.18. The spectra of remaining members are given in Appendix B.

From the infrared spectrum of **12SHB-OCH<sub>3</sub>**, the sharp and strong absorption peaks appeared at wavenumber of 2953, 2916 and 2850 cm<sup>-1</sup> were assigned to the methyl (-CH<sub>3</sub>) and methylene groups (-CH<sub>2</sub>-) of the long alkyl chain. The characteristic absorption peak of the carbonyl group (C=O) of the ester group was given as a sharp peak at wavenumber, 1759 cm<sup>-1</sup> and further confirmed by the presence of two sharp peaks at wavenumbers of 1197 and 1175 cm<sup>-1</sup> due to the C-O of the ester linkage. One of the peaks had a higher absorption intensity than the other one. This observation confirmed that the esterification was successful.

Apart from the corresponding peaks for the alkanoyloxy chain, the peak present at  $1634\text{ cm}^{-1}$  was assigned for the characteristic Schiff base imine linkage ( $\text{CH=N-}$ ) that connected both aromatic rings. The  $\text{sp}^2$  C–H hybridization stretching for two aromatic rings in the **12SHB-OCH<sub>3</sub>** appeared at  $3067\text{ cm}^{-1}$  and this peak assignment was further strengthened by the peaks at  $1602$  and  $1467\text{ cm}^{-1}$  which are characteristic signals of the carbon-carbon double bond ( $\text{C=C}$ ) of aromatic ring. These showed that the imination process had been successfully performed and the imine linkage had been introduced into the part of the structure of **12SHB-OCH<sub>3</sub>**.

The peak present at  $1248\text{ cm}^{-1}$  was assigned to the ether linkage that connected both aromatic rings together with a methyl group. This suggested that the substituent group, methoxy group was still present in the structure. The broad peak at  $3445\text{ cm}^{-1}$  was due to the presence of a lateral hydroxy group ( $\text{-OH}$ ). This can be further confirmed by the present of C–O stretch for phenol at  $1257\text{ cm}^{-1}$  together with a broad peak at  $1400 - 1300\text{ cm}^{-1}$  due to the C–O – H bond of the phenol group. These had evidenced that the hydroxy group was present in the structure. The several peak located between wavenumber  $900 - 800\text{ cm}^{-1}$  indicated that the aromatic ring is 1,2,4-trisubstituted (Pavia *et al.*, 2001) which match the structure of **12SHB-OCH<sub>3</sub>**.

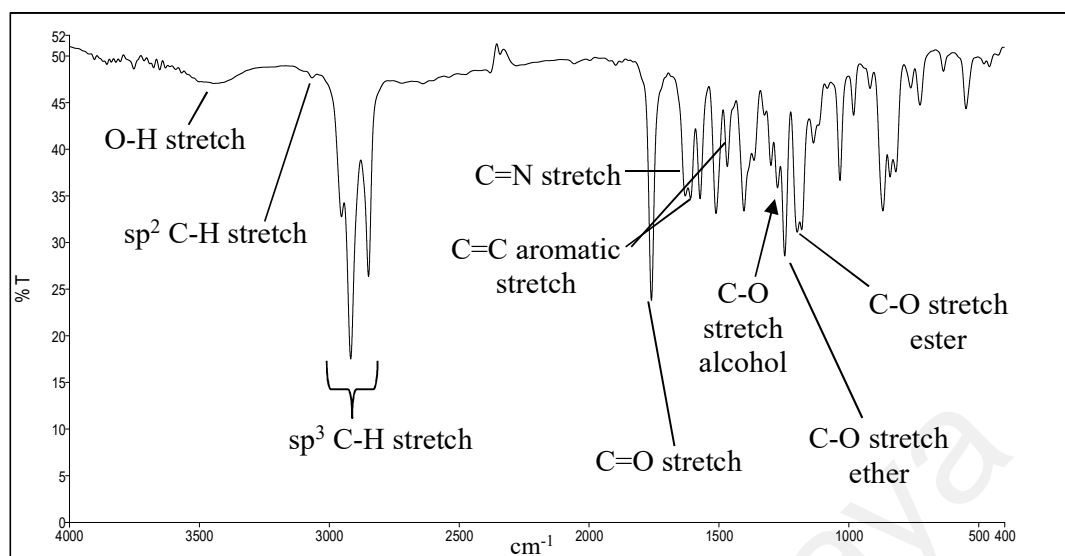


**Figure 4.25: FTIR spectrum of 12SHB-OCH<sub>3</sub>**

**Table 4.18: FTIR spectral data of nSHB-OCH<sub>3</sub>**

Functional group	IR $\nu$ (cm <sup>-1</sup> )						
	6SHB-CH <sub>3</sub>	8SHB-CH <sub>3</sub>	10SHB-CH <sub>3</sub>	12SHB-CH <sub>3</sub>	14SHB-CH <sub>3</sub>	16SHB-CH <sub>3</sub>	18SHB-CH <sub>3</sub>
O-H stretch	3438	3445	3474	3445	3504	3449	3445
sp <sup>2</sup> C-H stretch (Aromatic)	3064	3067	3063	3067	3067	3067	3071
sp <sup>3</sup> C-H stretch (Aliphatic)	2953 2924 2850	2957 2927 2865	2918 2953 2847	2953 2916 2850	2953 2920 2847	2957 2916 2846	2953 2916 2850
C=O (Ester)	1756	1759	1760	1759	1759	1763	1759
C=N (Schiff base)	1620	1620	1623	1634	1627	1627	1631
C=C (Aromatic)	1603 1465	1602 1465	1608 1469	1602 1467	1609 1465	1609 1469	1612 1465
C-O (Ether)	1252	1252	1248	1248	1245	1249	1249
C-O (Ester)	1182 1135	1197 1138	1197 1182	1197 1175	1201 1182	1201 1182	1197 1179

The  $^1\text{H}$  and  $^{13}\text{C}$  NMR spectra of **10SHB-OCH<sub>3</sub>** are given in Figures 4.27 – 4.28 and selected  $^1\text{H}$  and  $^{13}\text{C}$  NMR data are summarized in Tables 4.19 and 4.20. The remaining spectra of other members in the series are given in Appendix C.

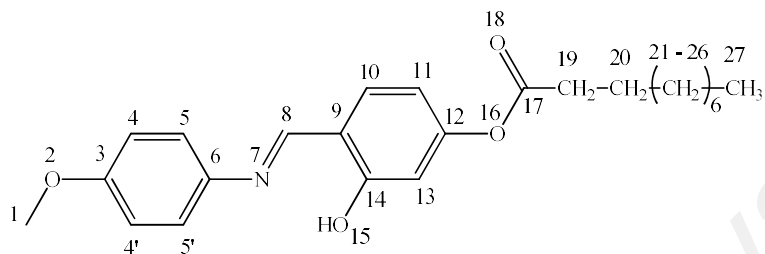


**Figure 4.26: Molecular structure with atomic numbering scheme for 10SHB-OCH<sub>3</sub>**

In the  $^1\text{H}$  NMR spectrum of **10SHB-OCH<sub>3</sub>** (Figure 4.27), a sharp peak appeared as a singlet at chemical shift,  $\delta = 8.61$  ppm which can be assigned to a **H8** proton located at the carbon atom in the Schiff base linkage ( $-\text{CH}=\text{N}-$ ). It was found that the chemical shift falls within the range that reported in the literature (Yeap *et al.* 2006). This was evidence of successful synthesis of the Schiff base group. The broader singlet peak located at chemical shift,  $\delta = 13.77$  ppm is assigned to the hydroxy group proton, **H15**. The peak was located at the most deshielded region as it was due to some local diamagnetic shielding caused by an electronegative atom, exchangeable proton and magnetic anisotropy effect by the aromatic ring.

In the higher chemical shift region range from chemical shift,  $\delta = 6.50 - 8.00$  ppm, five peaks were ascribed to the two aromatic rings. The doublet at chemical shift,  $\delta = 6.96 - 6.98$  ppm with a total integral of 2 protons was ascribed to **H4 & H4'** as it was closer to an electronegative atom, O. On the other hand, the doublet which appeared at chemical shift,  $\delta = 7.28 - 7.30$  ppm with a total integral of 2 protons was ascribed to **H5 & H5'**. For the doublet with a chemical shift,  $\delta = 7.37 - 7.39$  ppm was

ascribed to **H10**, where the doublet at chemical shift,  $\delta = 6.75 - 6.77$  ppm was ascribed to **H13**. The remaining doublet of doublets appeared at chemical shift,  $\delta = 6.69 - 6.72$  ppm was ascribed to **H11** due to *ortho* coupled with **H10** and *meta* coupled with **H13** which gave a doublet of doublet.

For the lower chemical shift region, a sharp singlet appeared at chemical shift,  $\delta = 3.86$  ppm which resulted from a strong electronegativity effect of the oxygen atom to **H1**. For the triplet present at chemical shift,  $\delta = 2.56 - 2.60$  ppm, it was assigned to **H19** as it was closer to the C=O which experienced a stronger diamagnetic effect. The quintet noticed at chemical shift,  $\delta = 1.76 - 1.82$  ppm was assigned to **H20** as it was located one bond further from the C=O compared to **H19**. Hence, it experienced less diamagnetic effect from the ester linkage. The multiplet was ascribed to the protons of the long alkyl chain (**H21 - H26**). Lastly, the triplet which appeared at the most shielded region,  $\delta = 0.90 - 0.93$  ppm was assigned to the methyl group in the long alkyl chain, **H27**.

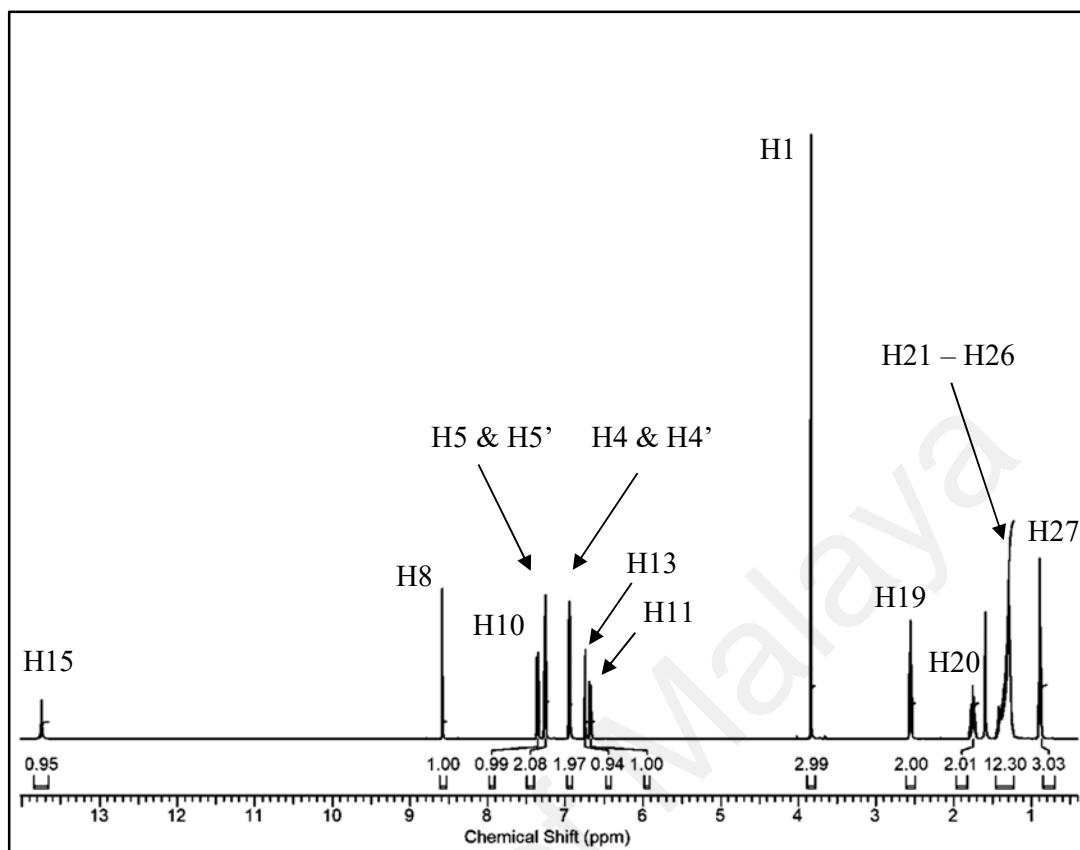


Figure 4.27:  $^1\text{H}$  NMR spectrum of 10SHB- $\text{OCH}_3$

Table 4.19:  $^1\text{H}$  NMR spectral data of compound 10SHB- $\text{OCH}_3$  in  $\text{CDCl}_3$

Proton number	Chemical shift, $\delta$ ppm	Integrals	Multiplicity	Coupling constant, $J$ (Hz)
H1	3.86	3	s	-
H4 & H4'	6.96 – 6.98	2	d	8.9
H5 & H5'	7.28 – 7.30	2	d	8.8
H8	8.61	1	s	-
H10	7.37 – 7.39	1	d	8.4
H11	6.69 – 6.72	1	dd	8.3 ( <i>ortho</i> ) 2.2 ( <i>meta</i> )
H13	6.76 – 6.77	1	d	2.2
H15	13.77	1	s	-
H19	2.56 – 2.60	2	t	7.5
H20	1.74 – 1.82	2	q	7.5
H21 – H26	1.31 – 1.44	12	m	-
H27	0.90 – 0.93	3	t	6.8

In the  $^{13}\text{C}$  NMR spectrum of **10SHB-OCH<sub>3</sub>** (Figure 4.28), the peak appeared at the highest chemical shift,  $\delta = 171.78$  ppm was ascribed to **C17** atom due to a strong electronegativity effect of two oxygen atoms attached nearby. The subsequent resonance signal at chemical shift,  $\delta = 162.35$  ppm corresponded to the aromatic carbon which bonded with a OH group, **C14**. The chemical shift,  $\delta = 159.52$  ppm corresponded to the carbon in a Schiff base linkage, **C8**.

The remaining nine peaks appeared between the chemical shift,  $\delta = 110.34 - 158.87$  ppm were attributed to the aromatic carbons in the two aromatic rings. Two peaks showed higher intensities ( $\delta = 114.62$  and  $122.25$  ppm) than the seven other peaks were assigned to the four aromatic carbons, **C4/4'** and **C5/5'**. **C3**, **C6** and **C12** atoms were either directly attached to an electronegative atom, N or O. The great impact of the electron withdrawing may had been led to the peaks shifted to higher chemical shift. The peaks were observed at chemical shift,  $\delta = 141.07$ ,  $154.10$  and  $158.87$  ppm. The chemical shift,  $\delta = 158.87$  ppm was ascribed to **C3** and peak with chemical shift,  $\delta = 141.07$  ppm was ascribed by **C6**. **C3** possessed higher chemical shift than **C6** as it was directly attached to a more electronegative atom O compared to N. The remaining peak at chemical shift,  $\delta = 154.10$  ppm was ascribed to **C12** as it was an ester carbon which directly attached to two electronegative oxygen atoms. This may had been reduced the diamagnetic effect.

In low field region, the peak with the chemical shift,  $\delta = 55.53$  ppm was attributed to **C1** as directly attached to an oxygen atom. The peak with the chemical shift,  $\delta = 34.43$  ppm was attributed by the **C19** in the long decanoyloxy chain. It showed the highest chemical shift among all the  $\text{sp}^3$  carbon in the decanoyloxy chain due to its direct attachment to the carbonyl group which experienced a strong  $\text{sp}^2$  hybridization

effect. **C20** atom was assigned to the chemical shift,  $\delta = 24.95$  ppm. This assignment made based on the previous reported work (Ha *et al.*, 2010) for the Schiff base derivatives with the pyridine core. It may have been due to the hyperconjugation effect with the carbonyl group of the ester linkage. For the methylene chain carbons **C21** – **C26** showed several signals in the chemical shift,  $\delta = 22.65 - 31.84$  ppm. The peak at chemical shift,  $\delta = 14.09$  ppm was attributed to the methyl group, **C27** at the end of the long alkanoyloxy chain.

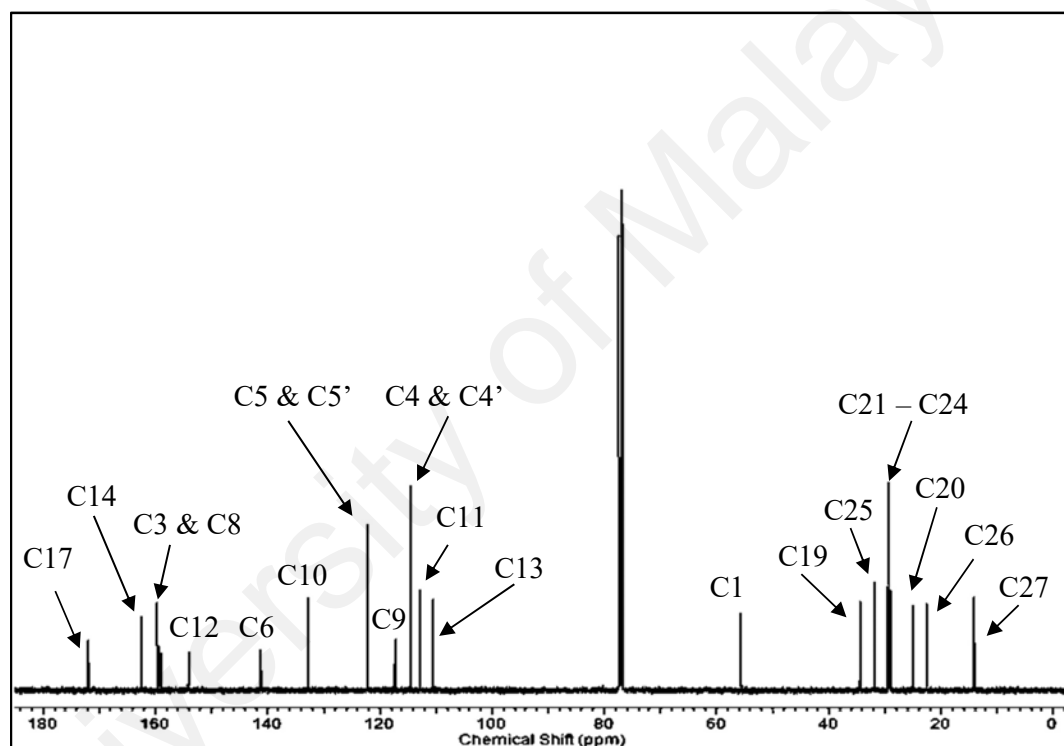


Figure 4.28:  $^{13}\text{C}$  NMR spectrum of 10SHB-OCH<sub>3</sub>



**Table 4.20:**  $^{13}\text{C}$  NMR spectral data of compound **10SHB-OCH<sub>3</sub>** in  $\text{CDCl}_3$

Carbon number	Chemical Shift, $\delta$ ppm
C1	55.53
C3	158.87
C4 & C4'	114.61
C5 & C5'	122.25
C6	141.07
C8	159.52
C9	117.27
C10	132.72
C11	112.71
C12	154.10
C13	110.33
C14	162.35
C17	171.78
C19	34.43
C20	24.87
C21 – C24	29.06
	29.23
	29.39
C25	31.84
C26	22.65
C27	14.09

<sup>a</sup> some of the signals attributed to C21 – C24 appear in the same column in the  $^{13}\text{C}$  NMR spectrum which resulted in less than 4 signals observed in the  $^{13}\text{C}$  NMR spectrum.

Based on the results obtained from infrared and NMR spectroscopy together with elemental analysis, the structure of **nSHB-CH<sub>3</sub>** was confirmed.

#### 4.2.2 Thermal Behavior and Mesomorphic Properties

The study of thermal and mesomorphic properties of **nSHB-OCH<sub>3</sub>** was carried out using DSC and POM methods. Representative DSC thermograms of **14SHB-OCH<sub>3</sub>** and **16SHB-OCH<sub>3</sub>** are depicted in Figures 4.29 and 4.30. The phase transition temperatures and associated enthalpy changes ( $\Delta H$ ) obtained from DSC analysis during the heating and cooling processes of **nSHB-OCH<sub>3</sub>** are tabulated in Table 4.21. The remaining DSC thermograms of **nSHB-OCH<sub>3</sub>** are given in Appendix D.

Early members (where  $n = 6, 8, 10$  and  $12$ ) possessed similar properties; there were two transition peaks observed in both heating and cooling cycles. They corresponded to the phase transitions of Cr-N and N-I. For **14SHB-OCH<sub>3</sub>**, there was an additional exotherm peak appeared in the cooling scan. However, the peak was hardly identified due to the energy released was minimal. It was unable to notice in the thermogram unless magnify the region. The presence of the additional peak which was later identified through POM as monotropic SmA phase (Dierking, 2003).

For **16SHB-OCH<sub>3</sub>**, both the heating and cooling cycles exhibited three transition peaks. They corresponded to the phase transitions of Cr-N, N-SmA and SmA-I. The nematic phase range of **16SHB-OCH<sub>3</sub>** was smaller than **14SHB-OCH<sub>3</sub>**, it was about 3 °C for the cooling scan.

The last member in the homologous series, **18SHB-OCH<sub>3</sub>**, showed only two transition peaks in both heating and cooling cycles. Under the observation of POM, the mesophase exhibited by the **18SHB-OCH<sub>3</sub>** was enantiotropic SmA phase (Dierking, 2003).

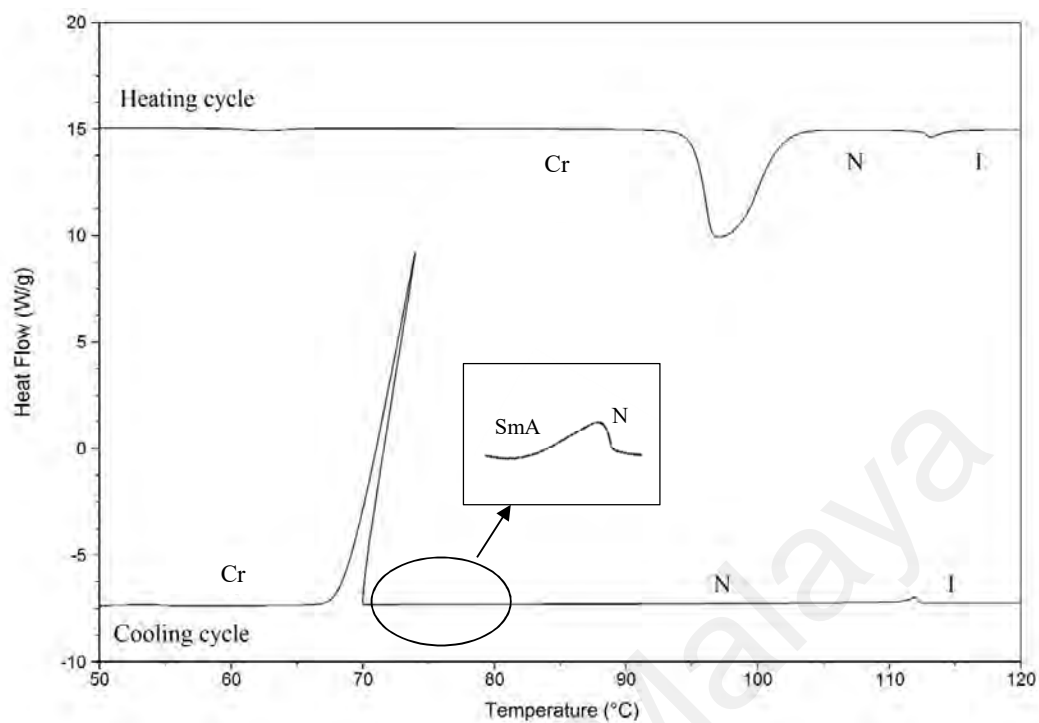


**Figure 4.29: DSC thermogram of 14SHB-OCH<sub>3</sub>**

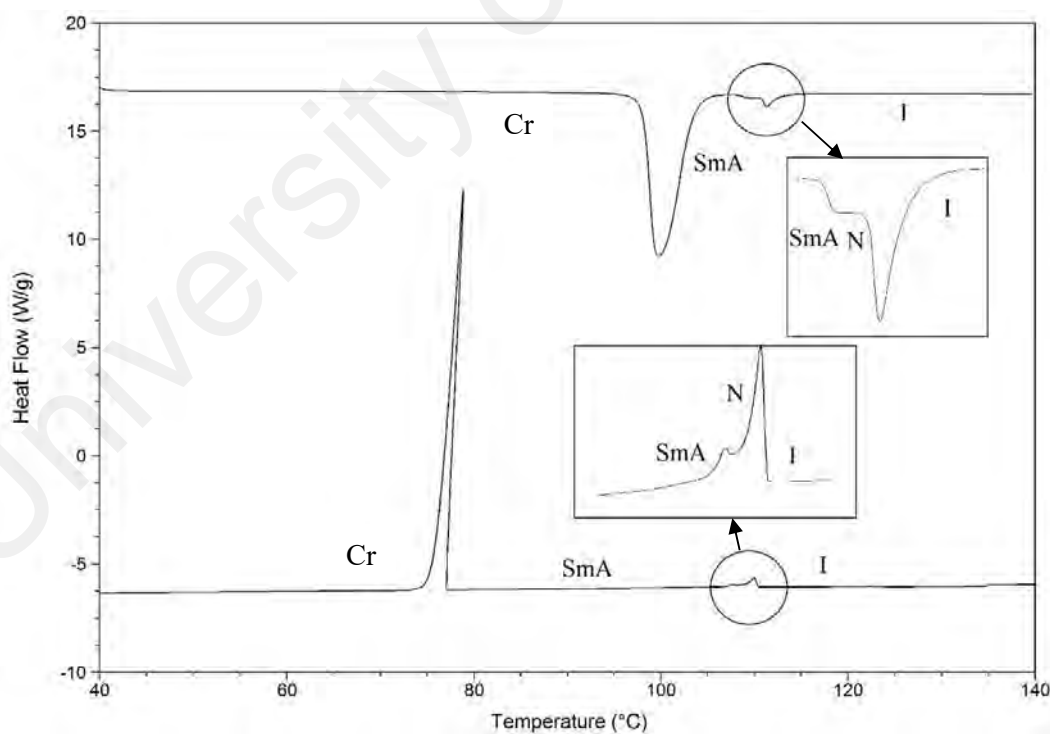


**Figure 4.30: DSC thermogram of 16SHB-OCH<sub>3</sub>**

**Table 4.21: Phase transition temperatures and associated enthalpy changes of series nSHB-OCH<sub>3</sub>**

Compound	Phase transition, °C
	(Corresponding enthalpy changes, kJ mol <sup>-1</sup> )
<b>6SHB-OCH<sub>3</sub></b>	Cr 80.11 (21.72) N 118.60 (0.79) I <i>I 113.20 (0.49) N 43.15 (17.34) Cr</i>
<b>8SHB-OCH<sub>3</sub></b>	Cr 86.49 (26.88) N 114.93 (0.49) I <i>I 114.25 (0.39) N 58.36 (23.10) Cr</i>
<b>10SHB-OCH<sub>3</sub></b>	Cr 89.13 (44.85) N 117.87 (1.21) I <i>I 116.60 (1.16) N 63.39 (40.79) Cr</i>
<b>12SHB-OCH<sub>3</sub></b>	Cr 94.10 (51.12) N 115.45 (1.52) I <i>I 114.04 (1.42) N 66.97 (50.56) Cr</i>
<b>14SHB-OCH<sub>3</sub></b>	Cr 97.03 (73.58) N 112.47 (1.65) I <i>I 111.96 (1.95) N 74.47 (0.09) SmA 73.98 (63.01) Cr</i>
<b>16SHB-OCH<sub>3</sub></b>	Cr 99.76 (78.13) SmA 108.59 N (0.13) 110.66 (3.00) I <i>I 110.01 (1.93) N 107.65 (0.10) SmA 78.85 (76.10) Cr</i>
<b>18SHB-OCH<sub>3</sub></b>	Cr 103.38 (81.25) SmA 111.37 (3.70) I <i>I 109.33 (3.22) SmA 85.10 (79.49) Cr</i>

The types of mesophases of **nSHB-OCH<sub>3</sub>** were identified using polarizing optical microscopy. The optical photomicrographs of **12SHB-OCH<sub>3</sub>**, **16SHB-OCH<sub>3</sub>** and **18SHB-OCH<sub>3</sub>**, are shown in Figures 4.31 – 4.33. The graph of transition temperature during heating or cooling cycles against the number of carbon atoms in the alkanoyloxy chain for **nSHB-OCH<sub>3</sub>** are plotted and shown in Figures 4.34 and 4.35.

Upon cooling **12SHB-OCH<sub>3</sub>**, nematic phase with schlieren texture (Dierking, 2003) was observed. The nematic phase was first appeared as nematic droplets and coalesced into schlieren texture. Further cooling from nematic phase, the texture had been transformed directly into crystal phase.

During the cooling of **16SHB-OCH<sub>3</sub>**, an additional transition from nematic phase into SmA phase was observed. The SmA phase with focal conic fan-shaped texture was observed for **16SHB-OCH<sub>3</sub>** (Ha *et al.*, 2012, Yeap *et al.*, 2012).

Upon cooling of **18SHB-OCH<sub>3</sub>**, the smectic phase batonnet was first observed under the POM and slowly aggregated into the focal conic fan-shaped texture of smectic A phase (Ha *et al.*, 2011). The nematic phase was absent for **18SHB-OCH<sub>3</sub>**.

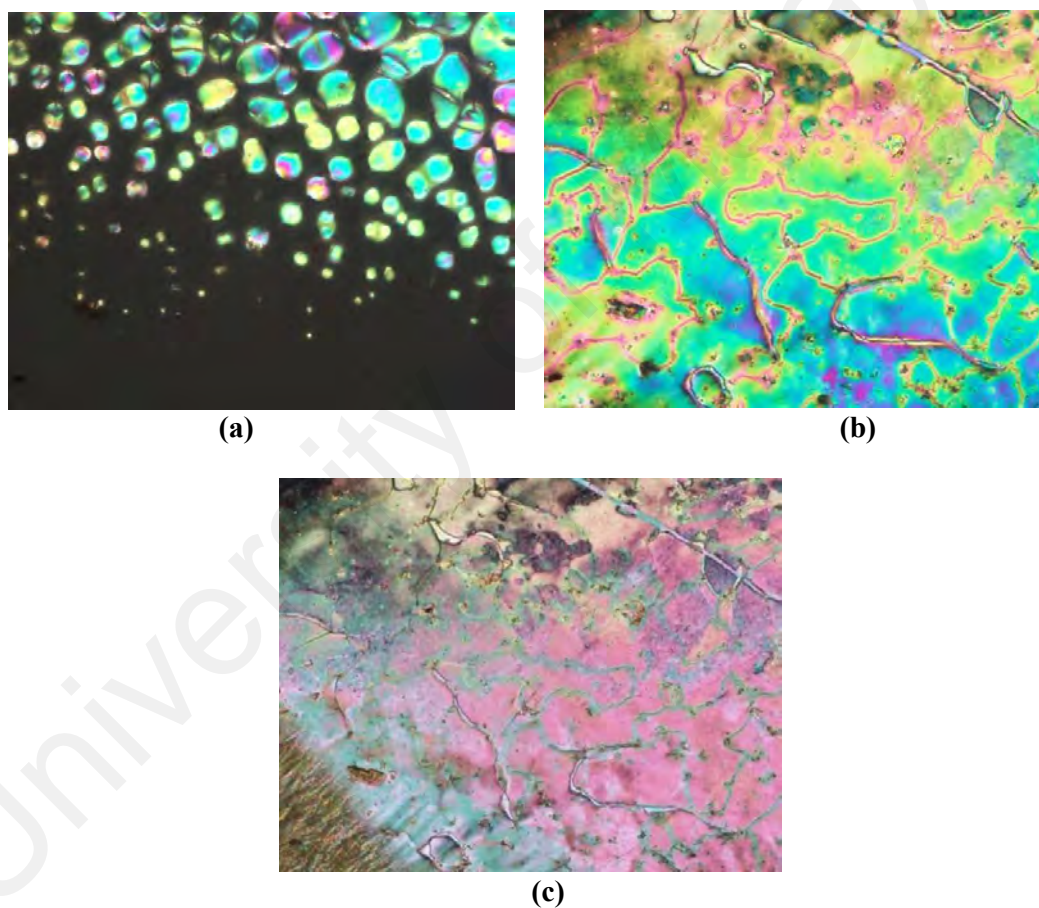


**Figure 4.31: Optical photomicrographs of compound 12SHB-OCH<sub>3</sub> exhibiting nematic phase only during cooling cycle**

- (a) Isotropic phase transforms into nematic droplet at 114 °C
- (b) Schlieren nematic phase texture at 81 °C
- (c) Nematic phase transform into crystal phase at 67 °C

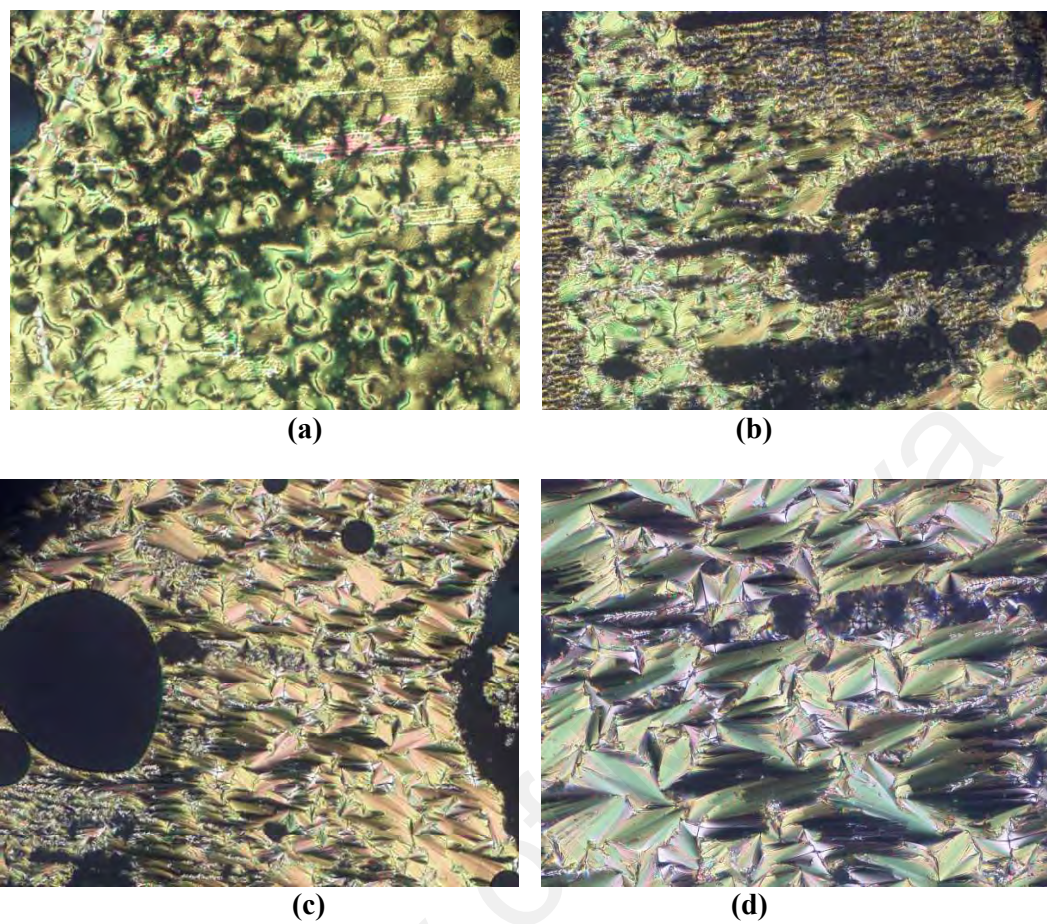


**Figure 4.32: Optical photomicrographs of compound 16SHB-OCH<sub>3</sub> exhibiting nematic phase and smectic A phase during cooling cycle**

- (a) Nematic phase texture at 108 °C
- (b) Nematic to Smectic A phase texture at 107 °C
- (c) Smectic A phase with at 100 °C
- (d) Smectic A phase with fan-shaped at 85 °C



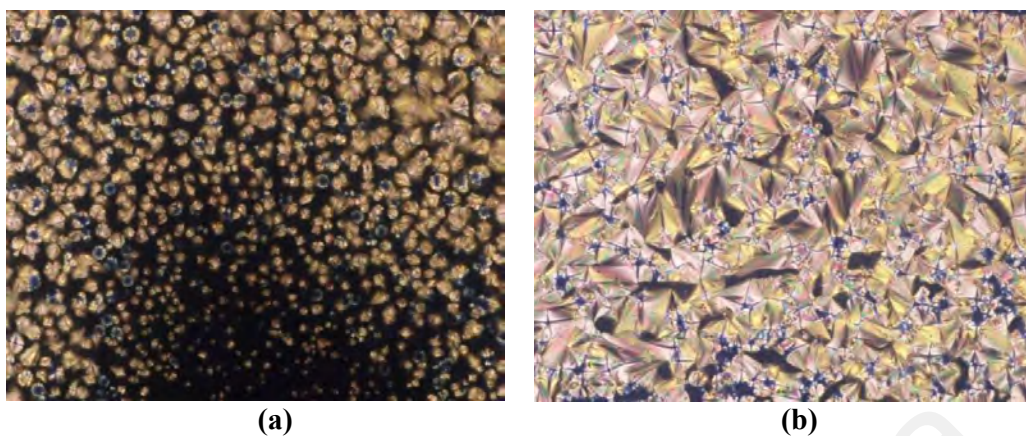


**Figure 4.33: Optical photomicrographs of compound 18SHB-OCH<sub>3</sub> exhibiting smectic A phase only during cooling cycle**

- (a) Smectic batonnet is formed at 108 °C
- (b) Smectic A phase with fan-shaped texture at 90 °C

As the methylene chain length increased (Figures 4.34 – 4.35), clearing temperatures of **nSHB-OCH<sub>3</sub>** showed a decreasing trend. Increased in flexibility for methylene chain has reduced the interaction between molecules and, thus, reduced the isotropization point. However, melting temperatures showed an increasing trend. As number of carbon increased, the strength of the VDW force increased and promoted a stronger electrostatic force to held the molecules tightly. Enantiotropic nematic phase was observed from *n*-hexanoyloxy to the *n*-hexadecanoyloxy derivatives. As the number of carbons increased, the nematic phase stability ( $T_N$ ) was decreased as shown in Figures 4.34 – 4.35. The flexibility of the molecules had been increased with the number of carbon. This excessive of flexibility which due to the extra long alkanoyloxy chain tends to disrupt the orientation of the molecules packing. It may have been helped in generated nematic phase. In other words, the longer the alkanoyloxy chain will emerge a lamellar packing which leads to the formation of the smectic phase. Therefore, the *n*-tetradecanoyloxy derivative exhibited SmA during the cooling cycle whereas *n*-hexadecanoyloxy and *n*-octadecanoyloxy derivatives showed the SmA phase as enantiotropic mesophase.

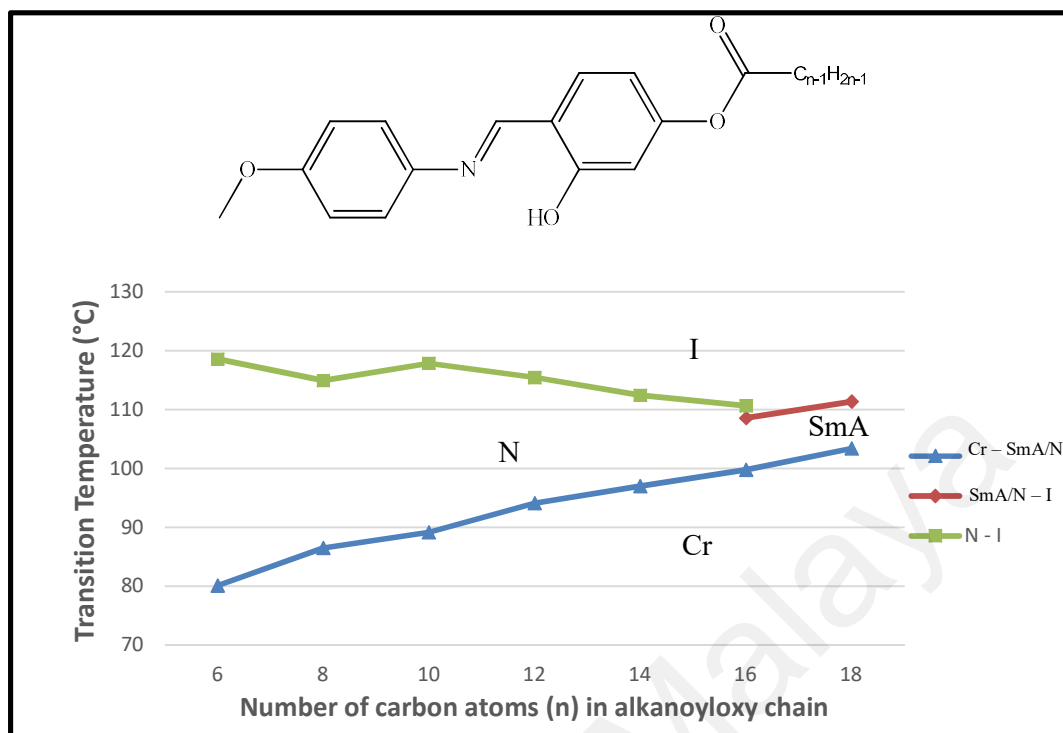


Figure 4.34: Plot of transition temperatures of  $n\text{SHB-OCH}_3$  during heating cycle as a function of the number of carbon atoms

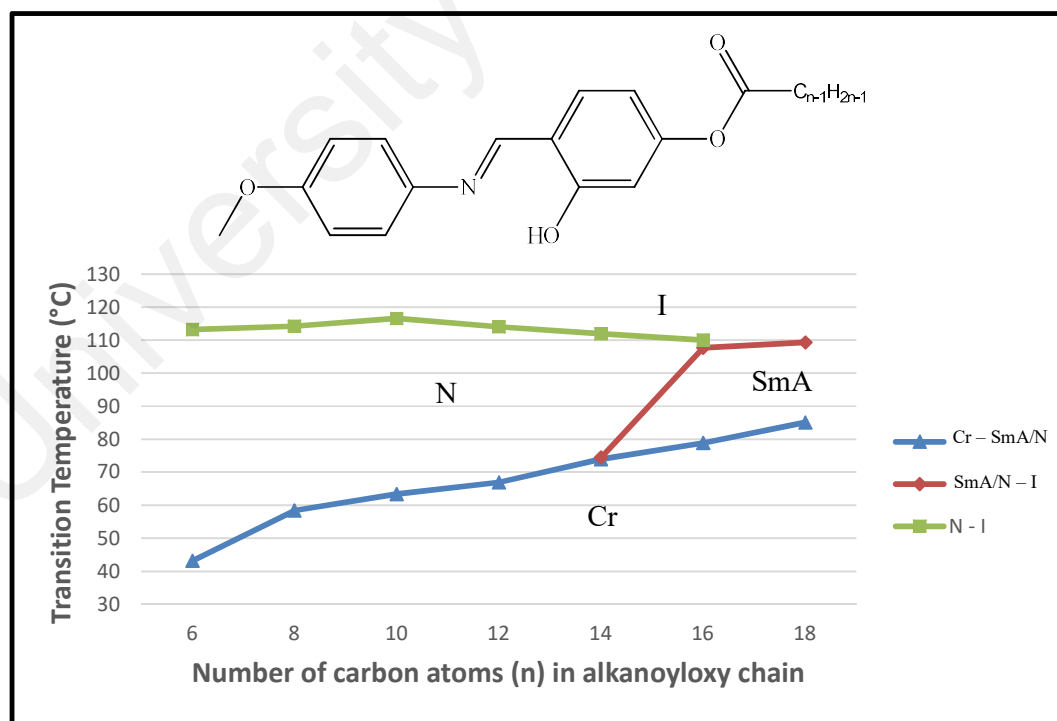
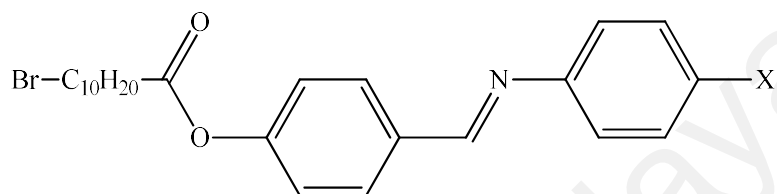


Figure 4.35: Plot of transition temperatures of  $n\text{SHB-OCH}_3$  during cooling cycle as a function of the number of carbon atoms



### 4.3 Series 3

The chemical structure of **OBSB-R** is given in Figure 4.36 and the percentage yields are summarized in Table 4.21. The TLC  $R_f$  value for **OBSB-R** is tabulated in Appendix A.



Where  $\text{X} = \text{H}, \text{Cl}, \text{Br}, \text{CH}_3, \text{OCH}_3$  and  $\text{N}(\text{C}_2\text{H}_5)_2$

**Figure 4.36: Structural formula of OBSB-R**

**Table 4.22: Percentage yields OBSB-R**

Compound	Yield (%)
<b>OBSB-H</b>	38
<b>OBSB-Cl</b>	42
<b>OBSB-Br</b>	47
<b>OBSB-CH<sub>3</sub></b>	41
<b>OBSB-OCH<sub>3</sub></b>	44
<b>OBSB-NDEA</b>	39

#### 4.3.1 Structural Elucidation

Elemental analytical data are tabulated in Table 4.23. The analytical data agreed with calculated values (within 0.5 %). The molecular formula of **OBSB-R** has been suggested according to the data below together with those obtained from the spectral analysis.

**Table 4.23: Micro-elemental analytical data of OBSB-R**

R	Experimental analysis found ( <i>calculated</i> ) / %					
	C		H		N	
H	64.53	(64.86)	6.97	(6.80)	3.07	(3.15)
CH <sub>3</sub>	65.31	(65.50)	7.12	(7.04)	3.01	(3.06)
OCH <sub>3</sub>	62.82	(63.29)	6.94	(6.80)	2.88	(2.95)
N(C <sub>2</sub> H <sub>5</sub> ) <sub>2</sub>	64.80	(65.23)	7.81	(7.63)	5.26	(5.43)
Cl	59.82	(60.20)	6.14	(6.10)	2.91	(2.93)
Br	54.64	(55.08)	5.68	(5.59)	2.63	(2.68)

Infrared spectrum for **OBSB-Br** is given in Figure 4.37, and selected data for **OBSB-R** are summarized in Table 4.24. Remaining spectra are provided in Appendix B. From the spectrum, the absorption peaks located at 2928 & 2851 cm<sup>-1</sup> were assigned to the sp<sup>3</sup> hybridization C–H stretch of the methylene (–CH<sub>2</sub>–) chain while a characteristic strong absorption peak at 1750 cm<sup>-1</sup> was ascribed to a carbonyl group (C=O) of the ester linkage. Two sharp peaks presented at 1161 & 1135 cm<sup>-1</sup> corresponded to C–O of ester group of which one peak was broader and stronger than another one. These observations indicated the esterification between 11-bromoundecanoic acid and the intermediate compound was successful and led to the formation of the **OBSB-Br**.

The aromatic C–H stretch appeared at 3012 cm<sup>-1</sup> ascribed to sp<sup>2</sup> C–H stretch of phenyl rings. This further strengthen by the peaks appeared at 1600 & 1468 cm<sup>-1</sup> which were assigned to the C–C stretch for phenyl rings. Schiff base group (C=N) indicated by the peak found at 1622 cm<sup>-1</sup> and this value conformed with those reported in the infrared spectra for various compound possess the formulation of the benzylidene aniline group (Ha *et al.*, 2011 and Yeap *et al.*, 2006). The other characteristic absorption peak such as CH<sub>2</sub>-Br bent of long ω-bromoalkanoyloxy chain appeared at 1201 cm<sup>-1</sup>,

and aliphatic C-Br stretching showed the absorption peak at 543  $\text{cm}^{-1}$ . For the C-Br of the aromatic ring, it had been revealed by the absorption peak at 1038  $\text{cm}^{-1}$ .

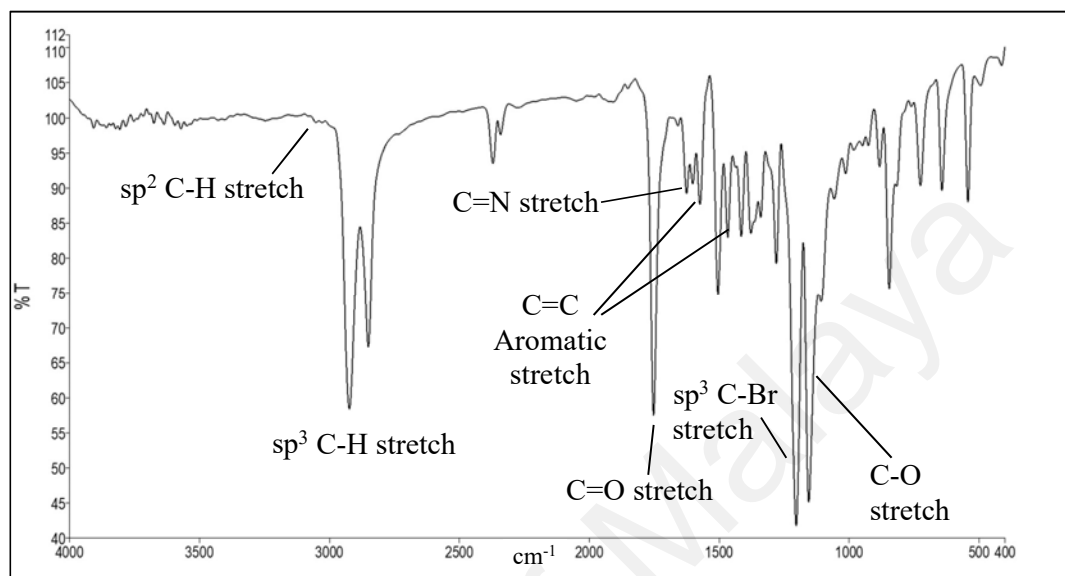


**Figure 4.37: Infrared spectrum of OBSB-Br**

**Table 4.24: FTIR spectrum data of OBSB-Br**

Functional group	IR $\nu$ ( $\text{cm}^{-1}$ )					
	OBSB-H	OBSB-Cl	OBSB-Br	OBSB-CH <sub>3</sub>	OBSB-OCH <sub>3</sub>	OBSB-NDEA
sp <sup>2</sup> C-H stretch (Aromatic)	3012	3001	3001	3006	3036	3071
sp <sup>3</sup> C-H stretch (Aliphatic)	2928 2851	2927 2854	2921 2853	2920 2850	2924 2850	2971 2927 2858
C=O (Ester)	1750	1759	1756	1756	1756	1752
C=N (Schiff base)	1622	1620	1621	1627	1623	1623
C=C (Aromatic)	1600 1468	1598 1469	1602 1468	1601 1469	1601 1469	1590 1469
C-O (Ester)	1161 1135	1160 1124	1124 1100	1157 1105	1138 1105	1131 1050
sp <sup>3</sup> CH <sub>2</sub> -Br	1201	1208	1205	1205	1212	1201
Aliphatic C-Br stretch	543	540	538	543	543	543

The  $^1\text{H}$  and  $^{13}\text{C}$  NMR spectra of **OBSB-OCH<sub>3</sub>** are given in Figures 4.39 – 4.40 and selected  $^1\text{H}$  and  $^{13}\text{C}$  NMR data for **OBSB-OCH<sub>3</sub>** are summarized in Tables 4.25 and 4.26. The spectra of the remaining members in the series are given in Appendix C.  $^1\text{H}$  &  $^{13}\text{C}$  NMR spectral analysis was performed for a representative compound, **OBSB-OCH<sub>3</sub>**. The molecular structure with an atomic numbering scheme for **OBSB-OCH<sub>3</sub>** is depicted in Figure 4.38.

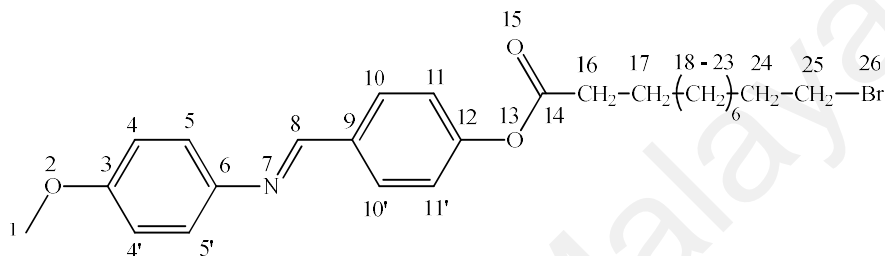


**Figure 4.38: Molecular structure with atomic numbering scheme for OBSB-OCH<sub>3</sub>**

In the  $^1\text{H}$  NMR spectrum of **OBSB-OCH<sub>3</sub>** (Figure 4.39), a sharp peak appeared as a singlet at chemical shift,  $\delta = 8.46$  ppm corresponded to a Schiff base proton, **H8** ( $-\text{CH}=\text{N}-$ ). This indicated that reaction between 4-methylaniline and 4-hydroxybenzaldehyde was successful reacted. The peaks appeared at chemical shift,  $\delta = 6.92 - 7.92$  ppm were assigned to the four sets of chemically equivalent aromatic protons, but magnetically inequivalent protons of benzylidene fragment ( $-\text{C}_6\text{H}_4-\text{C}=\text{N}-\text{C}_6\text{H}_4-$ ) and had been agreed with the reported data (Ha *et al.*, 2011). This proton was highly deshielded by strong anisotropy effect which generated by the  $\pi$ -electron density of the aromatic rings. Two doublets appeared at chemical shift,  $\delta = 7.19$  and  $7.93$  ppm were assigned to **H11/11'** and **H10/10'** respectively and the other two doublets with the chemical shift,  $\delta = 6.93$  and  $7.23$  ppm corresponded to the **H4/4'** and **H5/5'** respectively.

In low field region, the proton of the aromatic methoxy (Ar-OCH<sub>3</sub>) group, **H1**, was ascribed to the chemical shift,  $\delta = 3.83$  ppm as a singlet. The closer proton to the bromine atom (-CH<sub>2</sub>-Br), **H25**, exhibited the signal at chemical shift,  $\delta = 3.41$  ppm whereas the closer proton to the carbonyl group (C=O), **H16**, showed the signal at chemical shift,  $\delta = 2.57$  ppm. These protons were greatly influenced by the electron withdrawing effect and the  $\pi$ -bond magnetic anisotropy effect of the bromine atom and carbonyl group. It had been given a triplet due to the spin-spin interaction with **H17** and **H24** atoms. For the proton, **H25**, its chemical shift was higher than **H16**, due to the electronegativity effect which may have been strongly influenced compare to the  $\pi$ -bond magnetic anisotropy effect. Hence, **H25** was more deshielded than **H16**. For the second closer proton to the bromine atom and carbonyl group, **H24** and **H17**, showed the signal at chemical shift,  $\delta = 1.86$  and  $1.77$  ppm. Although **H24** and **H17** were one bond further from the bromine atom and carbonyl group, the magnetic anisotropy effect was still shifted the peak to higher chemical shift. The multiplet at chemical shift,  $\delta = 1.29$  ppm was attributed to **H18** – **H23**.

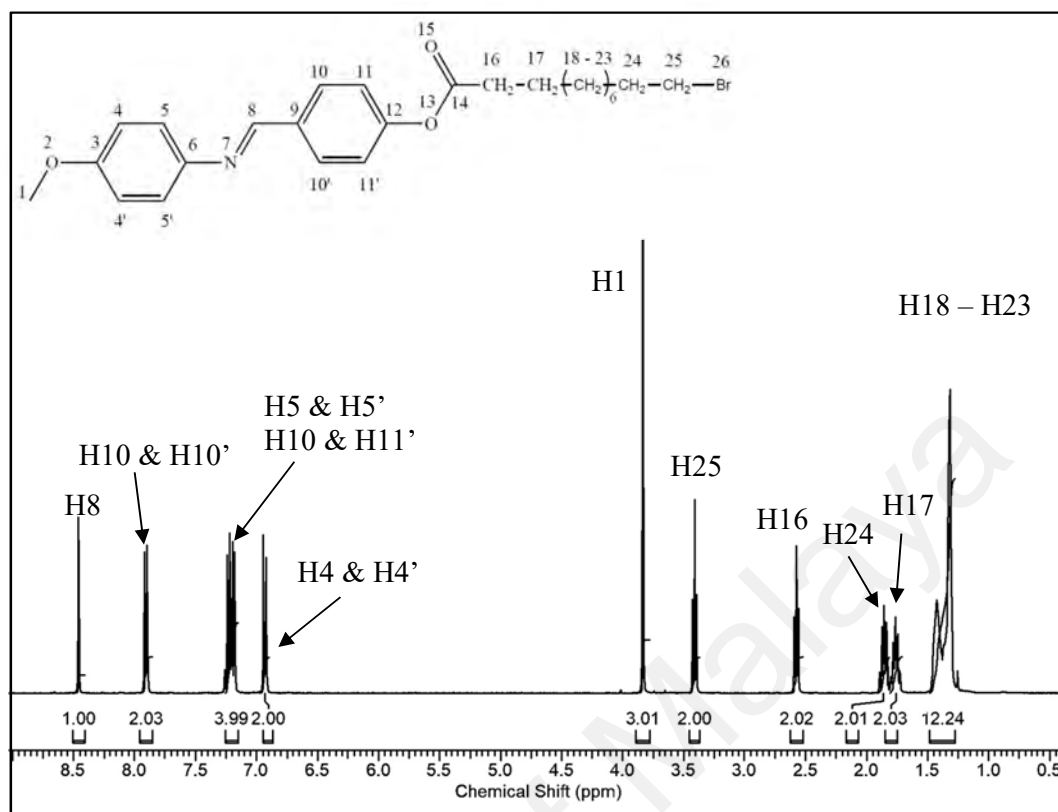


Figure 4.39:  $^1\text{H}$  NMR spectrum of OBSB- $\text{OCH}_3$

Table 4.25:  $^1\text{H}$  NMR spectral data of compound OBSB- $\text{OCH}_3$  in  $\text{CDCl}_3$

Proton number	Chemical shift, $\delta$ ppm	No of Proton	Multiplicity	Coupling constant, $J$ (Hz)
H1	3.83	3	s	-
H4 & H4'	6.92 – 6.94	2	d	8.8
H5 & H5'	7.22 – 7.24	2	d	8.8
H8	8.46	1	s	-
H10 & H10'	7.90 – 7.92	2	d	8.6
H11 & H11'	7.18 – 7.20	2	d	8.6
H16	2.56 – 2.59	2	t	7.5
H17	1.73 – 1.80	2	q	7.4
H18 – H23	1.32 – 1.43	12	m	-
H24	1.82 – 1.89	2	q	7.1
H25	3.39 – 3.43	2	t	6.9

In the  $^{13}\text{C}$  NMR spectrum of **OBSB-OCH<sub>3</sub>** (Figure 4.40), **C14** atom was an ester carbon bonded to two electronegative oxygen atoms and showed the highest chemical shift,  $\delta = 171.96$  ppm. The similar chemical shift was reported literally (Ha *et al.*, 2010). The peak at chemical shift,  $\delta = 157.12$  ppm was ascribed to the carbon atom of a Schiff base linkage, **C8**. The remaining eight peaks between chemical shift,  $\delta = 114.80 - 158.35$  ppm were attributed by the aromatic carbons in the two phenyl rings. There were four peaks which have higher intensities ( $\delta = 114.80, 121.98, 122.20$  and  $129.71$  ppm) than four other peaks assigned to the eight aromatic carbons, **C4/4'**, **C5/5'**, **C10/10'** and **C11/11'**. The resonance signal at chemical shift,  $\delta = 158.35$  ppm corresponded to the aromatic carbon, **C3**, that directly attached to a methoxy group. The present of electronegative oxygen atom was highly deshielded the electron cloud around the carbon atom.

In low field region, the peak with the chemical shift,  $\delta = 55.51$  ppm was attributed to the **C1** of the methoxy group attached to phenyl rings. The strong impact of the electron withdrawing effect by the oxygen atom had led shifting of the peaks to a lower chemical shift region. For the  $\omega$ -bromodecanoyloxy, the **C25** showed the highest chemical shift,  $\delta = 34.43$  ppm due to directly attached to an electronegative atom, bromine. For **C16** atom which was directly connected to the carbonyl group experienced the strong  $\text{sp}^2$  hybridization effect and the signal showed at chemical shift,  $\delta = 34.04$  ppm. Along the methylene ( $-\text{CH}_2-$ ) chain, **C18** – **C23** showed several signals at the chemical shift,  $\delta = 28.16 - 29.36$  ppm. The peak at chemical shift,  $\delta = 32.83$  ppm was attributed to the **C24**, second closer carbon atom to the bromine atom in the  $\omega$ -bromodecanoyloxy chain.

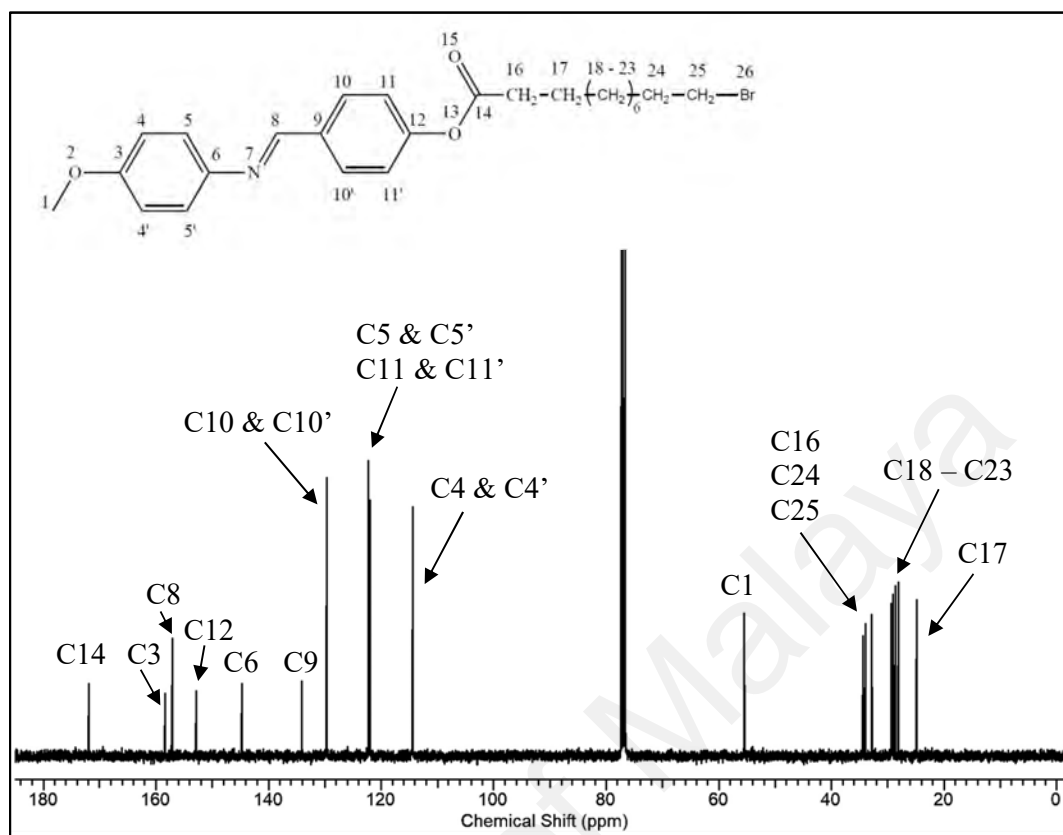


Figure 4.40:  $^{13}\text{C}$  NMR spectrum of OBSB- $\text{OCH}_3$



**Table 4.26:**  $^{13}\text{C}$  NMR spectral data of compound OBSB-OCH<sub>3</sub> in CDCl<sub>3</sub>

Carbon number	Chemical Shift, $\delta$ ppm
C1	55.51
C3	158.35
C4 & C4'	114.41
C5 & C5'	122.20
C6	144.80
C8	157.12
C9	134.08
C10 & C10'	129.71
C11 & C11'	121.98
C12	152.85
C14	171.96
C16	34.04
C17	24.87
	29.07
	29.32
	29.36
C18 – C23	29.20
	28.74
	28.16
C24	32.83
C25	34.42

#### 4.3.2 Thermal Behavior and Mesomorphic Properties

The study of thermal and mesomorphic properties of **OBSB-R** (where R = H, CH<sub>3</sub>, OCH<sub>3</sub>, Cl, Br and N(C<sub>2</sub>H<sub>5</sub>)<sub>2</sub>) were carried out using DSC and POM methods. Representative DSC thermograms **OBSB-CH<sub>3</sub>**, **OBSB-OCH<sub>3</sub>** and **OBSB-Cl**, are depicted in Figures 4.41 – 4.43. The phase transition temperatures and associated enthalpy changes ( $\Delta H$ ) obtained from DSC analysis of **OBSB-R** are tabulated in Table 4.27. The remaining DSC thermograms of **OBSB-R** are given in Appendix D.

From the DSC thermogram of **OBSB-Cl**, a total of two exotherm peaks observed in cooling cycle while there was only one endotherm peak appeared in the heating cycle. The two exotherm peaks were identified by POM and corresponded to the phase transitions of I-N and N-Cr, while the endotherm peak represented the direct transition of crystal into the isotropic phase. The compound exhibited monotropic nematic phase (Dierking, 2003).

From the DSC thermograms of **OBSB-OCH<sub>3</sub>** revealed that it was an enantiotropic nematogen. Two transition peaks were observed both in the heating and cooling cycles. This had been indicated the presence of mesophases and identified as a nematic phase by POM. While comparing with **OBSB-CH<sub>3</sub>**, **OBSB-CH<sub>3</sub>** did not show any mesophases transition. This could be concluded from the DSC thermogram, where **OBSB-CH<sub>3</sub>** exist only one transition peak for both the heating and cooling cycles. This indicated that the crystal phase of **OBSB-CH<sub>3</sub>** was direct gone through isotropization process upon heating.

The compounds having either chloro (**Cl**) or methoxy group (**OCH<sub>3</sub>**) substituent showed the presence of liquid crystal mesophases while the other showed direct isotropization process into the liquid phase.

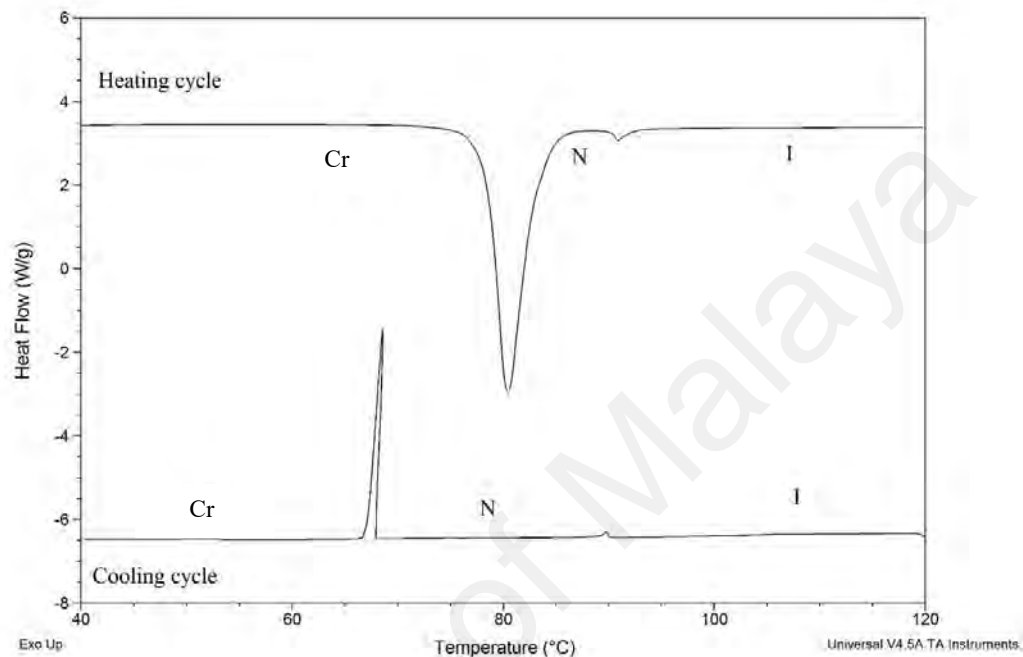


**Figure 4.41: DSC thermogram of OBSB-OCH<sub>3</sub>**

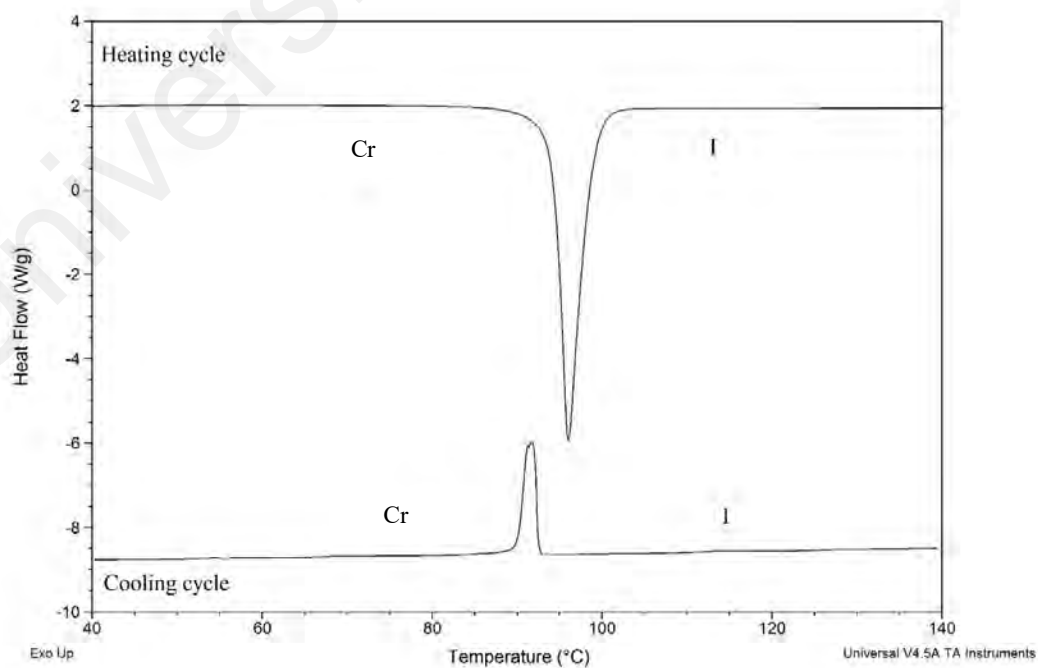


**Figure 4.42: DSC thermogram of OBSB-CH<sub>3</sub>**

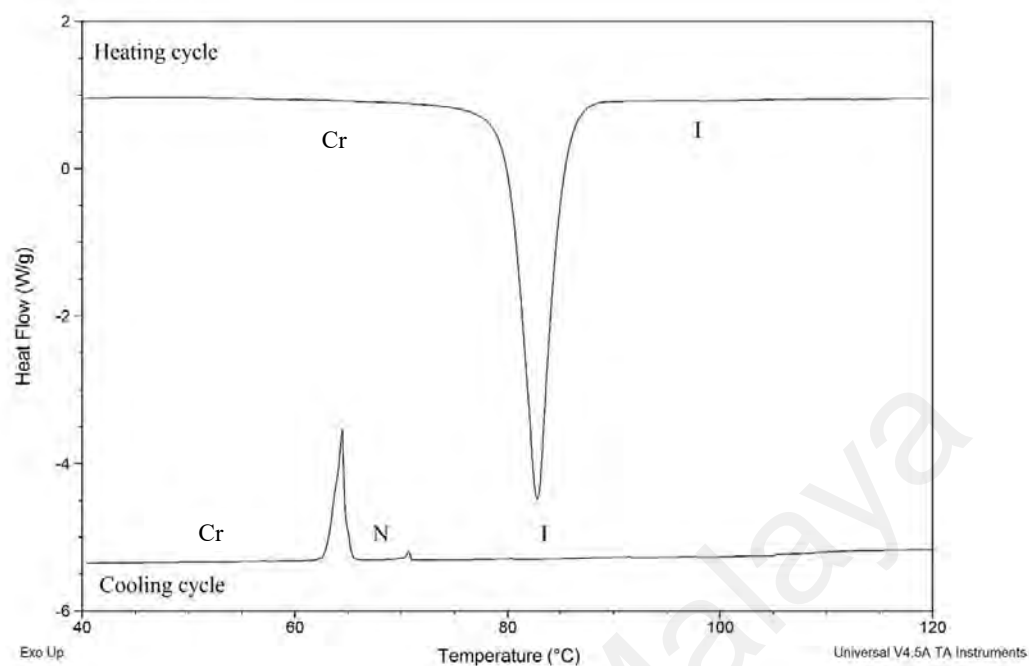


**Figure 4.43: DSC thermogram of OBSB-Cl**

**Table 4.27: Phase transition temperatures and associated enthalpy changes of series OBSB-R**

Compound	Phase transition, °C (Corresponding enthalpy changes, kJ mol <sup>-1</sup> )
OBSB-H	Cr 84.22 (51.51) I I 49.10 (46.88) Cr
OBSB-Cl	Cr 82.82 (52.72) I I 70.69 (1.39) N 64.5 <sup>a</sup> SmA 63.76 (50.8) Cr
OBSB-Br	Cr 96.38 (74.62) I I 90.29 (71.27) Cr
OBSB-CH <sub>3</sub>	Cr 96.05 (70.60) I I 91.71 (66.70) Cr
OBSB-OCH <sub>3</sub>	Cr 80.42 (60.77) N 90.92 (0.90) I I 89.79 (0.97) N 68.57 (60.03) Cr
OBSB-NDEA	Cr 84.66 (51.05) I I 57.74 (46.32) Cr

<sup>a</sup> denote the result obtained from POM analysis

Types of mesophases for entire synthesized compounds were identified using polarizing optical microscopy. The optical photomicrographs of **OBSB-OCH<sub>3</sub>** and **OBSB-Cl** are shown in Figures 4.44 and 4.45.

Upon cooling of **OBSB-OCH<sub>3</sub>**, nematic phase with schlieren texture (Imrie *et al.*, 2007) was observed during the cooling cycle. On further cooling from nematic phase, the texture was directly transformed into crystal phase. However, upon cooling of **OBSB-Cl**, the isotropic liquid phase was first transformed into nematic phase with schlieren texture. On further cooling, an additional mesophase which was SmA phase was observed for a short while before transformed into crystal phase. The SmA phase was present, and the texture was identified as the focal conic texture (Ha *et al.*, 2010). Although the SmA phase was shown in the POM analysis, due to the phase range of the observed SmA phase was just about 1 °C. Hence, it was unable to be detected using the DSC analysis.

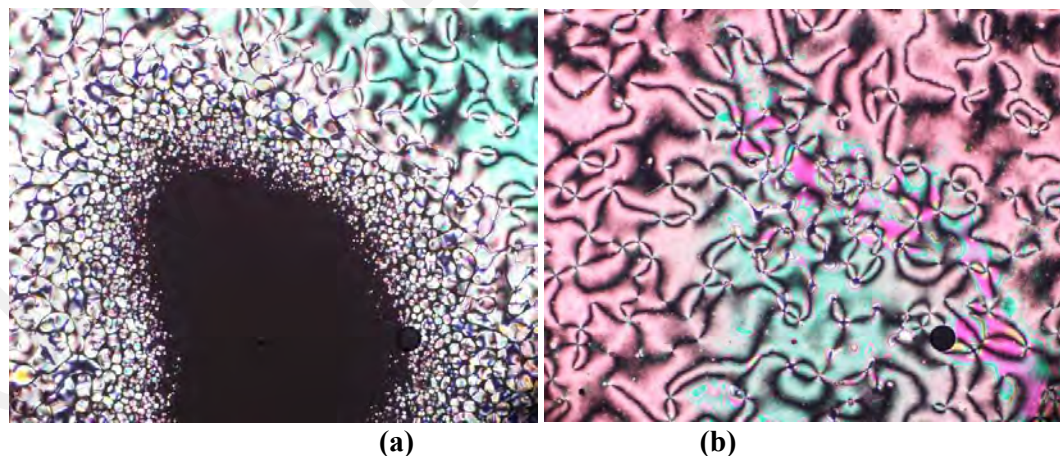


**Figure 4.44: Optical photomicrograph of compound OBSB-OCH<sub>3</sub> exhibiting nematic phase during cooling cycle**

- (a) Isotropic phase transforms into Nematic phase at 89.0 °C
- (b) Schlieren nematic phase texture at 80.0 °C

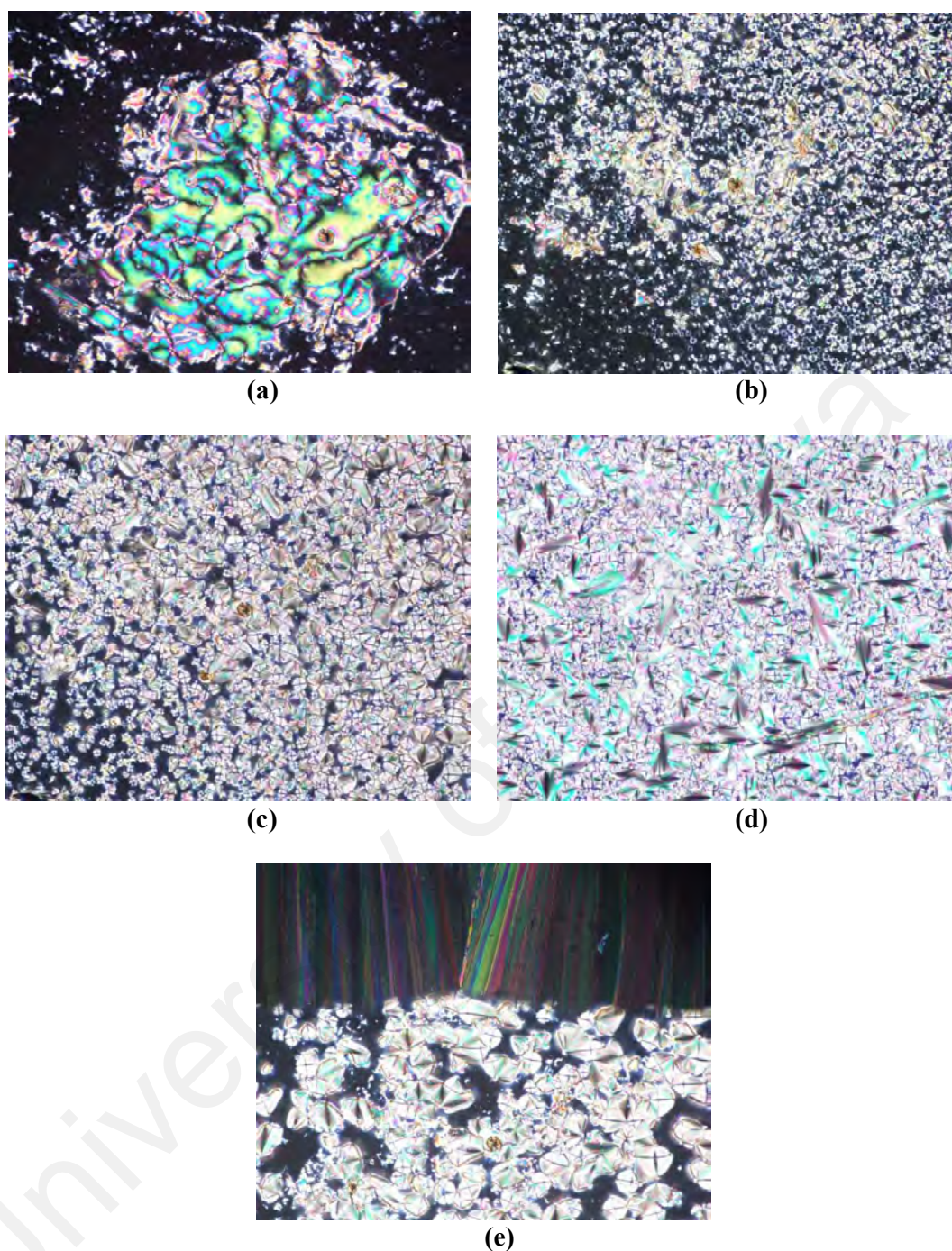
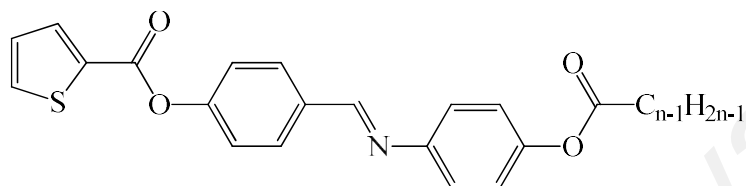


**Figure 4.45: Optical photomicrograph of compound OBSB-Cl exhibiting nematic phase and smectic A phase during cooling cycle**

- (a) Schlieren and homeotropic nematic phase at 69.0 °C
- (b) Nematic phase start to transform into smectic A phase (batonnet) at 64.5 °C
- (c) Smectic A phase growth at 64.5 °C
- (d) Smectic A phase with focal conic structure at 64.0 °C
- (e) Transform of smectic A phase into crystal phase at 63.0 °C

#### 4.4 Series 4

The chemical structure of **nAPTP** is given in Figure 4.46 and the percentage yields are summarized in Table 4.28.



Where  $n = 6, 8, 10, 12, 14, 16$  and  $18$

**Figure 4.46: Structural formula of nAPTP**

**Table 4.28: Percentage yields of nAPTP**

Compound	Yield (%)
<b>6APTP</b>	19
<b>8APTP</b>	23
<b>10APTP</b>	29
<b>12APTP</b>	35
<b>14APTP</b>	42
<b>16APTP</b>	39
<b>18APTP</b>	40

##### 4.4.1 Structural Elucidation

Structural elucidation of **nAPTP** was done by microscopy techniques such as FTIR,  $^1\text{H}$  NMR,  $^{13}\text{C}$  NMR and micro-elemental analysis. The purity of **nAPTP** was monitoring through TLC analysis. Composition data are tabulated in Table 4.29. The analytical data agreed with the calculated values (within 0.5%). The molecular formula of the compounds had been suggested accordingly with those obtained from the spectra.



**Table 4.29: Micro-elemental analytical data of nAFTP**

n	Experimental analysis found ( <i>calculated</i> ) / %					
	C		H		N	
6	68.57	(68.39)	5.67	(5.50)	3.79	(3.32)
8	69.15	(69.46)	6.18	(6.05)	3.06	(3.12)
10	70.42	(70.41)	6.77	(6.54)	2.98	(2.93)
12	70.98	(71.26)	7.08	(6.98)	2.73	(2.77)
14	71.71	(72.01)	7.45	(7.37)	2.58	(2.62)
16	72.53	(72.69)	7.76	(7.72)	2.47	(2.49)
18	73.08	(73.31)	8.11	(8.03)	2.34	(2.37)

The infrared spectrum of **16AFTP** is given in Figure 4.47 and the selected data for **nAFTP** are summarized in Table 4.30. The remaining spectra are presented in Appendix B. From the spectrum of **16AFTP**, the absorption peaks at 2955, 2918, 2873 and 2849  $\text{cm}^{-1}$  were assigned to the symmetric and asymmetric  $\text{sp}^3$  hybridization C–H stretch in the long alkyl group while a characteristic sharp absorption peak at 1729  $\text{cm}^{-1}$  was ascribed to the carbonyl group (C=O) of an ester linkage. The two strong peaks present at 1205 and 1157  $\text{cm}^{-1}$  represented C–O of the ester group where one of the peaks was broader and stronger the other. These observations indicated that the esterification reaction between a hexadecanoic acid and the intermediate compound was successful reacted and formed **16AFTP**.

The aromatic C–H stretch of **16AFTP** appeared at 3075  $\text{cm}^{-1}$  along with the peaks at 1602 & 1469  $\text{cm}^{-1}$  were assigned to the carbon-carbon double bond (C=C) of aromatic rings. These prove that the structure contains aromatic rings. Schiff base group (C=N) indicated by the presence of a peak at 1626  $\text{cm}^{-1}$  and was confirmed with those reported in literature possesses benzylidene aniline group ( $-\text{C}_6\text{H}_5\text{CH}=\text{NC}_6\text{H}_5-$ ) (Ha, *et*



*al.*, 2010, Yeap, *et al.*, 2006). Other characteristic was shown by the absorption peak of **16AFTP** is the C–S–C stretch of the thiophene ring at 862 cm<sup>-1</sup>.

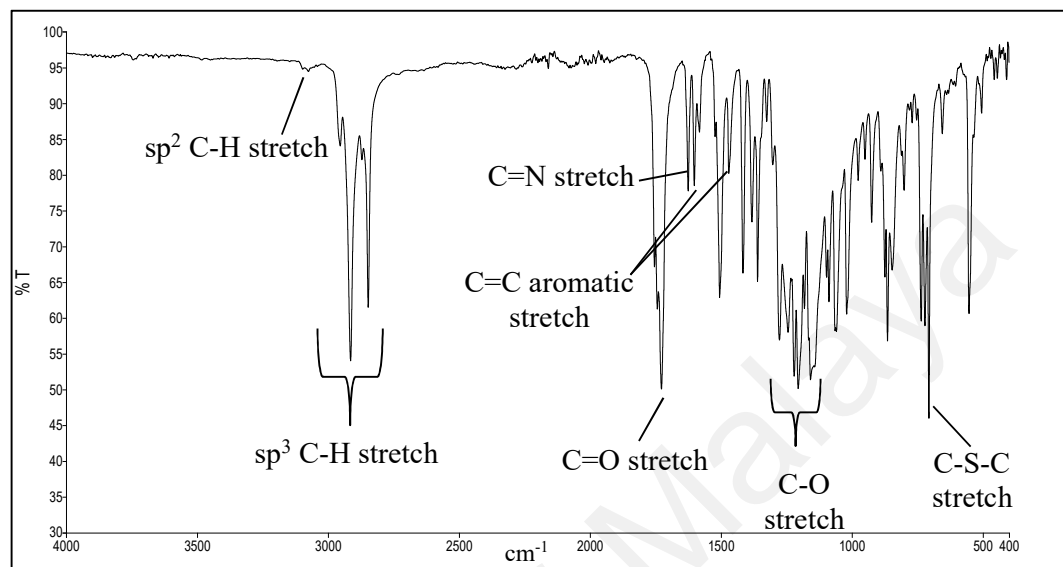


**Figure 4.47: Infrared spectrum of 16AFTP**

**Table 4.30: FTIR spectral analysis data of nAFTP**

Functional group	IR v (cm <sup>-1</sup> )						
	6AFTP	8AFTP	10AFTP	12AFTP	14AFTP	16AFTP	18AFTP
sp <sup>2</sup> C–H stretch aromatic	3075	3076	3075	3075	3075	3075	3075
sp <sup>3</sup> C–H stretch aliphatic	2955 2928 2872	2957 2921 2870 2849	2959 2921 2873 2849	2959 2918 2873 2849	2955 2918 2873 2849	2955 2918 2873 2849	2955 2918 2873 2849
C=O Ester	1728	1728	1726	1726	1729	1729	1729
C=N Schiff base	1626	1626	1626	1626	1626	1626	1626
C=C Aromatic	1602 1467	1602 1467	1602 1469	1602 1469	1602 1472	1602 1469	1602 1469
C–O Ester	1201 1157	1201 1141	1205 1143	1202 1143	1205 1143	1205 1157	1205 1157
C–S–C Thiophene	863	862	862	862	862	862	862

The  $^1\text{H}$  and  $^{13}\text{C}$  NMR spectra of **10AFTP** are given in Figures 4.49 – 4.50 and the selected  $^1\text{H}$  and  $^{13}\text{C}$  NMR data for **10AFTP** are summarized in Tables 4.31 and 4.32. The spectrum of the remaining members in the series is given in Appendix C.

$^1\text{H}$  and  $^{13}\text{C}$  NMR spectral analysis were performed on representative compounds **10AFTP**. The molecular structure with atomic numbering scheme for **10AFTP** is depicted in Figure 4.48.

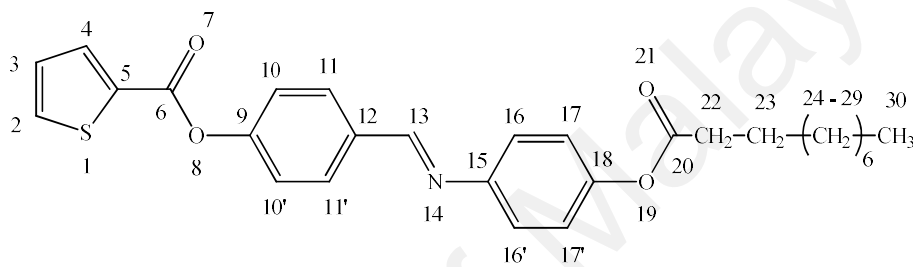


**Figure 4.48: Molecular structure with atomic numbering scheme for 10AFTP**

In the  $^1\text{H}$  NMR spectrum of **10AFTP** (Figure 4.49), a sharp peak appeared as a singlet at chemical shift,  $\delta = 8.46$  ppm corresponded to a Schiff base proton, **H13** ( $-\text{CH}=\text{N}-$ ). The similar chemical also reported by Ha *et al.*, (2011). This gave evidence that imination reaction was successful reacted between 4-aminophenol and intermediate, 4-formylphenyl thiophene-2-carboxylate. The three thiophene protons appeared at chemical shift,  $\delta = 8.01$ , 7.70 and 7.21 ppm and these values agreed with the reported data by Yeap *et al.*, (2009). The triplet at chemical shift,  $\delta = 7.21$  ppm assigned to the **H3** as there were two neighboring protons. **H2** was closer to the electronegative atom, S compared to **H4** as it was deshielded. Hence, the peak at chemical shift,  $\delta = 8.01$  ppm ascribed to **H2** while chemical shift,  $\delta = 7.70$  ppm attributed to **H4**.

In the higher chemical shift region, a total of two pairs of chemical equivalence, but magnetically inequivalence protons appeared as four doublets assigned to the eight aromatic protons. These protons were highly deshielded by a strong anisotropy effect which generated by the delocalized  $\pi$ -electron system of aromatic rings. Two doublets appeared at chemical shift,  $\delta = 7.98$  and  $7.36$  ppm were assigned to **H11/11'** and **H10/10'** respectively and the other two at chemical shift,  $\delta = 7.24$  and  $7.12$  ppm corresponded to **H16/16'** and **H17/17'** respectively.

In the lower chemical shift region, the proton closer to the carbonyl group, **H22**, showed a signal at chemical shift,  $\delta = 2.57$  ppm. This proton was greatly influenced by electron withdrawing effect and  $\pi$ -bond magnetic anisotropy effect. It gave a triplet due to the spin-spin interaction with an **H23** atom. Proton that one bond further from a carbonyl group, **H23**, showed a signal at chemical shift,  $\delta = 1.77$  ppm. Although **H23** was one bond further from the carbonyl group, the magnetic anisotropy effect was still deshielded the **H23**. The multiplet at chemical shift,  $\delta = 1.29$  ppm attributed to **H24 – H29**. The most shielded peak at chemical shift,  $\delta = 0.89$  ppm was assigned to **H30**, and a triplet observed due to spin-spin interaction caused by the protons of the adjacent carbon atom. This chemical shift agreed with the value reported for 4-n-octadecanoyloxybenzylidene-4'-iodoanilines (Ha *et al.*, 2011).

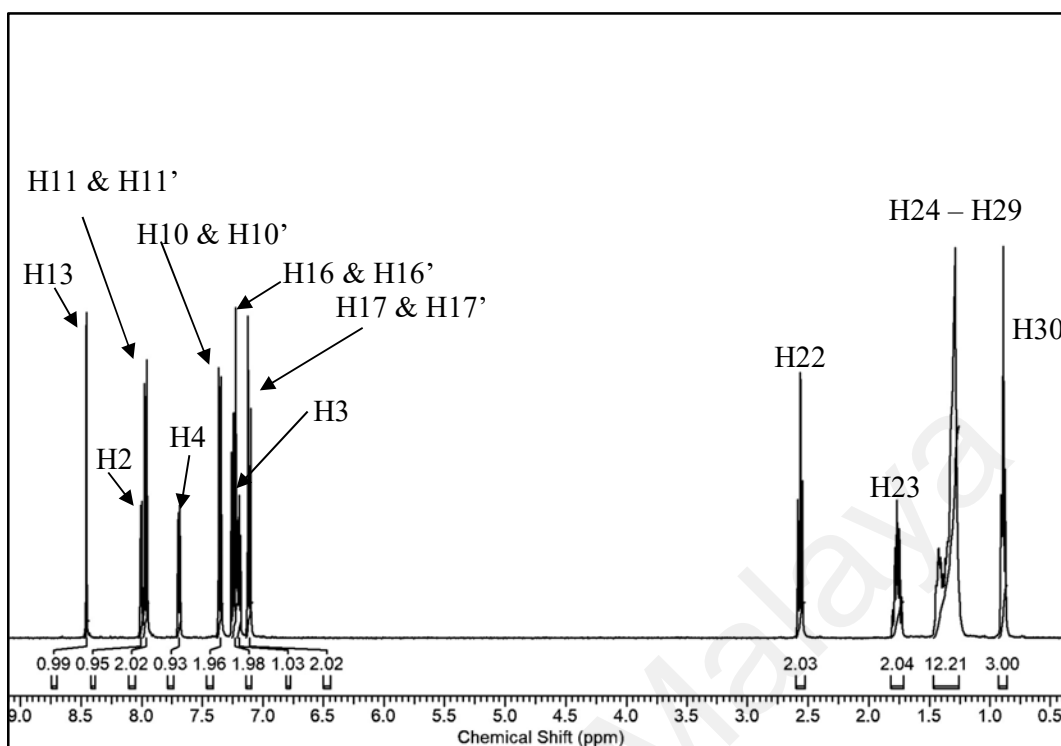


**Figure 4.49:**  $^1\text{H}$  NMR spectrum of compound 10AFTP

**Table 4.31:**  $^1\text{H}$  NMR spectral data of compound 10AFTP in  $\text{CDCl}_3$

Proton number	Chemical shift, $\delta$ ppm	No of Proton	Multiplicity	Coupling constant, $J$ (Hz)
H2	8.00 – 8.01	1H	d	3.7
H3	7.19 – 7.21	1H	t	4.3
H4	7.69 – 7.70	1H	d	4.9
H10, H10'	7.34 – 7.36	2H	d	8.6
H11, H11'	7.95 – 7.98	2H	d	8.6
H13	8.46	1H	s	-
H16, H16'	7.22 – 7.24	2H	d	8.7
H17, H17'	7.10 – 7.12	2H	d	8.8
H22	2.55 – 2.58	2H	t	7.5
H23	1.73 – 1.80	2H	q	7.5
H24 – H29	1.29 – 1.43	12H	m	-
H30	0.87 – 0.91	3H	t	6.7

In the  $^{13}\text{C}$  NMR spectrum of **10AFTP** (Figure 4.50), **C20** atom was an ester carbon which bonded with two electronegative oxygen atoms and gave the peak with the highest chemical shift,  $\delta = 172.45$  ppm. For the ester carbon atom, **C6** near a thiophene ring, it appeared at chemical shift,  $\delta = 160.21$  ppm. A similar chemical shift reported by Yeap *et al.*, (2009). The peak at chemical shift,  $\delta = 159.16$  ppm corresponded to the carbon in Schiff base linkage, **C13**. The remaining twelve peaks between chemical shift,  $\delta = 121.77 - 152.97$  ppm attributed to the aromatic carbons in the two aromatic rings and one thiophene ring. There are four peaks with higher intensities ( $\delta = 121.77, 122.14, 122.25$  and  $130.06$  ppm) than other eight peaks assigned to the eight aromatic carbons, **H10/10'**, **H11/11'**, **H16/16'** and **H17/17'**. **C9**, **C15** and **C18** atoms were either directly attached to an electronegative atom, N or O. The impact from electron withdrawing effect was significant and shifting the peaks to a higher chemical shift region at chemical shift,  $\delta = 148.98, 149.38$  and  $152.97$  ppm. The peak with the chemical shift,  $\delta = 34.43$  attributed to the **C22** and showed the highest chemical shift for the octanoyloxy chain. It may due to direct attached to the carbonyl group and experienced a strong  $\text{sp}^2$  hybridization effect. **C23** atom assigned to a chemical shift,  $\delta = 24.95$  ppm. This assignment was based on previously reported work by Ha *et al.*, (2010) for the Schiff base derivatives with the pyridine core. It may have been due to hyper-conjugation effect with the carbonyl group of the ester linkage. For the methylene groups, **C24 – C29** showed several signals at chemical shift,  $\delta = 22.65 - 31.85$  ppm. The peak at chemical shift,  $\delta = 14.09$  ppm attributed to the methyl group of the alkanoyloxy chain.

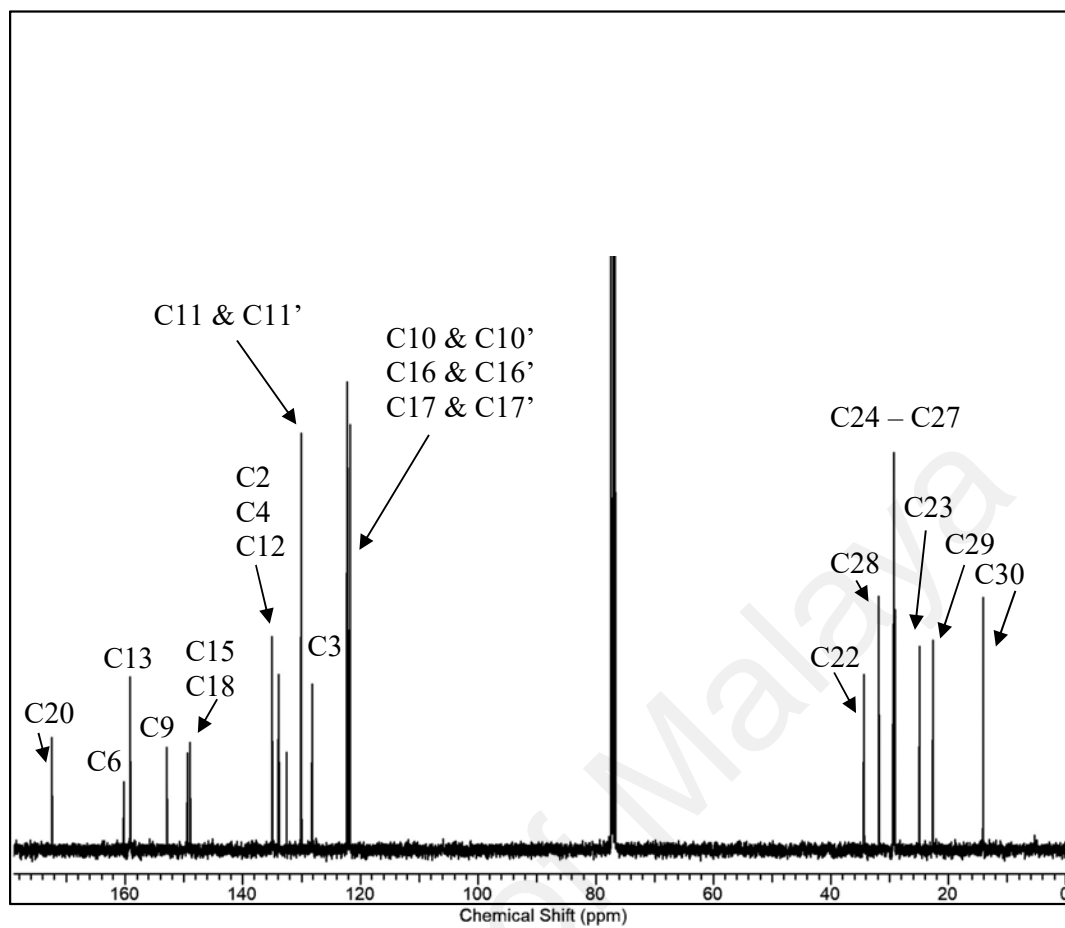


Figure 4.50:  $^{13}\text{C}$  NMR spectrum of compound 10A TP

**Table 4.32:**  $^{13}\text{C}$  NMR spectra data of compound 10AFTP in  $\text{CDCl}_3$

Carbon number	Chemical Shift, $\delta$ ppm
C2	133.83
C3	128.11
C4	134.95
C5	133.92
C6	159.14
C9	152.94
C10, C10'	122.11
C11, C11'	130.04
C12	132.52
C13	160.18
C15	148.96
C16, C16'	121.74
C17, C17'	122.22
C18	149.35
C20	172.43
C22	34.40
C23	24.95
C24 – C27 <sup>a</sup>	29.10
	29.24
	29.40
C28	31.85
C29	22.65
C30	14.09

<sup>a</sup> some of the signals attributed to C24 – C27 appear in the same column in the  $^{13}\text{C}$  NMR spectrum which resulted in less than 4 signals observed in the  $^{13}\text{C}$  NMR spectrum.

#### 4.4.2 Thermal Behavior and Mesomorphic Properties

The study of thermal and mesomorphic properties of **nAFTP** (where  $n = 6, 8, 10, 12, 14, 16$  and  $18$ ) were carried out using DSC and POM methods. Representative DSC thermograms **8AFTP** and **16AFTP** are depicted in Figures 4.51 and 4.52. The phase transition temperatures and associated enthalpy changes ( $\Delta H$ ) obtained from DSC analysis for **nAFTP** are tabulated in Table 4.33. The remaining DSC thermograms of **nAFTP** are given in Appendix D.

From the DSC thermogram of **8AFTP**, a total of two transition peaks observed in both heating and cooling cycles. It corresponds to the phase transition of Cr-N and N-I. For **16AFTP**, there was an additional exothermic peak in the cooling cycle compared to heating cycle. The compound was exhibited monotropic smectic C phase.

An additional exotherm for **16AFTP** during cooling cycle indicated the presence of monotropic mesophases and confirmed as SmC through POM (Dierking, 2003). For the last member of the homologous series, **18AFTP**, the SmC phase existed in both heating and cooling cycles. The DSC thermograms of **nAFTP** revealed that they were enantiotropic nematogen.



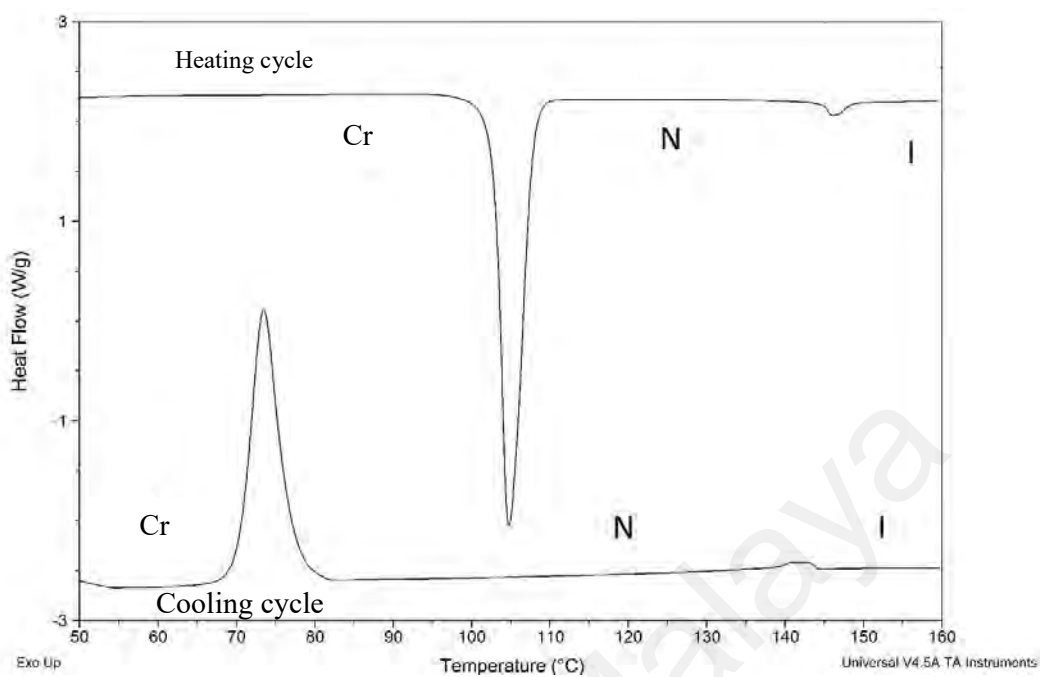


**Figure 4.51: DSC thermogram of 8AOTP**

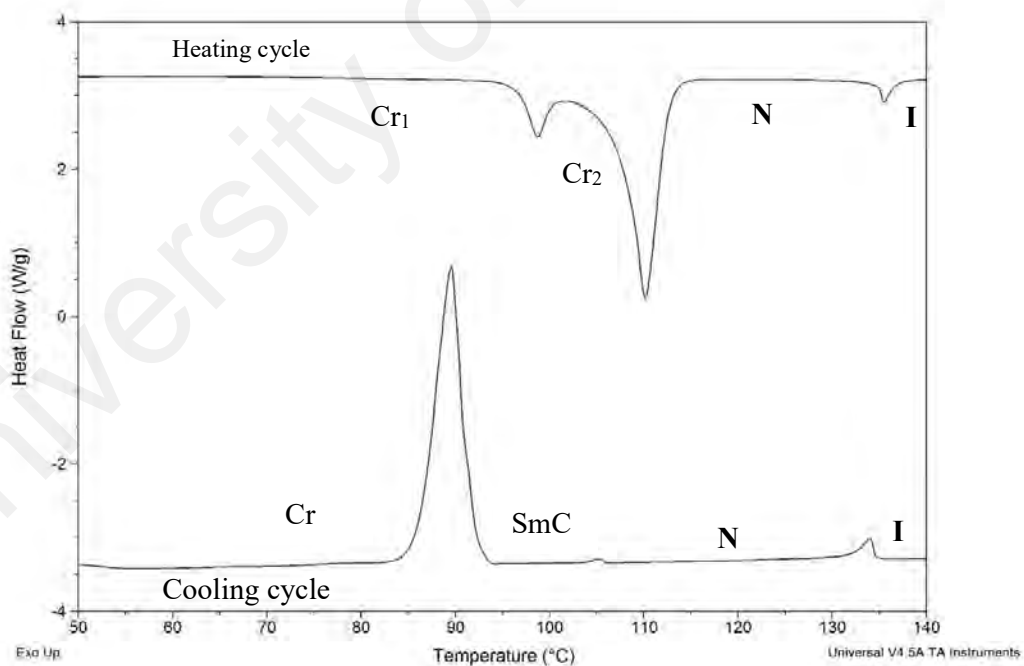


**Figure 4.52: DSC thermogram of 16AOTP**

**Table 4.33: Phase transition temperatures and associated enthalpy changes of series nAOTP**

Compound	Phase transition, °C	
	(Corresponding enthalpy changes, kJ mol <sup>-1</sup> )	
<b>6AOTP</b>	Cr <sub>1</sub> 85.08 (5.88) Cr <sub>2</sub> 95.43 (24.65) N 156.81 (0.55) I <i>I 156.69 (0.47) N 75.86 (20.72) Cr</i>	
<b>8AOTP</b>	Cr 104.75 (38.67) N 146.10 (1.06) I <i>I 143.30 (1.02) N 73.49 (33.61) Cr</i>	
<b>10AOTP</b>	Cr <sub>1</sub> 84.45 (0.95) Cr <sub>2</sub> 105.51 (28.03) N 141.04 (1.09) I <i>I 136.30 (0.71) N 81.14 (29.07) Cr</i>	
<b>12AOTP</b>	Cr <sub>1</sub> 89.51 (0.81) Cr <sub>2</sub> 108.08 (31.92) N 142.25 (0.91) I <i>I 141.15 (1.01) N 84.53 (34.72) Cr</i>	
<b>14AOTP</b>	Cr <sub>1</sub> 89.53 (0.66) Cr <sub>2</sub> 108.96 (38.21) N 141.93 (1.27) I <i>I 139.27 (1.37) N 82.90 (40.61) Cr</i>	
<b>16AOTP</b>	Cr <sub>1</sub> 100.34 (3.88) Cr <sub>2</sub> 111.01 (33.26) N 135.67 (2.10) I <i>I 134.15 (2.37) N 105.48 (0.32) SmC 89.75 (47.45) Cr</i>	
<b>18AOTP</b>	Cr <sub>1</sub> 91.78 (2.67) Cr <sub>2</sub> 105.76 (32.30) SmC 109.76 (0.02) N 132.92 (2.01) I <i>I 131.05 (1.60) N 107.43 (0.14) SmC 90.82 (42.39) Cr</i>	

The optical photomicrographs of **10AOTP** and **18AOTP** are shown in Figures 4.53 and 4.54. The graph of transition temperature during heating or cooling cycles against the number of carbon atoms in the alkanoyloxy chain ( $n = 6, 8, 10, 12, 14, 16$  and 18) for **nAOTP** are plotted and shown in Figures 4.55 and 4.56.

Upon cooling of **10AOTP**, nematic phase (Figure 4.53) with schlieren texture was observed during the cooling cycle. On further cooling from nematic phase, the texture directly transformed into crystal phase (region B). During the cooling cycles of **18AOTP**, the nematic phase was observed and transited into SmC phase upon further cooling. It illustrated in Figure 4.54. A characteristic bar transition texture (Dierking, 2003) was observed. The SmC phase with schlieren texture was observed for **18AOTP**.

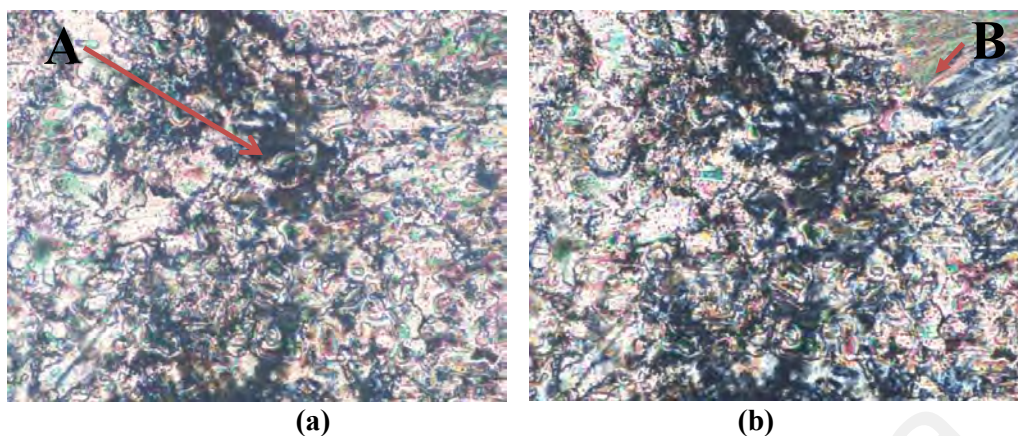


**Figure 4.53: Optical photomicrograph of compound 8AOTP exhibiting nematic phase during cooling cycle**

- (a) Nematic phase and homeotropic texture (Region A) at 90 °C
- (b) Crystal phase (Region B) started to form at 74 °C

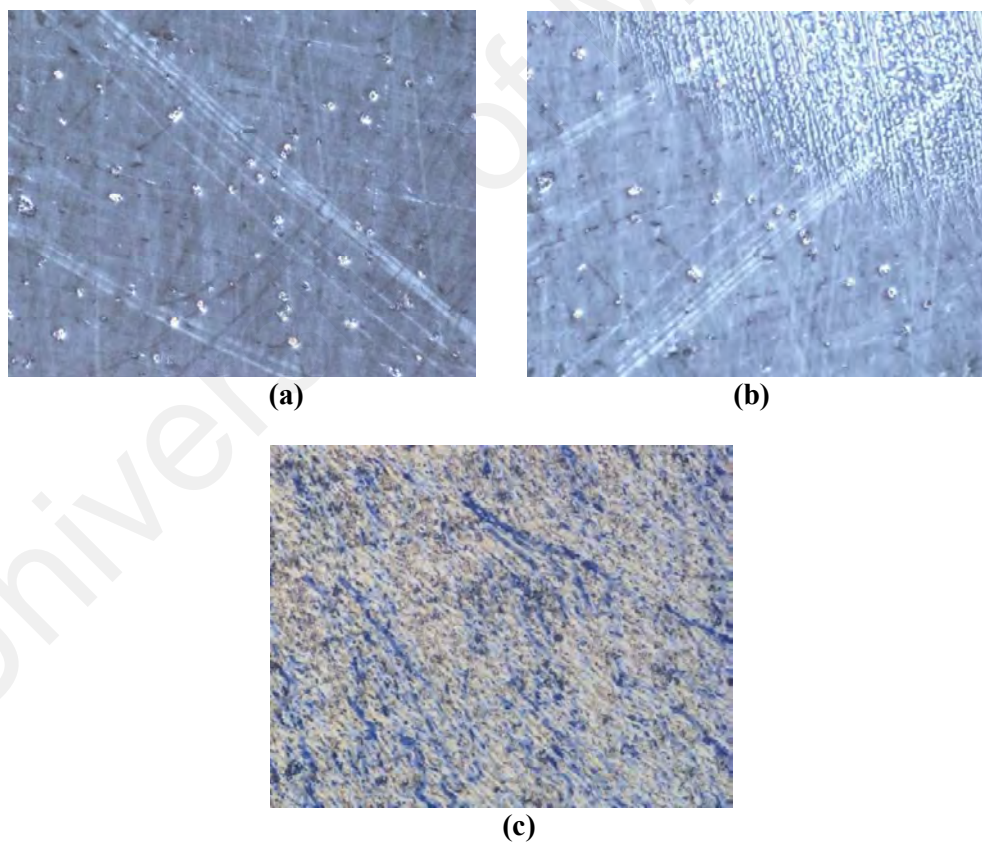


**Figure 4.54: Optical photomicrograph of compound 18AOTP exhibiting SmC phase upon further cooling from nematic phase**

- (a) Homeotropic texture of nematic phase at 105 °C
- (b) Bar transition of nematic (left) to SmC (right) phase at 91 °C
- (c) SmC phase with schlieren texture at 85 °C

As the length of carbon atoms increased (Figures 4.55 – 4.56), the clearing temperatures of **nAPTP** showed a decreasing trend. This may have been coming from the flexibility of the alkanoyloxy chain that reduced the interaction between molecules. Thus, isotropization temperature had been reduced. However, the melting temperatures showed an increasing trend as the carbon chain increased. As the number of carbons increased, the strength of the van der Waals force increased and held the molecules strongly. Hence, extra energy needed to separate the molecules.

The enantiotropic nematic phase observed from *n*-hexanoyloxy to the *n*-octadecanoyloxy derivatives. However, the nematic phase stability ( $T_N$ ) is decreased as the number of carbons increased. It may have been due to the flexibility of the molecules. This excess in flexibility tends to disrupt the packing of the molecules which required for the generation of the nematic phase. In other words, the alkanoyloxy chain emerged lamellar packing which led to the presence of the smectic phase. This showed by the *n*-hexadecanoyloxy and *n*-octadecanoyloxy derivatives where the SmC phase present as monotropic mesophase for *n*-hexadecanoyloxy derivative and enantiotropic smectic C phase for the *n*-octadecanoyloxy derivative.

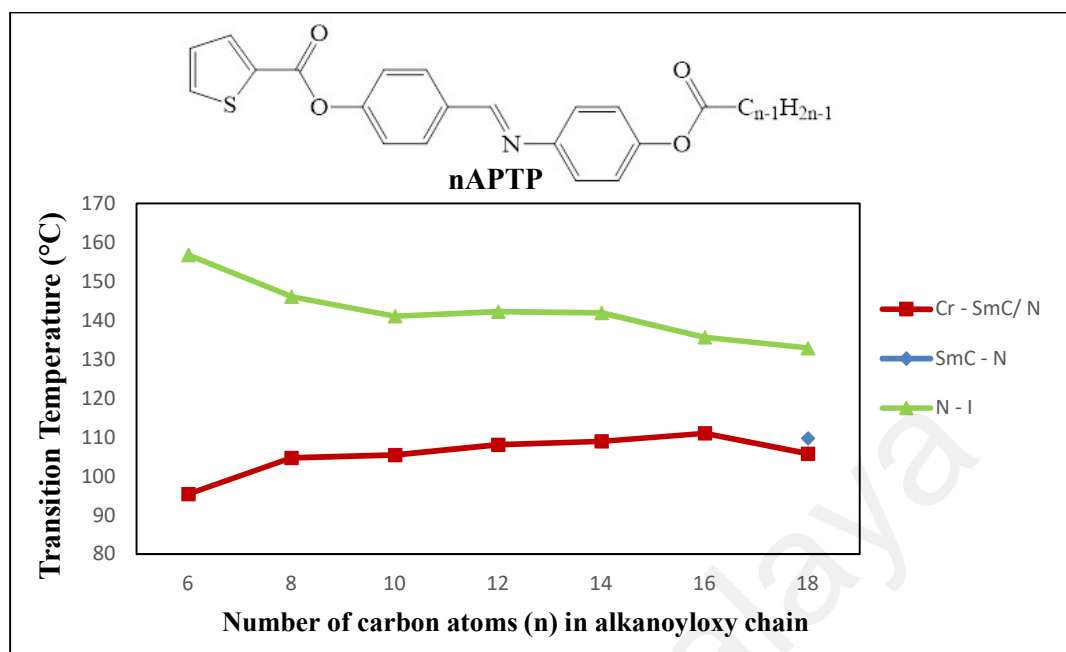


Figure 4.55: Plot of transition temperatures of nAOTP during heating cycle as a function of the number of carbon atoms

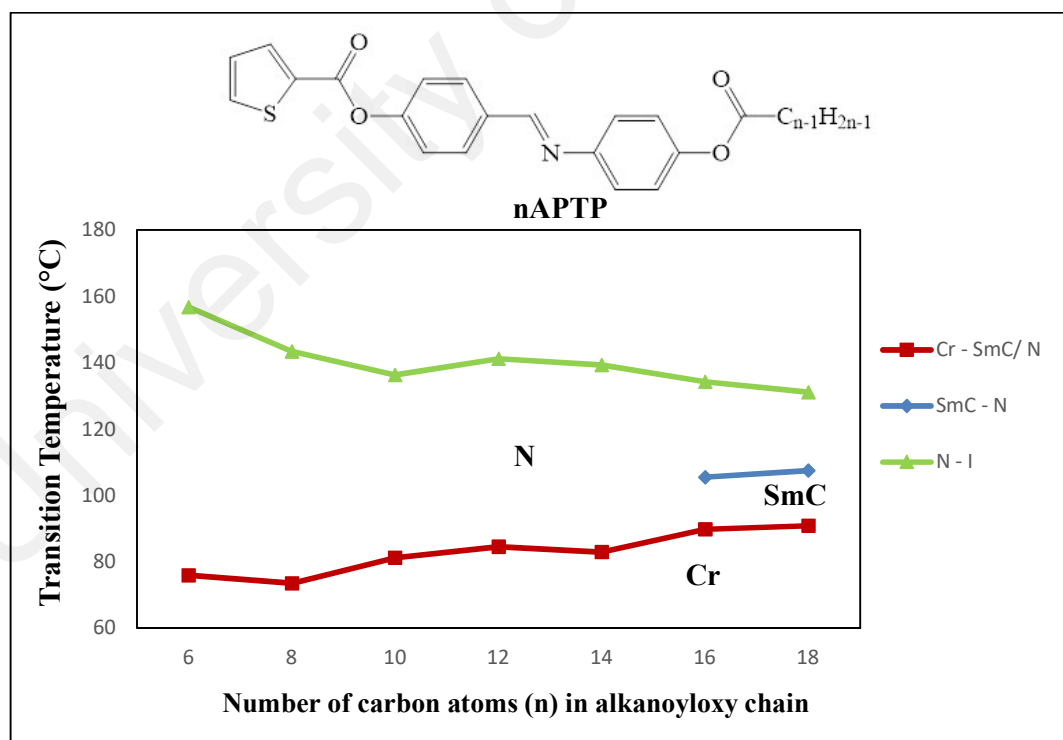


Figure 4.56: Plot of transition temperatures of nAOTP during cooling cycle as a function of the number of carbon atoms

## CHAPTER 5: CONCLUSION & FUTURE WORK

Schiff base liquid crystals with alkanoyloxy chain or terminated-alkanoyloxy chain are not extensively study in literature. A total of four series of rod-like liquid crystals possessing either two to four mesogenic cores, which was not studied previously in literature has been successfully synthesized and characterized. The results of each series are concluded in the following sections. These results can fill up the parts that were not being explored by other researchers, also capable to strengthen the fundamental knowledge of the science of liquid crystals and able to provide any possible studies on their prospect applications.

### 5.1 Series 1

Three sub-series of two aromatic rings Schiff's base liquid crystal were successfully synthesized. For sub-series 1, all **nSB-CH<sub>3</sub>** compounds exhibited liquid crystalline properties. Shorter members ( $n = 8$  &  $10$ ) showed monotropic nematic mesophase except *n*-hexanoyloxy derivative is non-mesogenic. The presence of monotropic SmA phase was observed at longer carbon chain compounds ( $n = 12, 14, 16$  &  $18$ ). Additional SmB phase had been observed for the homologous members ( $n = 14, 16$  &  $18$ ). For *n*-tetradecanoyloxy derivative, it showed the richest mesomorphism properties. For **nSB-CH<sub>3</sub>** sub-series, all compounds were nematogens. Shorter members ( $n = 6, 8, 10$  &  $12$ ) showed the enantiotropic nematic phase in both heating and cooling cycles. Later compounds ( $n = 14, 16$  &  $18$ ), monotropic nematic phase was observed. This may arise due to the dilution of the core by the long alkyl chain and increased in van der Waals' force. Hence, the nematic phase had been depleted. All compounds in **nSB-NDEA** were non-mesogenic compounds. This is due to the present bulky group

(N,N-diethylamino) which blocked the molecules from orientated closer to each other to generate the liquid crystal properties.

## 5.2 Series 2

A series of seven liquid crystals comprising two mesogenic core units connected by Schiff base linkage were successfully synthesized and characterized. All the compounds showed mesomorphic properties. For short chain members ( $n = 6, 8, 10, 12, 14$  &  $16$ ), enantiotropic nematic phase was observed. The SmA had been started to emerge as monotropic mesophase from *n*-tetradecanoyloxy derivative with the later two members ( $n = 16$  &  $18$ ) showed the enantiotropic smectic A phase. The nematic phase was absent for *n*-octadecanoyloxy derivatives. This may have been due to the alkyl chain provided excess flexibility which increased the lateral intermolecular force of the molecules. This had been given a better chance for the smectic phase (lamellar packing).

## 5.3 Series 3

A series of six liquid crystals comprised two mesogenic core units connected by Schiff base linkage with a  $\omega$ -bromoundecanoyloxy chain were successfully synthesized and characterized. The compound with the terminal substituent  $R = Cl$  and  $OCH_3$  showed liquid crystal properties whereas the others showed non-mesogenic properties. For **OBSB- $OCH_3$** , the enantiotropic nematic phase was observed. Meanwhile, **OBSB- $Cl$**  showed monotropic nematic and SmA phases. SmA phase existed only for a short range of temperature.

## 5.4 Series 4

A series of seven thiophene-based liquid crystals comprised three mesogenic core units connected by Schiff base linkage were successfully synthesized and characterized. Enantiotropic nematic phase was observed from *n*-hexanoyloxy to the *n*-octadecanoyloxy derivatives. For a longer alkanoyloxy chain, it was favoured to lamellar packing and led to the presence of the smectic phase. This was shown by the *n*-hexadecanoyloxy where the SmC phase existed as monotropic mesophase, whereas enantiotropic SmC phase was observed for the *n*-octadecanoyloxy derivative.

## 5.5 Recommendations for Future Work

Discovery of new molecular structures for thermotropic liquid crystals as advanced functional materials has grabbed the attention of many scientists. There are still numbers of researchable potentials in the applications. The conventional nematic liquid crystal device for example, has the fast switching properties that can be achieved in microsecond region. In order to improve this characteristic, certain studies can be carried out to further enhancement of viscosity, elastic constant and dielectric anisotropy.



## REFERENCES

- Ahmed, H. A., Naoum, M. M., & Saad, G. R. (2016). Mesophase behaviour of 1:1 mixtures of 4-n-alkoxyphenylazo benzoic acids bearing terminal alkoxy groups of different chain lengths. *Liquid Crystals*, 1-9.
- Ajeetha, N., & Ohja, D. P. (2009). Influence of oxygen on phase behaviour of N-(p-n-octyloxybenzylidene)-p-n-alkoxyanilines: a comparative study. *Molecular Crystals and Liquid Crystals*, 501, 86-93.
- Ajeetha, N., & Ohja, D. P. (2010). The influence of oxygen on mesomorphic behaviour of benzylidene anilines - the effect of end chain. *Molecular Crystals and Liquid Crystals*, 528(1), 96-102.
- Ajeetha, N., & Pisipati, V. (2003). The influence of the position of oxygen on the phase behaviour of benzylidene anilines. *Zeitschrift für Naturforschung A*, 58(12), 735-737.
- Ajeetha, N., Rao, M., Prasad, P., & Pisipati, V. (2005). Phase transitions and pre-translational effects in m-(p-n-pentylbenzylidene)-p-n-pentylaniline (5.5) and its oxygen derivatives - a dilatometric study. *Zeitschrift für Naturforschung A*, 60(10), 749-752.
- Alshargabi, A., Yeap, G. Y., Takeuchi, D., & Ito, M. M. (2013). Synthesis and terminal chain effect on the phase transition behavior of azo-bridged benzothiazole-phenyl ethers. *Molecular Crystals and Liquid Crystals*, 575(1), 128-139.
- Belmar, J. (1999). New liquid crystals containing the benzothiazole unit: amides and azo compounds. *Liquid Crystals*, 26(3), 389-396.
- Buchs, J., Gebner, A., Heyne, B., Jabetz, D., & Sawade, H. (2018). Florescent liquid crystals with rod-shaped pi-conjugated hydrocarbon core. *Liquid Crystals*, 1-18.
- Chien, L. C., Cada, L. G., & Xie, L. (1992). Liquid crystalline behaviour of 4-( $\omega$ -aminoalkoxy)-4'-cyanobiphenyls and their side chain epoxy polymers. *Liquid Crystals*, 12(5), 853-861.
- Collings, P. J. (2002). *Liquid crystals: nature's delicate phase of matter*. New Jersey: Princeton University Press.
- Collings, P. J., & Hird, M. (1997). *Introduction to liquid crystals: chemistry and physics*. Philadelphia: Taylor & Francis Inc.
- Demus, D., Goodby, J., Gray, G. W., & Spiess, H. W. (1998). *Handbook of liquid crystals volume 2A: low molecular weight liquid crystal I*. Weinheim: WILEY-VCH Verlag GmbH & Co. KGaA.
- Dierking, I. (2003). *Textures of liquid crystals*. Weinheim: WILEY-VCH Verlag GmbH & Co. KGaA.

- Du, M., Li, L., Zhang, J., Li, K., Cao, M., Mo, L., . . . Yang, H. (2018). Photoresponsive iodine-bonded liquid crystals based on azopyridine derivatives with a low phase-transition temperature. *Liquid Crystals*, 1-8.
- Foo, K. L., Ha, S. T., Lin, C. M., Lin, H. C., Lee, S. L., Yeap, G. Y., & Sastry, S. S. (2015). Synthesis, characterisation and mesomorphic properties of new symmetrical dimer liquid crystals derived from benzothiazole. *Karbala International Journal of Modern Science*, 1(3), 152-158.
- Foo, K. L., Ha, S. T., Yeap, G. Y., & Lee, S. L. (2018). Mesomorphic behaviors of a series of heterocyclic thiophene-imine-ester-based liquid crystals. *Phase Transitions*, 1-12.
- Galewski, Z. (1987). Liquid crystalline properties of 4-chlorobenzylidene-4-alkylanilines. *Molecular Crystals and Liquid Crystals Incorporating Nonlinear Optics*, 151(1), 233-241.
- Galewski, Z. (1990). Liquid crystalline properties of 4-nitrobenzylidene-4-alkylanilines. *Molecular Crystals and Liquid Crystals Incorporating Nonlinear Optics*, 191(1), 211-218.
- Galewski, Z. (1994). Liquid crystalline properties of 4-halogenbenzylidene-4-alkylanilines. *Molecular Crystals and Liquid Crystals*, 249, 43-49.
- Galewski, Z., & Coles, H. J. (1999). Liquid crystalline properties and phase situation in 4-chlorobenzylidene-4'-alkylanilines. *Journal of Molecular Liquids*, 79(1), 77-87.
- Gandolfo, C., Grasso, D., Buemi, G., & Torquati, G. (1988). Phase transitions and structural studies of p-n-alkoxybenzylidene-p'-fluoro-anilines. *Il Nuovo Cimento D*, 10(2), 1363-1371.
- Godzwon, J., Sienkowska, M. J., & Galewski, Z. (2009). Liquid-crystalline properties of 4-octyloxybenzylidene-4'-alkyloxyanilines and their mixtures with 4-pentyloxybenzylidene-4'-heptylaniline. *Thermochimica Acta*, 491, 71-79.
- Gray, G. W. (1998). Reminiscences from a life with liquid crystals. *Liquid Crystals*, 24(1), 5-14.
- Gray, G. W., & Goodby, J. W. (1984). *Smectic liquid crystals: textures and structures*. Glasgow: Leonard Hill.
- Gray, G. W., Harrison, K. J., & Nash, J. A. (1973). New family of nematic liquid crystals for displays. *Electronics Letters*, 9(6), 130-131.
- Griffin, A. C., & Vaidya, S. R. (1989). effect of molecular structure on mesomorphism 22. liquid crystalline 1-alkanol derivatives. *Molecular Crystals and Liquid Crystals Incorporating Nonlinear Optics*, 173(1), 85-88.
- Ha, S. T., Lee, T. L., Lee, S. L., Yeap, G. Y., Yip, F. W., & Ong, S. T. (2012). Mesomorphic behaviour of new azomethine liquid crystals having terminal bromo substituent. *Chinese Chemical Letters*, 23(2), 177-180.

- Ha, S. T., & Lee, T. L. (2014). Synthesis and mesomorphic properties of new fluorinated schiff base liquid crystals. *ISRN Material Science*, 1-12.
- Ha, S. T., Koh, T. M., Lin, H. C., Yeap, G. Y., Yip, F. W., Ong, S. T., . . . Ong, L. K. (2009). Heterocyclic benzothiazole-based liquid crystals: synthesis and mesomorphic properties. *Liquid Crystals*, 36(9), 917-925.
- Ha, S. T., Lee, T. L., Lee, S. L., Yeap, G. Y., Lin, H. C., & Ito, M. M. (2014). Mesomorphic properties and x-ray diffraction studies of 4-alkanoyloxybenzylidene-4'-fluoroaniline. *Asian Journal of Chemistry*, 26(22), 7737-7740.
- Ha, S. T., Lee, T. L., Yeap, G. Y., Ito, M. M., Saito, A., & Watanabe, M. (2011). Mesomorphic behavior of new azomethine liquid crystals having terminal iodo group. *Chinese Chemical Letters*, 22(3), 749-752.
- Ha, S. T., Ong, L. K., Lee, S. L., Lin, H. C., Yip, F. W., & Ong, S. T. (2010). Synthesis and mesomorphic properties of schiff base esters possessing terminal chloro substituent. *Chinese Chemical Letters*, 22(6), 637-640.
- Ha, S. T., Ong, L. K., Ong, S. T., Yeap, G. Y., Wong, J. P., Koh, T. M., & Lin, H. C. (2009). Synthesis and mesomorphic properties of new schiff base ester with different alkyl chains. *Chinese Chemical Letters*, 20(7), 767-770.
- Ha, S. T., Ong, L. K., Yasodha, S., Yeap, G. Y., Boey, P. L., & lin, H. C. (2010). New mesogenic schiff base ester with polar chloro substituent: synthesis, thermotropic properties and x-ray diffraction studies. *American Journal of Applied Sciences*, 7(2), 214-220.
- Ha, S. T., Yeap, G. Y., & Boey, P. L. (2009). Synthesis and liquid crystalline properties of new schiff bases n-[4-(4-n-alkanoyloxybenzoyloxy)benzylidene]-4-cyano-, 4-hydroxy-, 4-thio- and 4-nitroanilines. *Australian Journal of Basic and Applied Sciences*, 3(4), 3417-3422.
- Hagar, M., Ahmed, H. A., & Saad, G. R. (2018). Mesophase stability of new schiff base ester liquid crystals with different polar substituents. *Liquid Crystals*, 1-9.
- Haramoto, Y., & Kamogawa, H. (1989). Optical properties of new ferroelectric liquid crystal materials: (+)-2-methylbutyl-4-(5-alkyl-1,3-dioxan-2-yl) benzoate. *Molecular Crystals and Liquid Crystals*, 173, 89-93.
- Haramoto, Y., Meki, M., & Kamogawa, H. (1993). New liquid crystal materials with chiral 2-methylbutyl group: (+)-2-methylbutyl-4-(5-alkyl-1,3-dioxan-2-yl) cinnamate and benzoate. *Molecular Crystals and Liquid Crystals*, 231(1), 175-182.
- Imrie, C. T., Lu, Z. B., Picken, S. J., & Yildirim, Z. (2007). Oligomeric rod-disc nematic liquid crystals. *Chemistry Communication*, 1245-1247.
- Jadav, N. D., Prajapati, B. A., & Prajapati, A. K. (2003). Azomesogens containing two fused ring moieties: synthesis and characterisatization. *Molecular Crystals and Liquid Crystals*, 399(1), 53-60.

- Jber, N. R., Shukur, M. M., & Najaf, A. A. (2014). Schiff base liquid crystals with terminal alkoxy group synthesis and thermotropic properties. *Journal of Al-Nahrain University*, 17(2), 64-72.
- Jia, Y. G., Luo, C. C., Zhu, Z. X., & Hu, J. S. (2016). Synthesis and properties of new (-)-menthol-derived chiral liquid crystal compounds with alkyl or alkoxy terminal groups. *Liquid Crystals*, 1-12.
- Kato, T., Hirai, Y., Nakaso, S., & Moriyama, M. (2007). Liquid-crystalline physical gels. *Chemical Society Reviews*, 36(12), 1845-2188.
- Korbecka, I., Pocięcha, D., & Galewski, Z. (2017). 4-Octylphenylazo-4'-phenyl alkanoates - homologous series of azomesogens with extremely rich liquid-crystalline polymorphism. *Liquid Crystals*, 1-7.
- Kotadiya, V. C., & Bhoya, U. C. (2015). The mesomorphic properties of chalcone dimer derivatives. *Molecular Crystals and Liquid Crystals*, 608(1), 116-124.
- Krishnan, S. A., Weissflog, W., Pelzl, G., Diele, S., Kresse, H., Vakhovskaya, Z., & Friedemann, R. (2006). DMT and MD studies on the influence of the orientation of ester linkage groups in banana-shape mesogens. *Physical Chemistry Chemical Physics*, 8, 1170-1177.
- Kumar, S. (2001). *Liquid Crystals: Experiment study of physical properties and phase transitions*. Cambridge: Cambridge University Press.
- Kumar, S., & Pal, S. K. (2005). The first examples of terminally thiol-functionalized alkoxy cyanobiphenyls. *Liquid Crystals*, 52(5), 659-661.
- Lunkwitz, R., Tschierske, C., & Diele, S. (2001). Formation of smectic and columnar liquid crystalline phases by cyclotrimeratrylene (ctv) and cyclotetraatrylene (cttv) derivatives incorporating calamitic structural units. *Journal of Material Chemistry*, 7(10), 2001-2011.
- McAllister, L. J., Prasang, C., Wong, J. P.-W., Thatcher, R. J., Whitwood, A. C., Donnio, B., . . . Bruce, D. W. (2013). Halogen-bonded liquid crystals of 4-alkoxystilbazoles with molecular iodone: a very short halogen bond and unusual mesophase stability. *Chemistry Communication*, 49, 3946.
- Mingos, D. M. (1999). *Liquid crystal II*. Berlin: Springer-Verlag GmbH.
- Mohammad, A. T., Alwari, R. Y., Srinivasa, H. T., Husain, S. M., & Alajrawy, O. I. (2018). Preparation, spectral and thermal properties of new isoflavone derivatives: mesomorphic properties and DFT studies. *Liquid Crystals*, 1-12.
- Ong, L. K., Ha, S. T., Yeap, G. Y., & Lin, H. C. (2018). Heterocyclic pyridine-based liquid crystals: synthesis and mesomorphic properties. *Liquid Crystals*, 1-11.
- Pavia, D. L., Lampman, G. M., & Kriz, G. S. (2001). *Introduction to spectroscopy: a guide for students of organic chemistry* (3rd ed.). United States of America: Thompson Learning, Inc. Thomson.

- Prajapati, A. K. (2000). Effect of a lateral methyl group on azomesogens containing the naphthalene moiety. *Liquid Crystals*, 27(8), 1017-1020.
- Prajapati, A. K. (2001). Mesogenic biphenyl derivatives with azo and ester central linkage. *Molecular Crystals and Liquid Crystals*, 364(1), 769-777.
- Prajapati, A. K., & Bonde, N. L. (2006). Mesogenic benzothiazole derivatives with methoxy substituents. *Journal of Chemical Science*, 118(2), 203-210.
- Prajapati, A. K., & Pandya, H. M. (2003). Effect of lateral chloro group on azomesogens containing naphthalene moiety. *Molecular Crystals and Liquid Crystals*, 393(1), 31-39.
- Prajapati, A. K., & Varia, M. .. (2008). Azomesogens with polar chloro, nitro and phenolic-oh substituents. *Liquid Crystals*, 1271-1277.
- Prajapati, A. K., Thakkar, V., & Bonde, N. (2003). New mesogenic homologous series of schiff base cinnamates comprising naphthalene moiety. *Molecular Crystals and Liquid Crystals*, 393(1), 41-48.
- Reddy, M. K., Reddy, K. S., Kumar, B. V., & Narasimhaswamy, T. (2014). Synthesis, structural and mesophase characterization of three ring based thiophene liquid crystals. *Molecular Crystals and Liquid Crystals*, 593, 1-24.
- Rosa, R. R., Tariq, M., Weber, C. S., Hameed, S., Silva, S., & Merlo, A. A. (2016). Hybrid liquid crystals tetrazolyl and isoxazolyl cinnamates. *Liquid Crystals*, 1-12.
- Sakagami, S., & Nakimzo, M. (1980). Liquid crystalline properties of n-(4-alkoxybenzylidene)-4-halogenoanilines. *Bulletin of the Chemical Society of Japan*, 53(1265), 266.
- Sakagami, S., Koga, T., & Takase, A. (2002). Liquid crystalline properties and photochromism of 4-halogeno-n-(4-alkoxysalicylidene)anilines. *Molecular Crystals and Liquid Crystals*, 373(1), 71-81.
- Sakurai, S., Takenaka, S., Miyake, H., Morita, H., & Ikemoto, T. (1989). Molecular structure and smectic properties. part 1. the effect of linkages on smectic a thermal stability in three aromatic ring compounds linked by ester groups. *Journal of the Chemical Society, Perkin Transactions 2*(9), 1199-1204.
- Schroeder, D. C., & Schroeder, J. P. (1974). P-phenylene di-p-amino and di-p-hydroxybenzoate. novel mesomorphism of an amine and a phenol. *Journal of the American Chemical Society*, 96, 4347-4348.
- Shanker, B. R., & Pisipati, V. G. (2011). *Liquid crystalline organic compounds and polymers as materials of the xxi century; from synthesis to applications. an overview of liquid crystals based on schiff base compounds*. Kerala: Transworld Research Network.
- Singh, S., & Dunmur, D. A. (2002). *Liquid crystals fundamentals*. New Jersey: World Scientific Publishing Co. Pte. Ltd.

- Starkulla, G. F., kapatsina, E., Baro, A., Giesselmann, F., Tussetchlager, S., Kaller, M., & Laschat, S. (2009). Influence of spacer chain lengths and polar terminal groups on the mesomorphic properties of tethered 5-phenylpyrimidines. *Beilstein Journal of Organic Chemistry*, 63(5), 1-10.
- Taki, S., Okabe, H., & Kai, S. (2003). Study of odd-even effect in molecular alignments of nOCB liquid crystals: stm observation and charge density distribution analysis. *Japan Journal of Applied Physics*, 42, 7053-7056.
- Taylor & Francis. (1984). Benzylidene anilines. *Molecular Crystals and Liquid Crystals*, 115 (1), 238 - 251.
- Thaker, B. T., & Kanojiya, J. B. (2011). Synthesis, characterization and mesophase behavior of new liquid crystalline compounds having chalcone as a central linkage. *Molecular Crystals and Liquid Crystals*, 542(1), 84-98.
- Thaker, B. T., Patel, B. S., Dhimmar, Y. T., Solanki, D. B., Chothani, N. J., Patel, N. B., . . . Makavana, U. (2012). Synthesis, characterization and mesomorphic properties of new rod-like thiophene based liquid crystals. *Molecular Crystals and Liquid Crystals*, 526, 98-113.
- Thaker, B. T., Patel, P. H., Vansadiya, A. D., & Kanojiya, J. B. (2009). Substitution effects on the liquid crystalline properties of thermotropic liquid crystals containing schiff base chalcone linkages. *Molecular Crystals and Liquid Crystals*, 515(1), 135-147.
- Thaker, B. T., Solanki, D. B., Patel, B. S., & Patel, N. B. (2013). Synthesis, characterization and liquid crystalline properties of some schiff base and cinnamate central linkages involving 1,3,5-trisubstituted pyrazolone ring system and their cu(ii) complexes. *Liquid Crystals*, 562, 1296-1309.
- Vora, R., & Prajapati, A. K. (1998). Mesogenic homologous series with a naphthalene moiety. *Liquid Crystals*, 25(5), 567-572.
- Vora, R., Prajapati, A. K., & Kevat, J. (2001). Effect of terminal branching on mesomorphism. *Molecular Crystals and Liquid Crystals*, 357(1), 229-237.
- Wong, J. P. W., Whitwood, A. C., & Bruce, D. W. (2012). Hydrogen-bonded complexes between 4-alkoxystilbazoles and fluorophenols in solid state structures and liquid crystallinity. *Chemistry European Journal*, 18, 16073-16089.
- Yeap, G. Y., Chan, T. N., Yam, W. S., Takeuchi, D., & Ito, M. M. (2011). Influence of bromoalkyloxy side chain on mesomorphic behavior in heterocyclic 7-(4-bromoalkyloxy)-3-(4'-decyloxyphenyl)-4H-1-benzopyran-4-ones. *Chinese Chemical Letters*, 22, 947-950.
- Yeap, G. Y., Ha, S. T., Boey, P. L., Mahmood, W. A., Ito, M. M., & Youhei, Y. (2006). Synthesis and characterization of some new mesogenic schiff base esters n-[4-(4-n-hexadecanoyloxybenzyloxy)-benzylidene]-4-substituted anilines. *Molecular Crystals and Liquid Crystals*, 452(1), 73-90.

- Yeap, G. Y., Hng, T. C., Takeuchi, D., Osakada, K., Madmood, W., & Ito, M. M. (2009). Non-symmetric liquid crystal dimers: high thermal stability in nematic phase enhanced by thiophene-2-carboxylate moiety. *Molecular Crystals and Liquid Crystals*, 506, 134-149.
- Yeap, G. Y., Ooi, W. S., Nakamura, Y., & Cheng, Z. (2002). Synthesis and mesomorphic properties of schiff base esters p-n-octadecanoyloxybenzylidene-p-cyano-,p-hydroxy-,p-nitro-, and p-carboxyanilines. *Molecular Crystals and Liquid Crystals*, 381(1), 169-178.
- Yeap, G. Y., Ooi, Y. H., Kubo, K., & Ito, M. M. (2012). Synthesis and mesomorphic properties of 4-(4-bromopropoxy)-4'-(4-alkyloxybenzylidene)anilines. *Chinese Chemical Letters*, 23, 769-772.
- Yuksel, F., Atilla, D., & Ahsen, V. (2007). Synthesis and characterization of liquid crystalline unsymmetrically substituted phthalocyanines. *Polyhedron*, 26, 4551-4556.

## LIST OF PUBLICATIONS AND PAPERS PRESENTED

### **Publication**

1. Chong, Y. T., Sarih, N. M., Ha, S. T., & Sheikh, M. R. K. (2016). New Homologues Series of Heterocyclic Schiff Base Ester: Synthesis and Characterization. *Advances in Physical Chemistry*, 2016, 1-7.

### **Poster Presentation**

1. Chong, Y. T., Sarih, N. M., Ha, S. T., & Sheikh, M. R. K. (2014). Synthesis and Mesomorphic Properties of Schiff Base Ester with Terminal Methoxy Substituent, 5th UM-NUS-CU Trilateral Mini Symposium & Scientific Meeting 2014, 2014-02-11 to 2014-02-12, Department of Chemistry, Faculty of Science, University of Malaya.